

12

NSWC TR 86-142

# NOTES ON A GENERIC PARACHUTE OPENING FORCE ANALYSIS

BY WILLIAM P. LUDTKE

UNDERWATER SYSTEMS DEPARTMENT

1 MARCH 1986

DTIC  
SELECTED  
AUG 14 1986  
S D  
*Handwritten initials*

Approved for public release; distribution is unlimited.

AD-A170 962

DTIC FILE COPY



## NAVAL SURFACE WEAPONS CENTER

Dahlgren, Virginia 22448-5000 • Silver Spring, Maryland 20903-5000

86 8 14 040



AD-A170962

REPORT DOCUMENTATION PAGE

1a. REPORT SECURITY CLASSIFICATION UNCLASSIFIED			1b. RESTRICTIVE MARKINGS			
2a. SECURITY CLASSIFICATION AUTHORITY			3. DISTRIBUTION/AVAILABILITY OF REPORT Approved for public release; distribution unlimited.			
2b. DECLASSIFICATION/DOWNGRADING SCHEDULE						
4. PERFORMING ORGANIZATION REPORT NUMBER(S) NSWC TR 86-142			5. MONITORING ORGANIZATION REPORT NUMBER(S)			
6a. NAME OF PERFORMING ORGANIZATION Naval Surface Weapons Center		6b. OFFICE SYMBOL (If applicable) (U13)	7a. NAME OF MONITORING ORGANIZATION			
6c. ADDRESS (City, State, and ZIP Code) 10901 New Hampshire Avenue Silver Spring, MD 20903-5000			7b. ADDRESS (City, State, and ZIP Code)			
8a. NAME OF FUNDING/SPONSORING ORGANIZATION		8b. OFFICE SYMBOL (If applicable)	9. PROCUREMENT INSTRUMENT IDENTIFICATION NUMBER			
8c. ADDRESS (City, State, and ZIP Code)			10. SOURCE OF FUNDING NUMBERS			
			PROGRAM ELEMENT NO. NA	PROJECT NO. 4U81VA	TASK NO. NA	WORK UNIT ACCESSION NO. NA
11. TITLE (Include Security Classification) NOTES ON A GENERIC PARACHUTE OPENING FORCE ANALYSIS						
12. PERSONAL AUTHOR(S) William P. Ludtke						
13a. TYPE OF REPORT Final		13b. TIME COVERED FROM FY 1985 TO 1986		14. DATE OF REPORT (Year, Month, Day) 86-3-1		15. PAGE COUNT
16. SUPPLEMENTARY NOTATION						
17. COSATI CODES			18. SUBJECT TERMS (Continue on reverse if necessary and identify by block number)			
FIELD	GROUP	SUB-GROUP				
01	03		Solid Cloth Parachutes Calculation Methods Parachute Technology Limiting Ballistic Mass Ratio Opening Shock Scaling			
19. ABSTRACT (Continue on reverse if necessary and identify by block number)						
<p>The determination of parachute opening shock forces is one of the most vital elements in decelerator system design. This report develops a generic opening shock analysis that permits calculation of velocity profiles, shock factors, maximum shock forces and their time of occurrence during deployment for many types of parachutes. Criteria are presented and methods of calculation developed.</p> <p>Application of the analysis to an apparent anomaly in solid cloth parachute finite mass deployment, verifies the parachute diameter effect shown in the test performance. This is illustrated by an example.</p>						
20. DISTRIBUTION/AVAILABILITY OF ABSTRACT <input type="checkbox"/> UNCLASSIFIED/UNLIMITED <input checked="" type="checkbox"/> SAME AS RPT. <input type="checkbox"/> DTIC USERS				21. ABSTRACT SECURITY CLASSIFICATION UNCLASSIFIED		
22a. NAME OF RESPONSIBLE INDIVIDUAL William P. Ludtke			22b. TELEPHONE (Include Area Code) (202) 294-1705		22c. OFFICE SYMBOL U13	

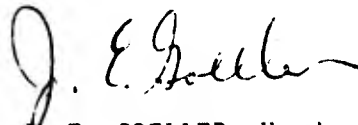
A

FOREWORD

The determination of parachute opening shock forces is one of the most vital elements in decelerator system design. This report develops a generic opening shock analysis that permits calculation of velocity profiles, shock factors, maximum shock forces and their time of occurrence during deployment for many types of parachutes. Criteria are presented and methods of calculation developed.

Application of the analysis to an apparent anomaly in solid cloth parachute finite mass deployment, verifies the parachute diameter effect shown in the test performance. This is illustrated by an example.

Approved by:



Dr. J. E. GOELLER, Head  
Underwater Weapons Division



Accession For	
NTIS CRA&i	<input checked="" type="checkbox"/>
DTIC TAB	<input type="checkbox"/>
Unannounced	<input type="checkbox"/>
Justification	
By	
Distribution/	
Availability Codes	
Dist	Avail and/or Special
A-1	

## CONTENTS

	<u>Page</u>
INTRODUCTION . . . . .	1
APPROACH . . . . .	2
THE EQUATION OF MOTION IN THE UNFOLDING PHASE OF INFLATION . . . . .	2
THE BALLISTIC MASS RATIO AS A SCALE FACTOR . . . . .	3
DEVELOPMENT OF THE GENERIC DEPLOYMENT ANALYSIS . . . . .	7
INTRODUCTION OF THE VARIABLE EXPONENT AND INITIAL DRAG AREA . . . . .	14
THE ELASTIC PHASE OF INFLATION . . . . .	21
ANALYSIS APPLICATION TO AN APPARENT SOLID CLOTH PARACHUTE DEPLOYMENT ANOMALY . . . . .	25
IMPULSE AND MOMENTUM DURING PARACHUTE INFLATION . . . . .	30
CONCLUSIONS . . . . .	40
REFERENCES . . . . .	41
APPENDIX A--AIAA PAPER NO. 73-477, "A TECHNIQUE FOR THE CALCULATION OF THE OPENING-SHOCK FORCES FOR SEVERAL TYPES OF SOLID CLOTH PARACHUTES" . . . . .	A-1
APPENDIX B--A GUIDE FOR THE USE OF APPENDIX A . . . . .	B-1
APPENDIX C--EFFECT OF INITIAL AREA RATIO ON THE LIMITING MASS RATIO AND SHOCK FACTOR FOR THE FINITE STATE OF SOLID CLOTH PARACHUTE DEPLOYMENT . . . . .	C-1

## ILLUSTRATIONS

<u>Figure</u>		<u>Page</u>
1	POINT MASS FORCE SYSTEM . . . . .	2
2	OPENING FORCE FACTOR VERSUS MASS RATIO . . . . .	4
3	VISUALIZATION OF THE SCHILLING CUBIC MASS RATIO CONCEPT . . . . .	5
4	RETARDED AUTOMOBILE . . . . .	5
5	VISUALIZATION OF THE BALLISTIC MASS RATIO CONCEPT . . . . .	6
6	VARIATION OF AFFECTED AIR MASS ALONG A FULLY INFLATED PARACHUTE TRAJECTORY . . . . .	6
7	DEPENDENCE OF MASS RATIO AND INFLATION REFERENCE TIME ON PARACHUTE GEOMETRY, AIRFLOW PROPERTIES, DRAG-AREA SIGNATURE, AND DEPLOYMENT CONDITIONS FOR SOLID CLOTH PARACHUTES . . . . .	8
8	TYPICAL INFINITE MASS FORCE-TIME HISTORY OF A SOLID CLOTH PARACHUTE IN A WIND TUNNEL . . . . .	9
9	DRAG-AREA RATIO VERSUS DIMENSIONLESS FILLING TIME . . . . .	11
10	OPENING FORCE REDUCTION FACTOR VERSUS BALLISTIC PARAMETER A . . . . .	15
11	COMPARISON OF DRAG AREAS DURING INFLATION . . . . .	17
12	EFFECT OF INITIAL AREA AND BALLISTIC MASS RATIO ON THE SHOCK FACTOR AND VELOCITY RATIO DURING THE UNFOLDING PHASE FOR SEVERAL VALUES OF $j$ . . . . .	19
13	EFFECT OF THE FILLING TIME EQUATION EXPONENT 0.9 ON THE TRAJECTORY VELOCITY AT PARACHUTE SUSPENSION LINE STRETCH . . . . .	26
14	FINITE MASS RATIO FORM OF DEPLOYMENT PERFORMANCE PROFILE FOR THE 24-FOOT AND 28-FOOT FLAT CIRCULAR PARACHUTES OF EXAMPLE 1 . . . . .	31
15	FINITE MASS REAL TIME DEPLOYMENT DRAG-AREA PROFILES FOR THE 24-FOOT AND 28-FOOT FLAT CIRCULAR PARACHUTES OF EXAMPLE 1 . . . . .	32
16	FINITE MASS REAL TIME DEPLOYMENT VELOCITY AND OPENING FORCE PROFILES FOR THE 24-FOOT AND 28-FOOT FLAT CIRCULAR PARACHUTES OF EXAMPLE 1 . . . . .	33
17	IMPULSE OF THE INFLATING CANOPY OF EXAMPLE 2 . . . . .	35
18	EFFECT OF ALTITUDE AND INFLATION REFERENCE TIME ON THE IMPULSE OF THE INFLATING CANOPY OF EXAMPLE 2 . . . . .	39

## TABLES

<u>Table</u>		<u>Page</u>
1	SUMMARY OF THE PERFORMANCE ANALYSIS DURING PARACHUTE DEPLOYMENT FOR SELECTED VALUES OF $j$ . . . . .	23
2	CANOPY FILL FACTOR, $n$ , FOR VARIOUS PARACHUTE TYPES . . . . .	27
3	SOLID CLOTH PARACHUTE CALCULATIONS FOR EXAMPLE 1 . . . . .	28
4	RIBBON PARACHUTE CALCULATIONS FOR EXAMPLE 1 . . . . .	34

## INTRODUCTION

In July 1985, the American Institute of Aeronautics and Astronautics, in conjunction with the University of Minnesota presented the Helmut G. Heinrich Short Course on Decelerator Systems Technology. This course was hosted by the Sandia National Laboratories, Albuquerque, New Mexico.

A principal topic presented in the course was the opening-shock force of various types of parachutes. One element of the opening-shock analysis was based upon the Pflanz method where the inflating canopy drag-area ratio ( $C_{DS}/C_{DS0}$ ) was expressed as a time ratio ( $t/t_f$ ) raised to an exponent of  $1/2$ , 1, or 2. Appendix A of this report is an approach to several solid cloth types of parachutes which uses a time-ratio exponent of 6. The several exponents denote the type of parachute under analysis, i.e., an exponent of 1 is indicative of geometrically porous Ribbon and Ringslot parachutes and Cross parachute canopies while an exponent of 6 is indicative of solid cloth canopies. Another property of parachute deployment, usually considered as small and therefore not usually addressed, is the concept of initial drag-area ratio ( $C_{DS_i}/C_{DS0}$ ) at the inflation time  $t = 0$  second is also included in the development.

Variation of the time-ratio exponent from  $1/2$  through 6 and the initial drag-area effect can be determined in a closed form theoretical approach. The purpose of this study is to analyze the opening-shock solution in a general way and to develop the equations for the velocity ratio, instantaneous shock factors, time of occurrence of the maximum opening shock in the finite mass, intermediate mass, and infinite mass ranges of performance and the limiting mass ratio for finite mass operation. The velocity-ratio and shock-factor performance of the various parachute types is presented in graphical format and as a tabular summary of the various equations.

As the study progressed application of the formulae to an apparent solid cloth parachute finite mass deployment anomaly, which had been noted in 1944, theoretically confirmed the test results.

Newton's third law of motion for constant mass is used in a horizontal deployment mode. A transform equation modifies the analysis to permit the development of velocity ratios in a generic form of a drag-area ratio signature and a performance scale factor. Instantaneous shock factors are derived from the velocity and drag-area ratios. The times of occurrence of the maximum shock force and the maximum force in the finite mass, intermediate mass, and infinite mass ranges are presented. Particular drag-area signatures and initial drag areas applied to the generic equations yield the performance profiles.

A method of addressing the impulse and momentum of an inflating parachute canopy was derived in Reference 3. The method is updated in this report to include the variable exponent and initial drag area.

## APPROACH

The study is based upon two conditions: (a) the premise that the Ballistic Mass Ratio satisfies stated criteria required for a genuine scale parameter, and (b) an opening-shock-force analysis that was presented at the fourth AIAA Aerodynamic Decelerator and Balloon Technology Symposium in 1973. Since the analysis is to be used extensively, the paper from the symposium is included as Appendix A for the convenience of the reader. Appendix B provides a worksheet for use as a guide on how to most effectively use Appendix A. The development of the subject matter is to be a combination of theoretical development combined with examples to demonstrate the results. It is suggested that for best understanding of this report the reader should review Appendix A first.

## THE EQUATION OF MOTION IN THE UNFOLDING PHASE OF INFLATION

Consider a point-mass system of analysis where the forces acting on the system are the system weight and the parachute aerodynamic drag force in a horizontal mode as in Figure 1.

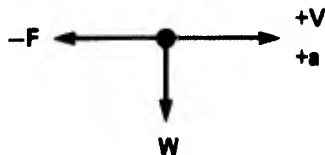


FIGURE 1. POINT MASS FORCE SYSTEM

$$-F = ma$$

$$-\frac{1}{2}\rho v^2 C_D S = \frac{W}{g} \frac{dv}{dt}$$

$$\int_0^t C_D S dt = \frac{2W}{g\rho} \int_{V_B}^V \frac{dv}{(-v^2)} \quad (1)$$

multiplying the right-hand term of Equation (1) by:

$$1 = \frac{C_D S_0 t_0 V_S}{C_D S_0 t_0 V_S}$$

This factor is the key to transforming Equation (1) to a form suitable for parachute analysis.

Equation (1) becomes

$$\frac{1}{t_0} \int_0^t \frac{C_D S}{C_D S_0} dt = \frac{2W}{\rho g C_D S_0 V_S t_0} V_S \int_{V_B}^V \frac{dv}{(-v^2)} \quad (2)$$

## THE BALLISTIC MASS RATIO AS A SCALE FACTOR

$$\text{Let } M = \frac{2W}{\rho g C_D S_0 V_{St_0}}$$

The Ballistic Mass Ratio,  $M$ , is a scale parameter that determines whether the mode of operation is finite mass, intermediate mass, or infinite mass. The Ballistic Mass Ratio as a scale parameter is discussed in detail in Reference 1. This dimensionless quantity has been known in parachute dynamics for a long time and is generally known as "Factor A."

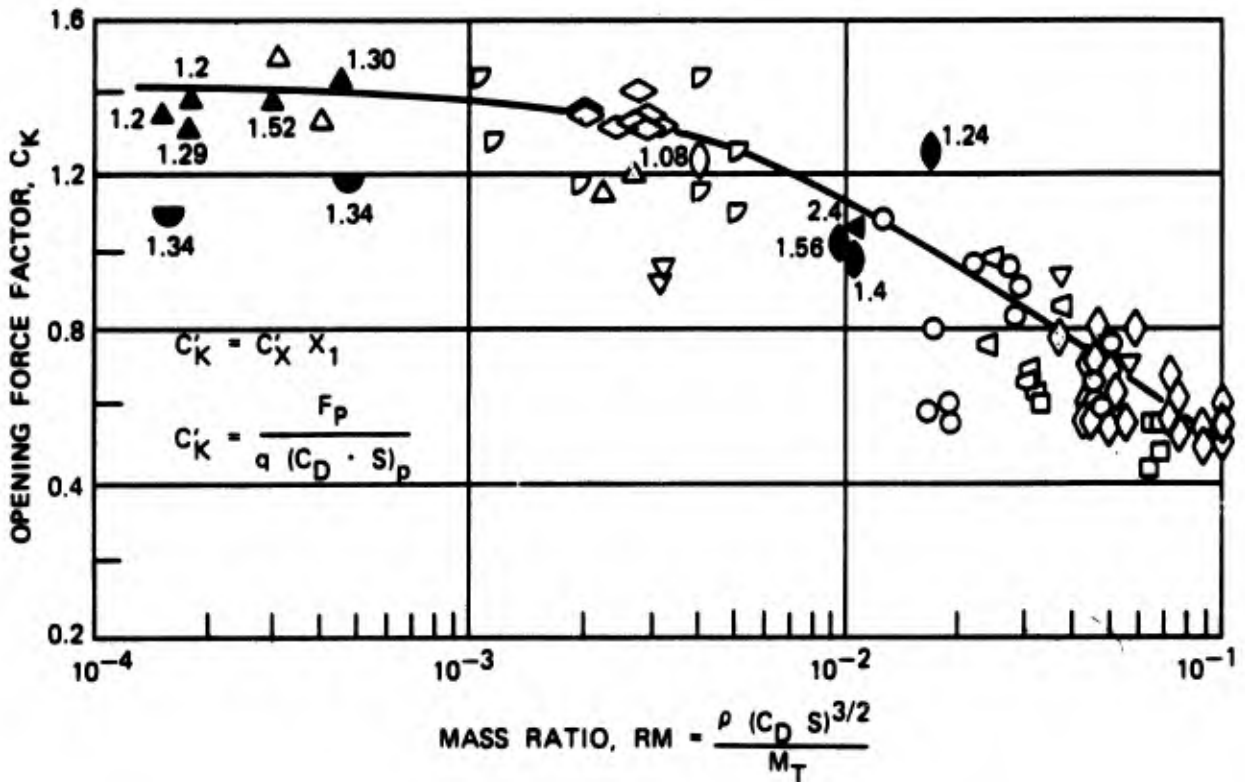
The worth of the parachute deployment performance calculation depends on the goodness-of-fit of the several elements. Equation (2) shows that accurate mathematical description of the dynamic drag area ratio ( $C_D S / C_D S_0$ ) and the inflation distance ( $V_{St_0}$ ) are necessary for reliable calculations. The inflation distance may also be a function of altitude; see Equation 14, page A-7 of Appendix A. Usually, such elements as retarded system weight,  $W$ , system-drag area,  $C_D S_0$ , and density,  $\rho$ , are sufficiently defined.

All methods of opening-shock-force calculations are based on formulae as if there were only a single solution. In reality the formulae are related to a flexible vibrating (inflating) device that may have considerable noise superimposed on the calculations. This noise results in a tolerance on the calculated force. From experience tolerance limits of  $\pm 15$  percent are realistic.

Schilling in 1957 recognized that the correlation of parachute-shock factors was improved by relating them to a dimensionless ratio of atmosphere mass to system mass as in Figure 2, reproduced from Reference 2. Visualizing the atmospheric mass component of the mass ratio of Figure 2 indicates that the parachute-opening shock is proportional to a cube of atmospheric mass as shown in Figure 3. I really have a problem trying to visualize parachute performance as being dependent on a cube of atmosphere.

For any quantity to be a valid scale factor in any process it must contain those variables which affect performance. Froude, Reynolds, and Mach numbers are not suitable for scaling parachute performance because they do not account for the effects of weight, time, and variable geometry. The mass ratio of Figure 2 does not allow for velocity or time effects. The retarded automobile of Figures 4, 5, and 6, from Reference 3, on a horizontal road illustrates how the Ballistic Mass Ratio affects the performance of the vehicle. Solution of Equation (1) for the fully open parachute retardation phase (constant  $C_D S_0$ ) yields the following velocity ratio.

$$\frac{V}{V_S} = \frac{1}{1 + \frac{\rho g V_{St} C_D S_0}{2W}} = \frac{1}{1 + \frac{1}{M}} \quad (3)$$



SYMBOL	PARACHUTE DATA				FOREBODY
	TYPE	D <sub>o</sub> , FT	REEFING RATIO	DEPLOY METHOD	
◇	APOLLO CONICAL RIBBON DROGUE	13.7	0.308	MORTAR	BUFF
▷	APOLLO CONICAL RIBBON DROGUE	16.5	0.428	MORTAR	BUFF
○	ADDPEP HEMISFLO	16.0	0.22-0.41	CANISTER	STREAMLINED
△	MERCURY CONICAL RIBBON	6.87	0.87	MORTAR	STREAMLINED
△	SANDIA CONICAL RIBBON	20.0	0.186	DROGUE GUN	STREAMLINED
◐	COOK CONICAL RIBBON	84.4	0.20-0.30	PILOT CHUTE	STREAMLINED
○	UAR RINGSAIL	20-30	0.16-0.31	PILOT CHUTE	STREAMLINED
□	CENTURY RINGSAIL	128	0.125	PILOT CHUTE	STREAMLINED
▽	ASSET RINGSAIL	29.6	0.10/0.20	PILOT CHUTE	STREAMLINED
△	APOLLO HVAIS RINGSAIL	83.5	0.08	PILOT CHUTE	STREAMLINED
◇	APOLLO BLK I AND II RINGSAIL	83.5	0.095	PILOT CHUTE	STREAMLINED

FILLED SYMBOLS INDICATE SUPERSONIC PARACHUTE DEPLOYMENT. NUMBERS ADJACENT TO DATUM POINTS IDENTIFY MACH NO. AT PARACHUTE LINE STRETCH.

- F<sub>p</sub> = PARACHUTE FORCE (REEFED OR UNREEFED)
- (C<sub>D</sub> · S)<sub>p</sub> = PARACHUTE DRAG AREA (REEFED OR UNREEFED)
- q = DYNAMIC PRESSURE AT LINE STRETCH OR DISREEF
- M<sub>T</sub> = SYSTEM MASS = W<sub>T</sub>/g (VEHICLE PLUS DECELERATOR)

FIGURE 2. OPENING FORCE FACTOR VERSUS MASS RATIO

Reproduced from reference 2

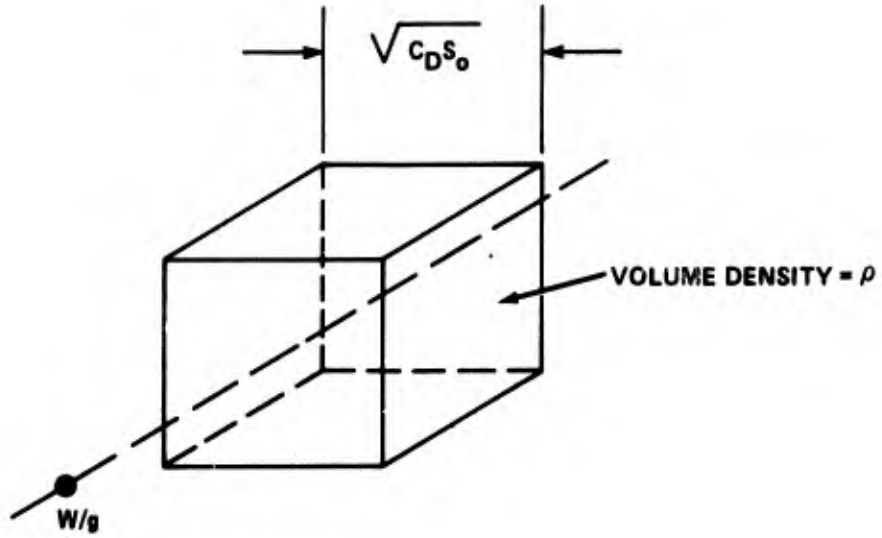


FIGURE 3. VISUALIZATION OF THE SCHILLING CUBIC MASS RATIO CONCEPT

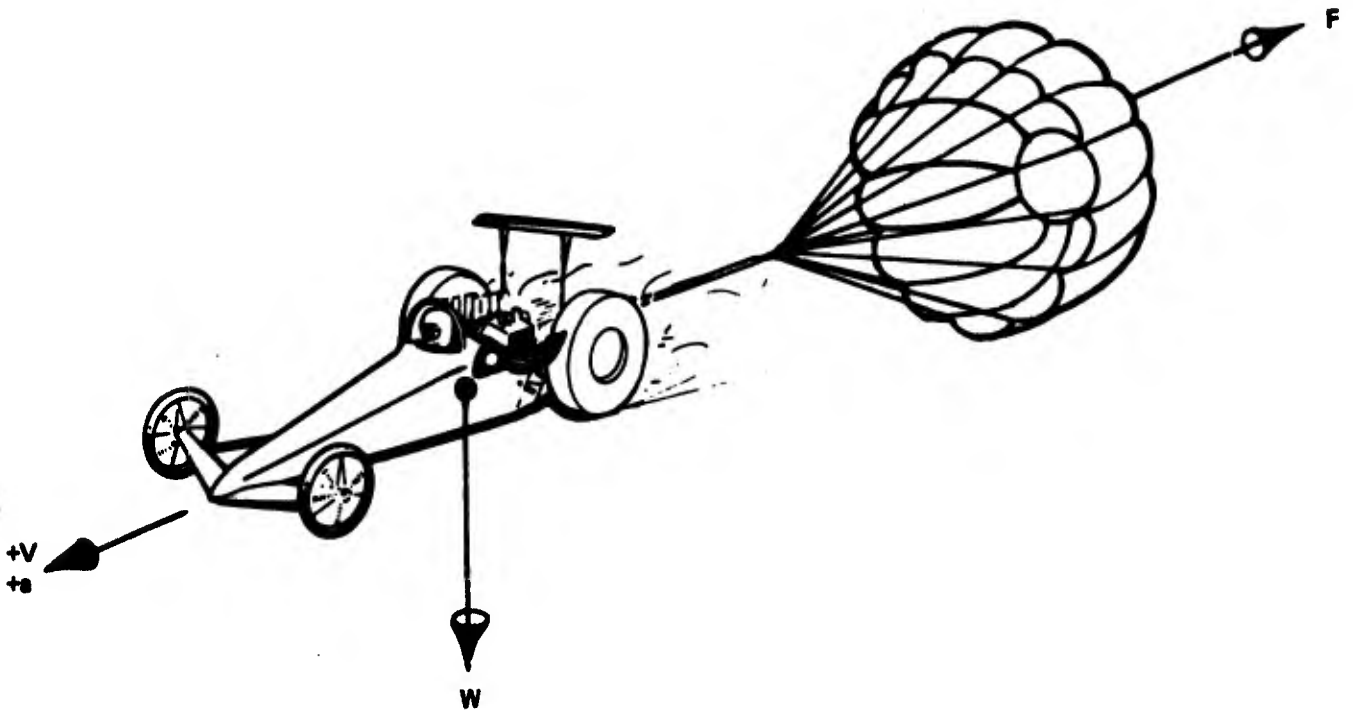


FIGURE 4. RETARDED AUTOMOBILE

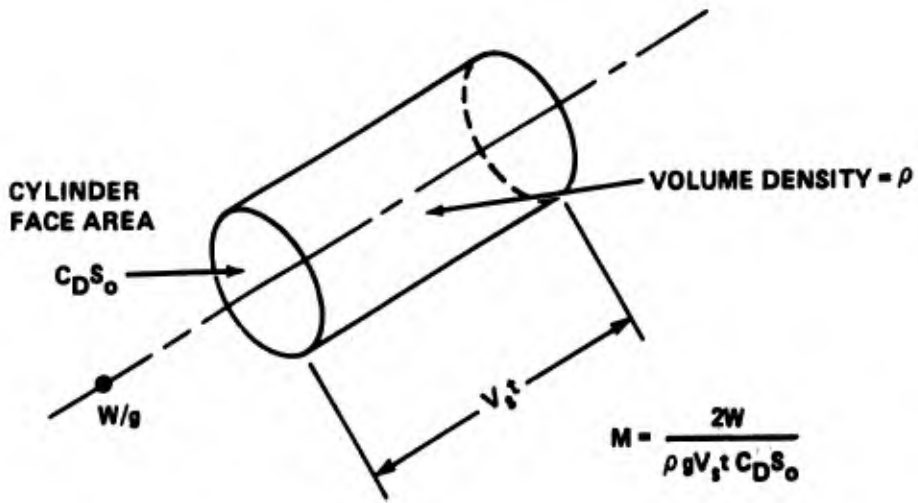


FIGURE 5. VISUALIZATION OF THE BALLISTIC MASS RATIO CONCEPT

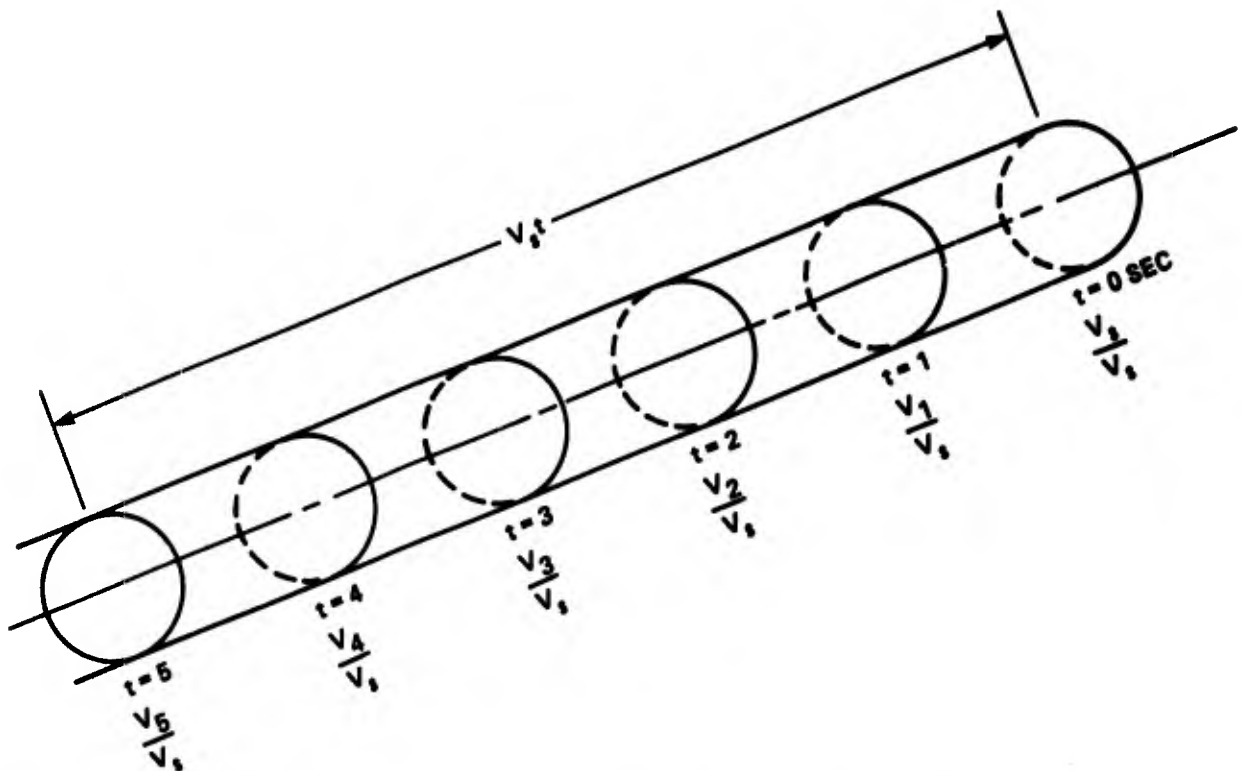


FIGURE 6. VARIATION OF AFFECTED AIR MASS ALONG A FULLY INFLATED PARACHUTE TRAJECTORY

Figure 5 visualizes the Ballistic Mass Ratio concept and Figure 6 illustrates how the Ballistic Mass Ratio varies with time. The air mass affected varies from instant to instant and at each instant a definite velocity ratio is associated with the Ballistic Mass Ratio.

Appendix A was developed for several types of solid cloth parachutes. Equation (14) on page A-7 gives the inflation time for a canopy inflating from  $C_{DS} = 0$  to  $C_{DS} = C_{DS0}$  for the first time.

$$t_0 = \frac{14W}{\rho g C_{DS0} V_S} \left[ \frac{g \rho V_0}{2W} \left[ \frac{C_{DS0}}{A_{M0} - A_{S0} k \left( \frac{C.P. \rho}{2} \right)^{1/2}} \right]^{-1} \right]$$

The flow chart of Figure 7 shows how the Ballistic Mass Ratio is affected by each of the parameters of solid cloth parachutes. This approach is probably true for other types of parachutes, but at the present time I have not been able to develop a similar analysis.

#### DEVELOPMENT OF THE GENERIC DEPLOYMENT ANALYSIS

Since the Ballistic Mass Ratio develops naturally in the mathematical analysis and interacts with the geometric and aerodynamic properties of the parachute, I believe that it represents the best scale parameter currently available. Rewriting Equation (2)

$$\frac{1}{t_0} \int_0^t \frac{C_{DS}}{C_{DS0}} dt = M V_S \int_{V_S}^V \frac{dV}{(-V^2)} \quad (4)$$

Integrating the right-hand term

$$\frac{1}{t_0} \int_0^t \frac{C_{DS}}{C_{DS0}} dt = M \left( \frac{V_S}{V} - 1 \right) \quad (4a)$$

velocity ratio

$$\frac{V}{V_S} = \frac{1}{1 + \frac{1}{M t_0} \int_0^t \frac{C_{DS}}{C_{DS0}} dt} \quad (5)$$

The opening-shock signature of Figure 8 defines the method of determining the shock factors during inflation. At any given instant the instantaneous force is:

$$F = \frac{1}{2} \rho V^2 C_{DS},$$

**W** - SYSTEM WEIGHT, LB  
 **$\rho$**  - DENSITY AT DEPLOYMENT ALTITUDE, SLUGS/FT<sup>3</sup>  
 **$V_s$**  - SYSTEM VELOCITY AT SUSPENSION LINE STRETCH, FPS  
 **$t_0$**  - REFERENCE TIME OF UNFOLDING PHASE OF CANOPY INFLATION, SEC  
 **$C_D S_0$**  - SYSTEM STEADY STATE DRAG AREA, FT<sup>2</sup>  
**g** - GRAVITY, FT/SEC<sup>2</sup>  
**P** - CANOPY CLOTH PERMEABILITY, FT<sup>3</sup>/FT<sup>2</sup>/SEC  
 **$V_0$**  - STEADY STATE CANOPY VOLUME, FT<sup>3</sup>  
 **$A_{M0}$**  - STEADY STATE MOUTH AREA, FT<sup>2</sup>  
 **$S_0 = A_{30}$**  - CANOPY SURFACE AREA, FT<sup>2</sup>  
 **$\frac{C_D S}{C_D S_0}$**  - DRAG AREA SIGNATURE  
 **$\eta$**  - INITIAL AREA  
 **$t/t_0$**  - DEPLOYMENT TIME RATIO  
**k & n** - CLOTH AIR FLOW CONSTANTS  
 **$C_p$**  - CANOPY PRESSURE COEFFICIENT  
**V** - INSTANTANEOUS TRAJECTORY VELOCITY, FPS

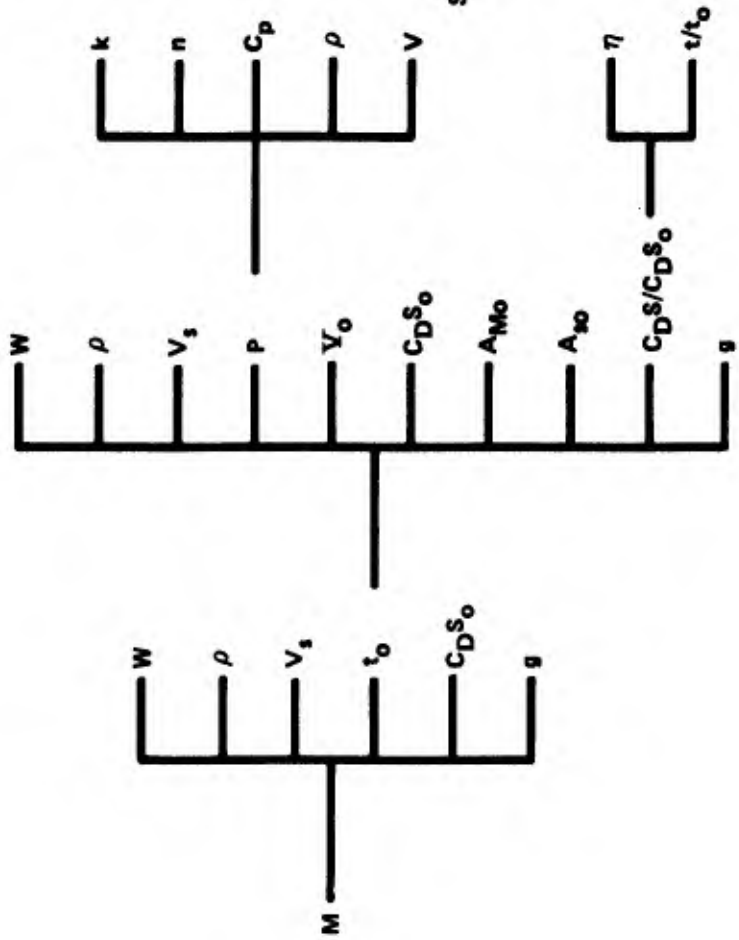


FIGURE 7. DEPENDENCE OF MASS RATIO AND INFLATION REFERENCE TIME ON PARACHUTE GEOMETRY, AIRFLOW PROPERTIES, DRAG-AREA SIGNATURE, AND DEPLOYMENT CONDITIONS FOR SOLID CLOTH PARACHUTES

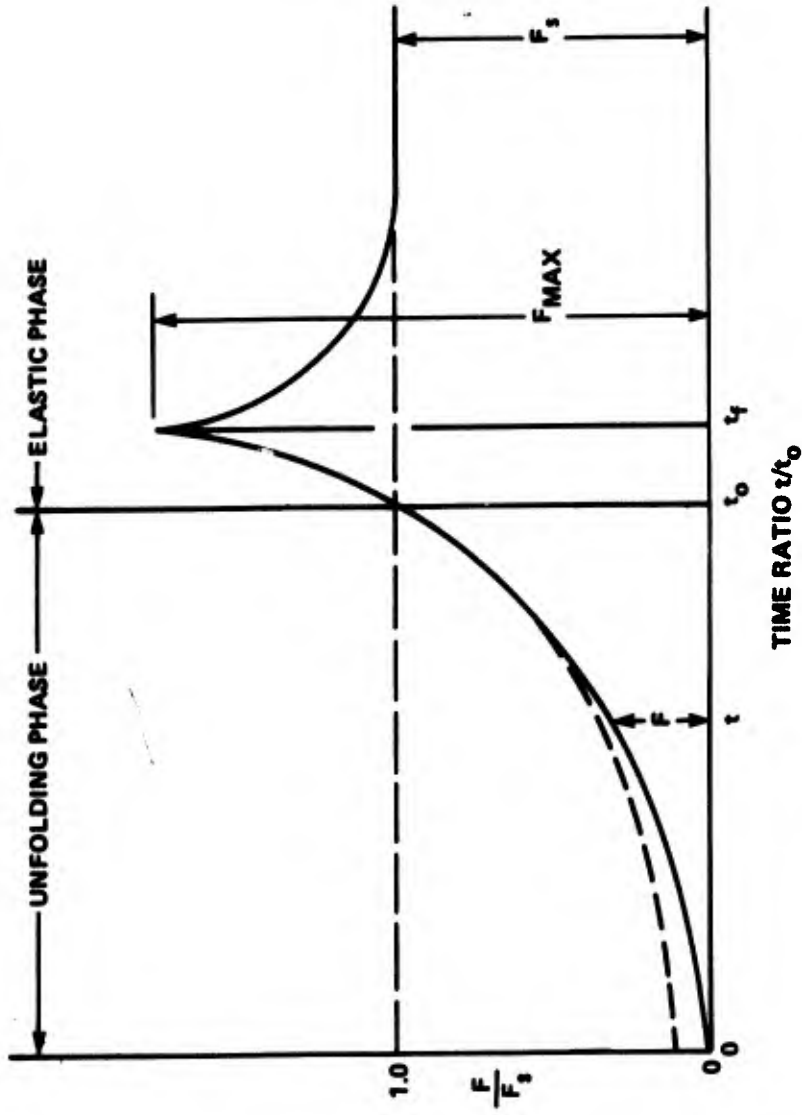


FIGURE 8. TYPICAL INFINITE MASS FORCE-TIME HISTORY OF A SOLID CLOTH PARACHUTE IN A WIND TUNNEL

and the wind tunnel steady-state drag force at deployment velocity  $V_S$  is:

$$F_S = \frac{1}{2} \rho V_S^2 C_D S_0$$

The ratio  $F/F_S$  is the instantaneous shock factor,  $x_1$ .

$$x_1 = \frac{F}{F_S} = \frac{1/2 \rho V^2 C_D S}{1/2 \rho V_S^2 C_D S_0}$$

$$x_1 = \left( \frac{V}{V_S} \right)^2 \frac{C_D S}{C_D S_0} \quad (6)$$

In wind tunnel infinite mass deployments the velocity remains constant and the shock factor becomes:

$$x_1 = \frac{C_D S}{C_D S_0} = f\left(\tau, \frac{t}{t_0}\right), \quad (7)$$

Dynamic drag-area signatures of various types of parachutes may be obtained in this manner. It has been demonstrated theoretically in Appendix A, and by actual test, Reference 4, Page 245, that the geometry of the inflating parachute is independent of altitude, velocity, and system mass. Dynamic drag-area signatures include the effects of apparent mass.

Figure 9, from Reference 2, defines dynamic drag areas for several types of parachutes.

In the general case the instantaneous shock factor is in accordance with Equations (5) and (6).

$$x_1 = \frac{\frac{C_D S}{C_D S_0}}{\left[ 1 + \frac{1}{M t_0} \int_0^t \frac{C_D S}{C_D S_0} dt \right]^2} \quad (8)$$

The time of occurrence of the maximum shock force can be determined by differentiating the shock factor with respect to time and setting the result equal to zero.

$$\frac{dx_1}{dt} = \left[ M + \frac{1}{t_0} \int_0^t \frac{C_D S}{C_D S_0} dt \right] \frac{d\left(\frac{C_D S}{C_D S_0}\right)}{dt} - \frac{2}{t_0} \left(\frac{C_D S}{C_D S_0}\right)^2 = 0 \quad (9)$$

The maximum shock factor can be determined by substituting the time ratio  $(t/t_0)$  from Equation (9) into Equation (8). As the Ballistic Mass Ratio increases from a small value, the time of occurrence and the maximum shock force develop later in the inflation process. When the maximum shock force occurs at

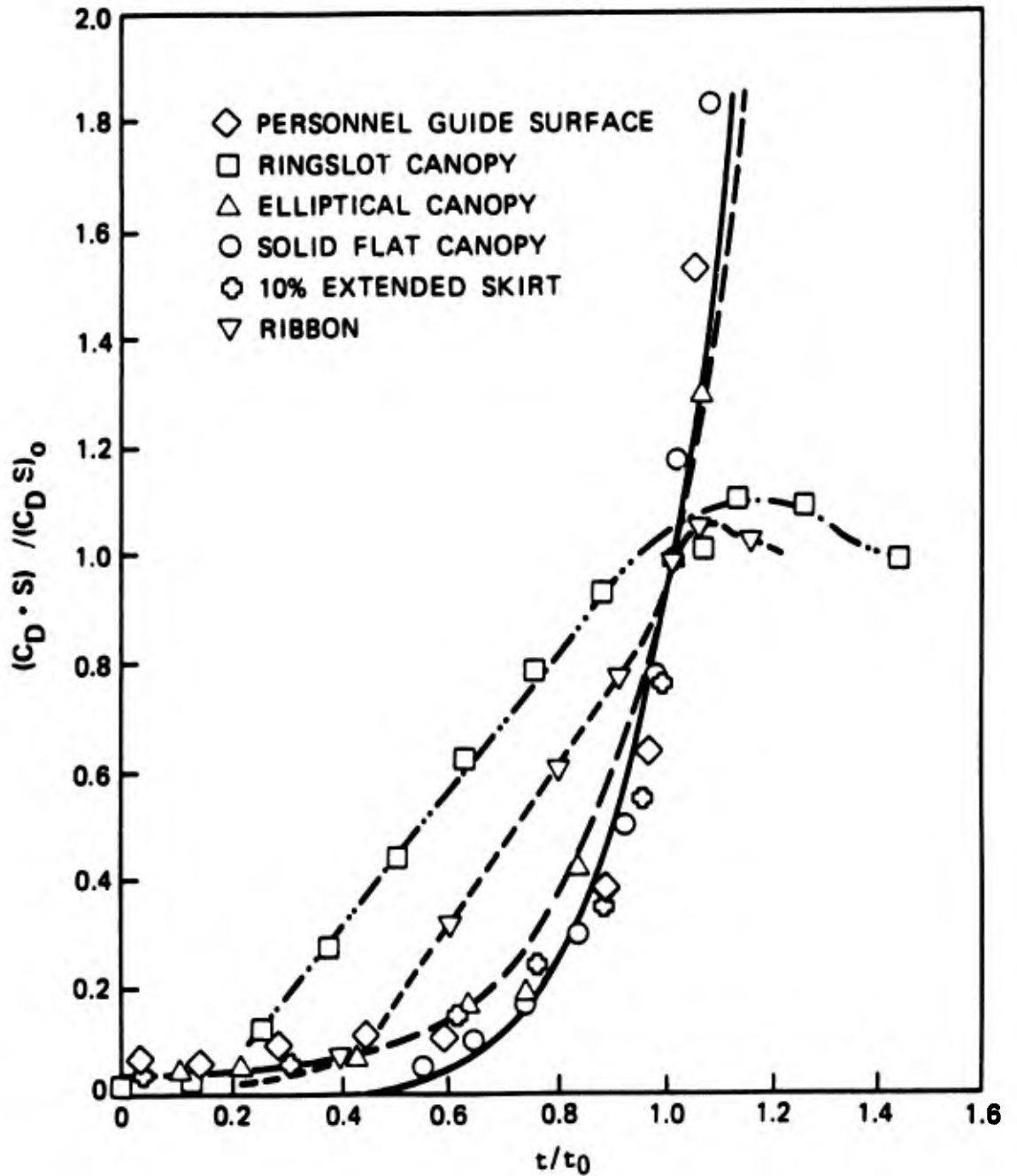


FIGURE 9. DRAG-AREA RATIO VERSUS DIMENSIONLESS FILLING TIME

Reproduced from Reference 2

the time  $t_0$ , the mass ratio associated with the occurrence of the maximum shock at  $t=t_0$  is the limiting mass ratio,  $M_L$ , for finite mass operation. A further increase in the Ballistic Mass Ratio causes the maximum force to occur after the inflation reference time,  $t_0$ , of the canopy, but to be much less than the infinite mass case. This is what I term the "Intermediate Mass" case. Eventually a further increase in the Ballistic Mass Ratio results in the classic infinite mass opening shock.

In summary:

velocity ratio

$$\frac{v}{v_s} = \frac{1}{1 + \frac{1}{Mt_0} \int_0^t \frac{C_D S}{C_D S_0} dt} \quad (5)$$

instantaneous shock factor

$$x_i = \frac{\frac{C_D S}{C_D S_0}}{\left[ 1 + \frac{1}{Mt_0} \int_0^t \frac{C_D S}{C_D S_0} dt \right]^2} \quad (8)$$

Time of occurrence of the finite mass maximum shock factor.

$$0 = \left[ M + \frac{1}{t_0} \int_0^t \frac{C_D S}{C_D S_0} dt \right] \frac{d\left(\frac{C_D S}{C_D S_0}\right)}{dt} - \frac{2}{t_0} \left(\frac{C_D S}{C_D S_0}\right)^2 \quad (9)$$

I call these equations Bill Ludtke's generic equations of parachute inflation. The analysis is generic since the drag-area signature has not been assigned.

The term  $d(C_D S/C_D S_0)/dt$  in Equation (9) is the inflation rate of the particular type of parachute. Figure 9 compares the dynamic drag-area signatures of the geometrically porous and the solid cloth canopies. The geometrically porous parachutes begin inflation slowly and then achieve a constant inflation rate until nearly fully open for the first time. The drag area then becomes self-limiting, and there is a decrease in the inflation rate. The inflation rate becomes zero for maximum drag-area ratios in the range of 1.05 to 1.1, which is the accepted range of infinite mass opening-shock factors for this family of canopies. The solid cloth parachutes begin inflation at a rate below the ribbon and ringslot parachutes. However, as the solid cloth canopies inflate, the inflation rate continues to increase. The high opening-shock force and tendency for man carrying solid cloth canopies to deflate at full opening are related to this property.

Even though Equations (5), (8), and (9) look formidable, they really are not.

For example:

let

$$\frac{C_D S}{C_D S_0} = \frac{t}{t_0}$$

then

$$\frac{d\left(\frac{C_D S}{C_D S_0}\right)}{dt} = \frac{1}{t_0}$$

and

$$\frac{1}{Mt_0} \int_0^t \frac{C_D S}{C_D S_0} dt = \frac{1}{2M} \left(\frac{t}{t_0}\right)^2$$

Therefore the velocity ratio becomes

$$\frac{v}{v_s} = \frac{1}{1 + \frac{1}{2M} \left(\frac{t}{t_0}\right)^2} \quad (9a)$$

Instantaneous shock factor

$$x_i = \frac{\frac{t}{t_0}}{\left[1 + \frac{1}{2M} \left(\frac{t}{t_0}\right)^2\right]^2} \quad (9b)$$

The time of occurrence of the maximum shock force

$$\frac{dx_i}{dt} = \left[M + \frac{1}{2} \left(\frac{t}{t_0}\right)^2\right] \cdot 2 \left(\frac{t}{t_0}\right)^2 = 0 \quad (9c)$$

$$\left(\frac{t}{t_0}\right)_{@x_{i_{\max}}} = \left(\frac{2M}{3}\right)^{1/2} \quad (9d)$$

The maximum shock factor

$$x_{i_{\max}} = \frac{\left(\frac{2M}{3}\right)^{1/2}}{\left[1 + \frac{1}{2M} \times \frac{2M}{3}\right]^2}$$

$$x_{i_{\max}} = \frac{9}{16} \left(\frac{2M}{3}\right)^{1/2} \quad (9e)$$

The maximum shock force

$$F_{\max} = F_s x_{i_{\max}}, \quad (9f)$$

where

$$F_s = \frac{1}{2} \rho V_s^2 C_D S_0$$

The limiting Ballistic Mass Ratio,  $M_L$ , for finite mass operation comes from Equation (9d) for  $t/t_0 = 1$ .

$$M_L = \frac{3}{2} \quad (9g)$$

Note that in the developed analysis, system performance is solely a function of the Ballistic Mass Ratio for a given value of  $j$  and  $\tau$ . Reference 3 demonstrated that the opening-shock force and stress distributions are constant, for all test altitudes, when a given parachute system is deployed at constant Ballistic Mass Ratio and dynamic pressure.

#### INTRODUCTION OF THE VARIABLE EXPONENT AND INITIAL DRAG AREA

In the general case many variations of drag area may be formulated as functions of time and applied in the analysis. Figure 10 from Reference 2 illustrates the Pflanz technique of using a drag-area signature of the form:

$$\frac{C_D S}{C_D S_0} = \left( \frac{t}{t_0} \right)^j,$$

where  $j$  has the values of  $1/2$ ,  $1$ ,  $2$ , etc. Appendix A uses a value of  $j = 6$ .

In general, drag-area signatures are not  $C_D S = 0$  at  $t = 0$ . There is some finite initial value of drag area,  $C_D S_i$ , that is dependent on the method of deployment; i.e., uncontrolled, deployment sleeve, deployment bag, quarter bag, etc. The objective is to make this feature as repeatable as possible so that it can be reliably accounted for.

$$\frac{C_D S_i}{C_D S_0} = \tau$$

In Appendix A,  $\eta$  is used to describe the initial area effects. The reason for the use of  $\tau$  in this report is that the basis of technology varies. While  $\tau$  is based on the ratio of initial drag area to the steady-state drag area,  $\eta$  was based upon the ratio of initial projected mouth area to the steady-state projected area.

$$\frac{C_D S}{C_D S_0} = (1 - \tau) \left( \frac{t}{t_0} \right)^j + \tau \quad (10)$$

$$X_{i_{max}} = \left[ \frac{(j+2)}{2(j+1)} \right]^2 \left( \frac{j(j+1)M}{(j+2)} \right)^{\frac{j}{j+1}} \quad (14)$$

n = j  
A = M

THIS FORMULA VALID FOR VALUES OF  $0 < X_{i_{max}} \leq 1$

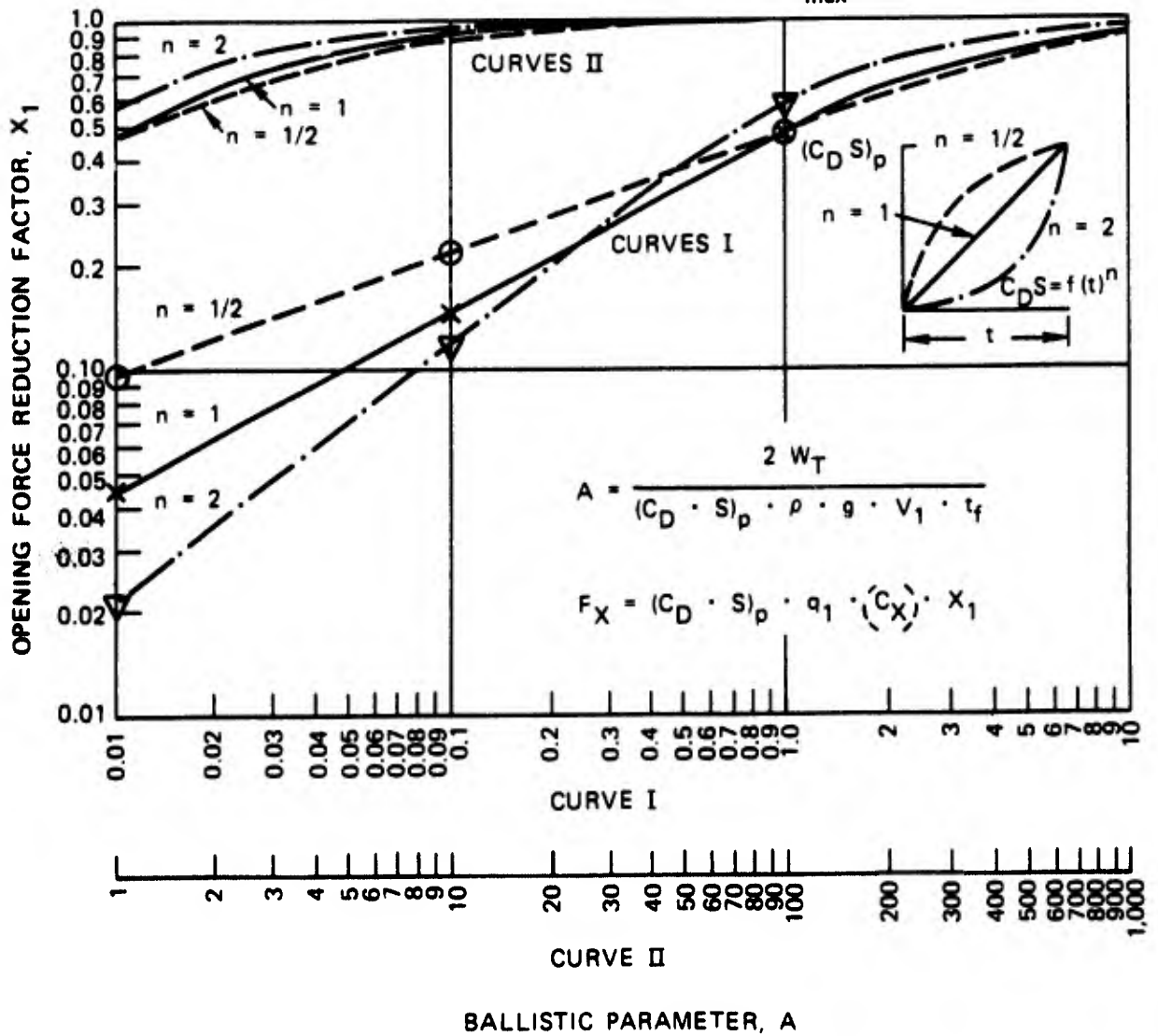


FIGURE 10. OPENING FORCE REDUCTION FACTOR VERSUS BALLISTIC PARAMETER A

Reproduced from Reference 2

The generalized Pflanz approach to drag area in Equation (10) is slightly different from Equation (4) of Appendix A. Figure 11 compares the Pflanz method and the method of Appendix A for initial drag area ratios of 0 and 0.1. For zero initial drag area both methods produce identical drag areas during the inflation sequence for a  $j$  value of 6. When an initial drag-area ratio of 0.1 is used, the generalized Pflanz method develops drag-area at a slower rate than the Appendix A method and probably yields higher opening-shock forces because of the lower rate of velocity decay during inflation.

The Pflanz method is the particular solution for Equation (10) when  $\tau = 0$ .

$$\frac{d\left(\frac{C_D S}{C_{D S_0}}\right)}{dt} = \frac{j(1-\tau)}{t_0} \left(\frac{t}{t_0}\right)^{j-1}$$

$$\frac{1}{M t_0} \int_0^t \left(\frac{C_D S}{C_{D S_0}}\right) dt = \frac{1}{M} \left[ \frac{(1-\tau)}{(j+1)} \left(\frac{t}{t_0}\right)^{j+1} + \tau \left(\frac{t}{t_0}\right) \right]$$

The general case velocity ratio is:

$$\frac{v}{v_s} = \frac{1}{1 + \frac{1}{M} \left[ \frac{(1-\tau)}{(j+1)} \left(\frac{t}{t_0}\right)^{j+1} + \tau \left(\frac{t}{t_0}\right) \right]} \quad (11)$$

The general case instantaneous shock factor

$$x_1 = \frac{(1-\tau) \left(\frac{t}{t_0}\right)^j + \tau}{\left[ 1 + \frac{1}{M} \left[ \frac{(1-\tau)}{(j+1)} \left(\frac{t}{t_0}\right)^{j+1} + \tau \left(\frac{t}{t_0}\right) \right] \right]^2} \quad (12)$$

The time of occurrence of the maximum shock force

$$0 = \left[ M + \frac{(1-\tau)}{(j+1)} \left(\frac{t}{t_0}\right)^{j+1} + \tau \left(\frac{t}{t_0}\right) \right] j(1-\tau) \left(\frac{t}{t_0}\right)^{j-1} - 2 \left[ (1-\tau) \left(\frac{t}{t_0}\right)^j + \tau \right]^2 \quad (13)$$

A closed solution to the general case of the time of occurrence of the maximum finite mass shock force has not been found except for when  $\tau = 0$ . For values of  $\tau$  other than zero, plotting  $x_1$  versus  $t/t_0$  is a suggested method.

When  $\tau = 0$

$$0 = \left[ M + \frac{1}{(j+1)} \left(\frac{t}{t_0}\right)^{j+1} \right] j \left(\frac{t}{t_0}\right)^{j-1} - 2 \left(\frac{t}{t_0}\right)^{2j}$$

- Eq. (4), APPENDIX A  $C_{DS}/C_{DS_0} = \left[ (1-\eta)(t/t_0)^3 + \eta \right]^2$
- - - - - Eq. (10), GENERALIZED Pflanz  $C_{DS}/C_{DS_0} = (1-\tau)(t/t_0)^6 + \tau$
- Eq. (10), AND (4) APPENDIX A FOR  $\tau = \eta = 0$

NOTE:  $\eta = \sqrt{\tau}$

$$\tau = C_{DSi}/C_{DS_0}$$

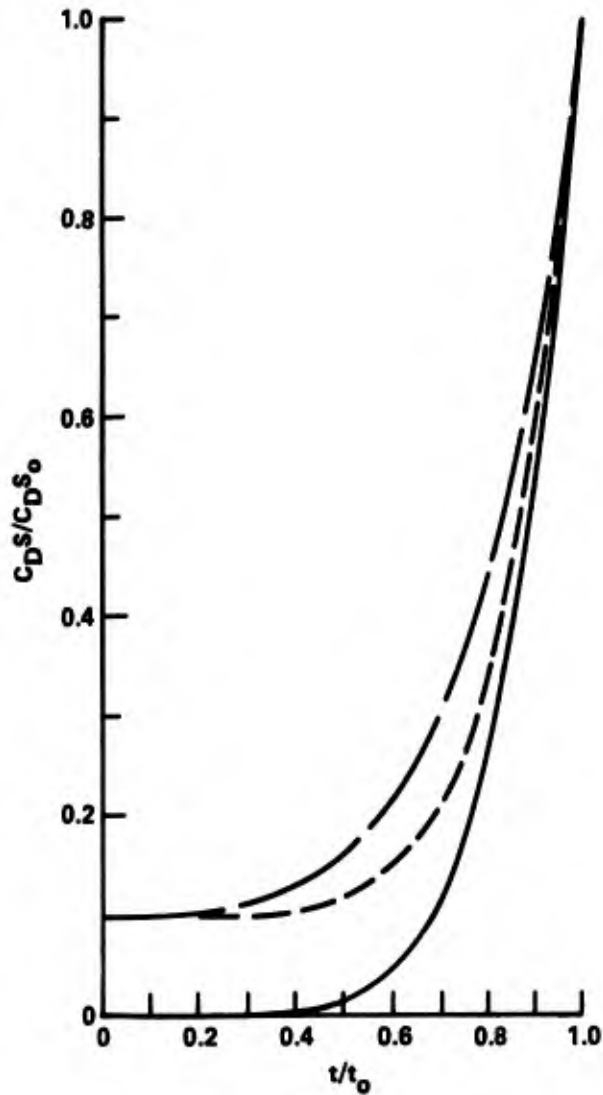


FIGURE 11. COMPARISON OF DRAG AREAS DURING INFLATION

$$\left(\frac{t}{t_0}\right)_{@x_{i_{\max}}} = \left(\frac{j(j+1)M}{(j+2)}\right)^{\frac{1}{j+1}} \quad (13a)$$

The finite mass limiting mass ratio when  $x_i$  max occurs at  $t/t_0 = 1$  is given by:

$$0 = \left[ M_L + \frac{(1-\tau)}{(j+1)} + \tau \right] j(1-\tau) - 2$$

$$M_L = \frac{2}{j(1-\tau)} - \frac{(1-\tau)}{(j+1)} - \tau \quad (13b)$$

For  $\tau = 0$  the limiting finite mass ratio is:

$$M_L = \frac{(j+2)}{j(j+1)} \quad (13c)$$

The maximum shock factor @  $(t/t_0)$  @  $x_{i_{\max}}$

$$x_{i_{\max}} = \left[ \frac{(j+2)}{2(j+1)} \right]^2 \left[ \frac{j(j+1)M}{(j+2)} \right]^{\frac{j}{j+1}} \quad (14)$$

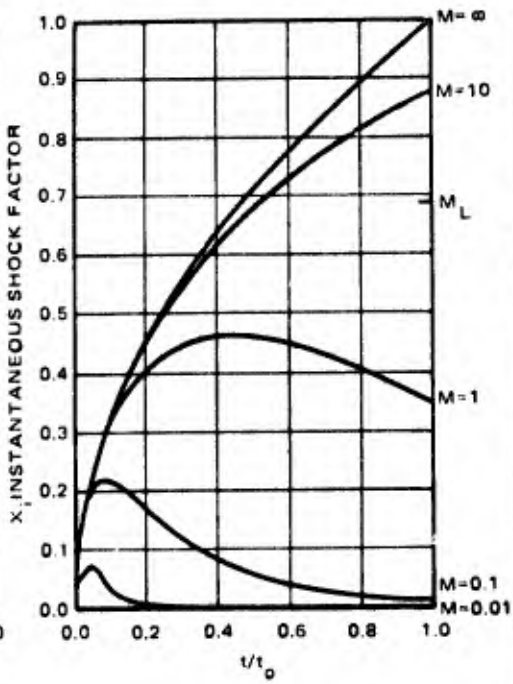
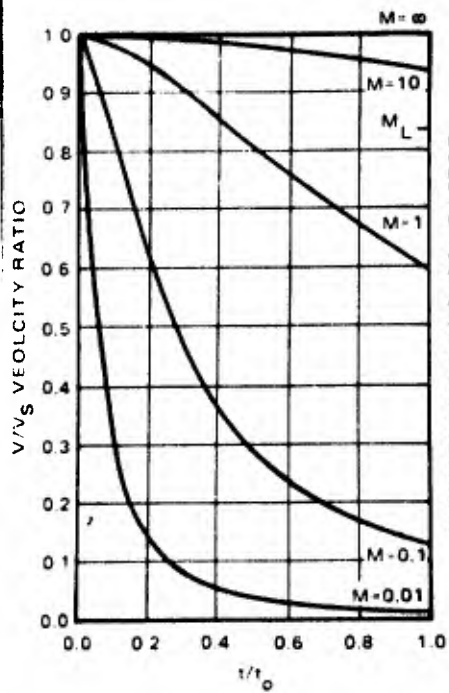
The results of Equation 14 are plotted in Figure 10 for several values of Ballistic Mass Ratio ( $M = A$ ) and ( $n = j$ ). The variable  $n$  was earlier used in Appendix A in the definition of cloth airflow. Hence,  $j$  was used to define the drag-area signature exponent in this report. There is excellent agreement between the plotted data and Equation 14.

The four analysis variables,  $t/t_0$ ,  $\tau$ ,  $j$ , and  $M$ , and the range of possible values for each, present numerous performance possibilities. A series of inflation model calculations were made to determine the velocity ratios and shock factors for values of  $\tau = 0$  and  $\tau = 0.2$ ;  $M = \text{infinity}, 10, 1, 0.1, \text{ and } 0.01$ ;  $j = 1/2, 1, 2, 3, 4, 5, \text{ and } 6$  as the time ratio,  $t/t_0$ , varied from 0 to 1.0. With 1400 data combinations available, it is impossible to discuss the results in meaningful narrative form. Figure 12 graphically presents the inflation model performance and permits simultaneous viewing of the interaction and effects of the analysis variables.

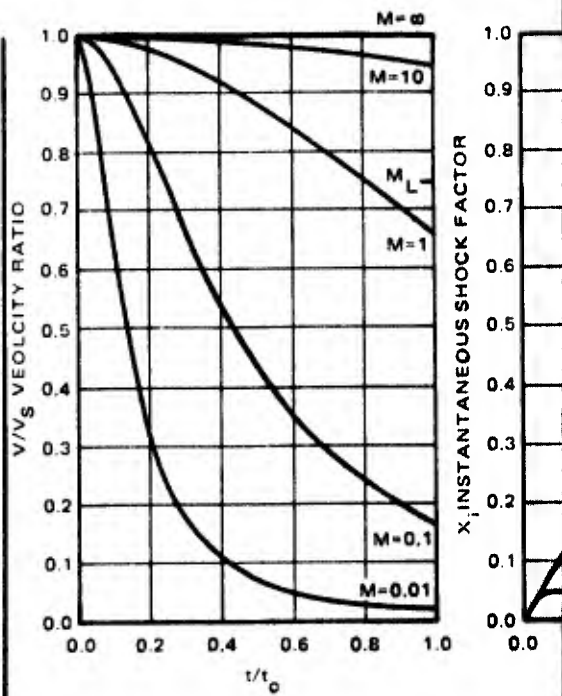
The value of  $\tau = 0.2$ , used in Figure 12, was to illustrate the effect of initial drag area on opening shock performance. The line-stretch snatch force of a parachute open that far would be very large. The effect of the Ballistic Mass Ratio is well illustrated in Figure 12. The limiting mass ratios,  $M_L$ , are marked on the ordinates at  $t/t_0 = 1$ . On page A-6 of Appendix A, a similar performance plot with additional Ballistic Mass Ratios provides a more detailed performance for  $j = 6$ .

When Ballistic Mass Ratios exceed the limiting value, the time of occurrence of the maximum shock force is greater than 1. In this event, Equation (14) cannot be used to calculate the shock factor. The elasticity of the parachute materials must be included in the analysis. The approach is similar to Section VI of Appendix A beginning on page A-9.

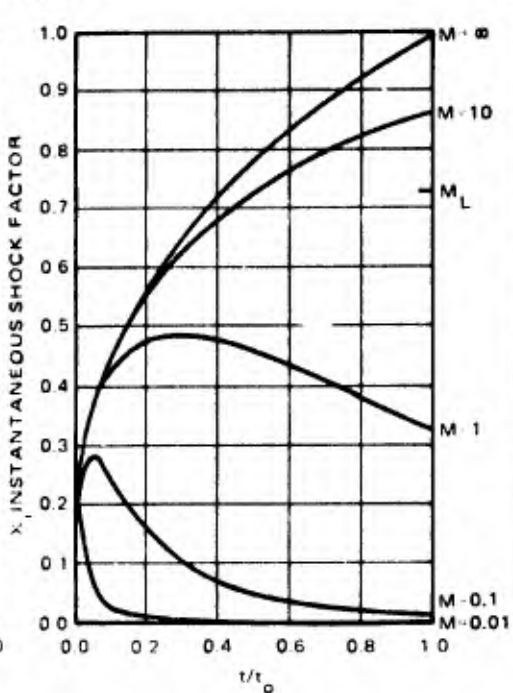
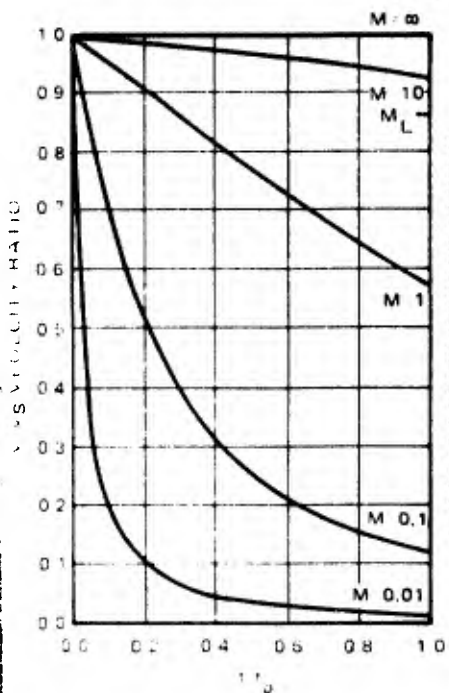
$\tau = 0; j = 0.5$



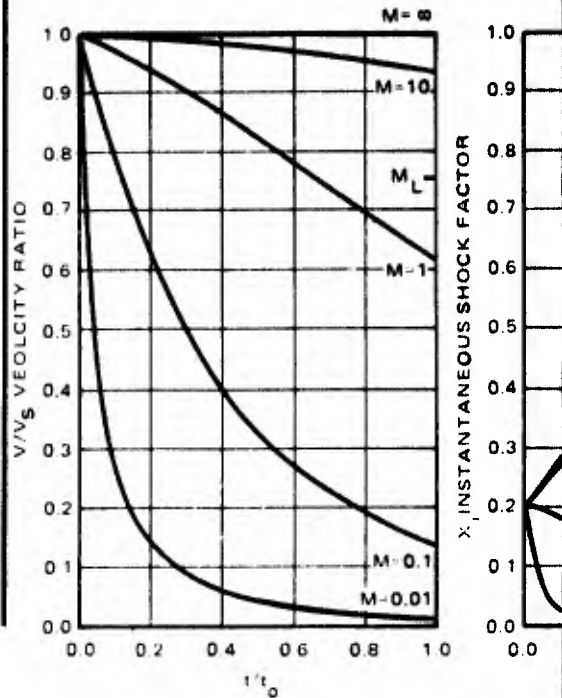
$\tau = 0; j = 1$



$\tau = 0.2; j = 0.5$

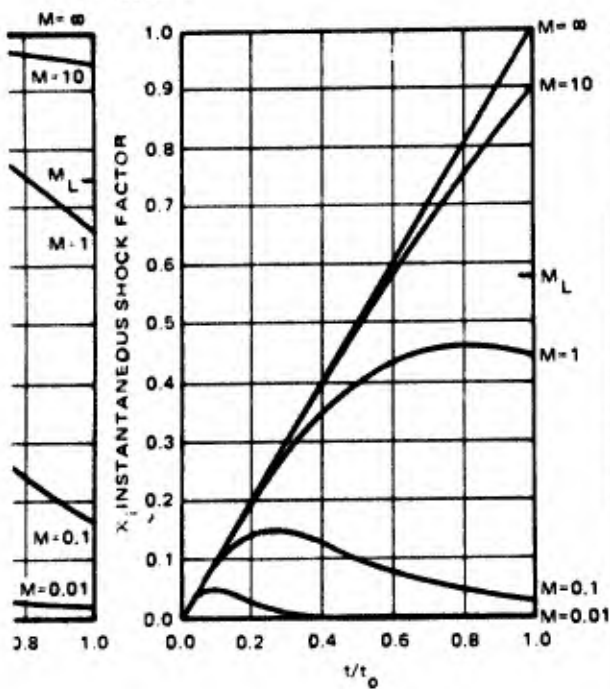


$\tau = 0.2; j = 1$

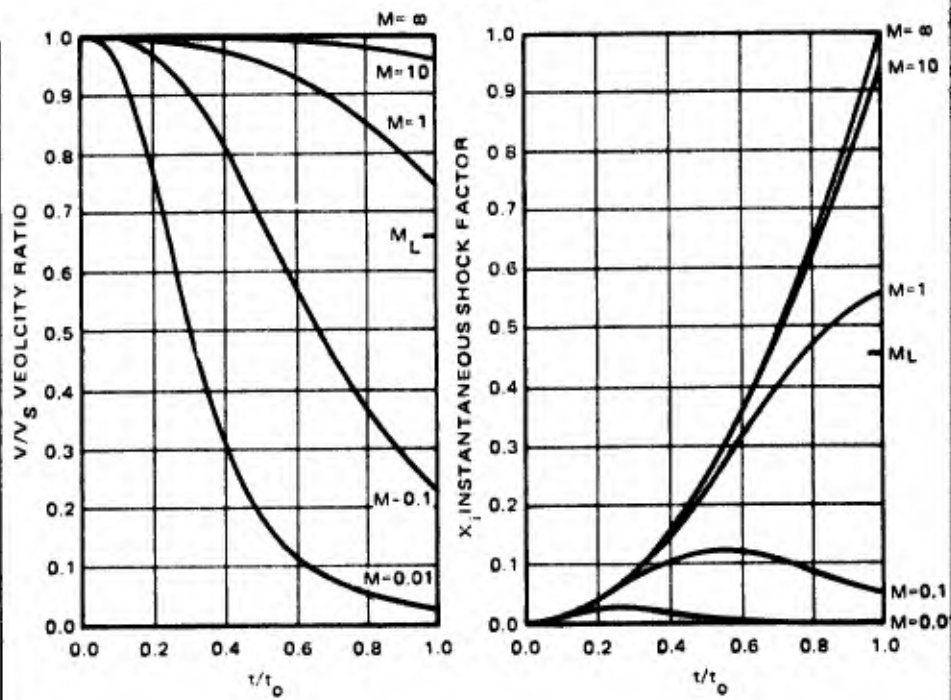


185

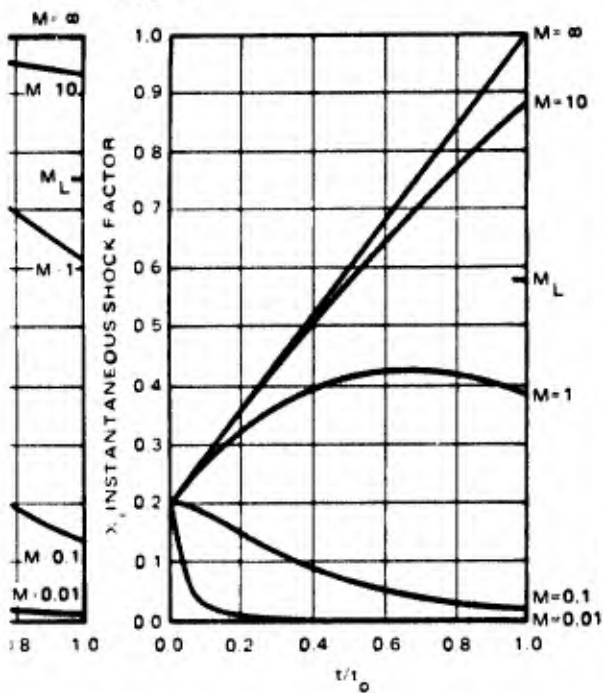
$\tau = 0; j = 1$



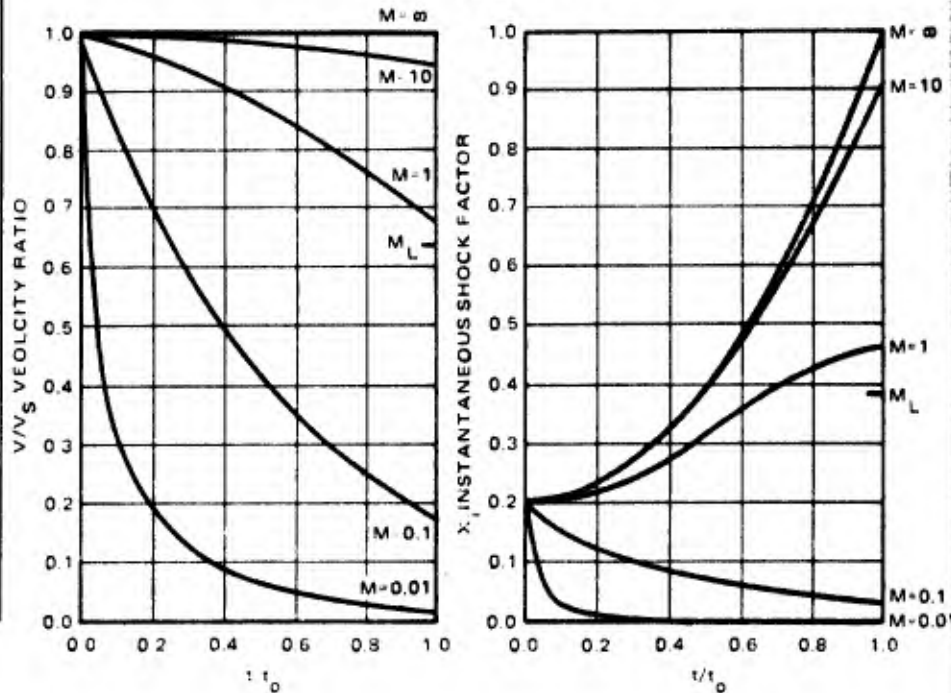
$\tau = 0; j = 2$



$\tau = 0.2; j = 1$

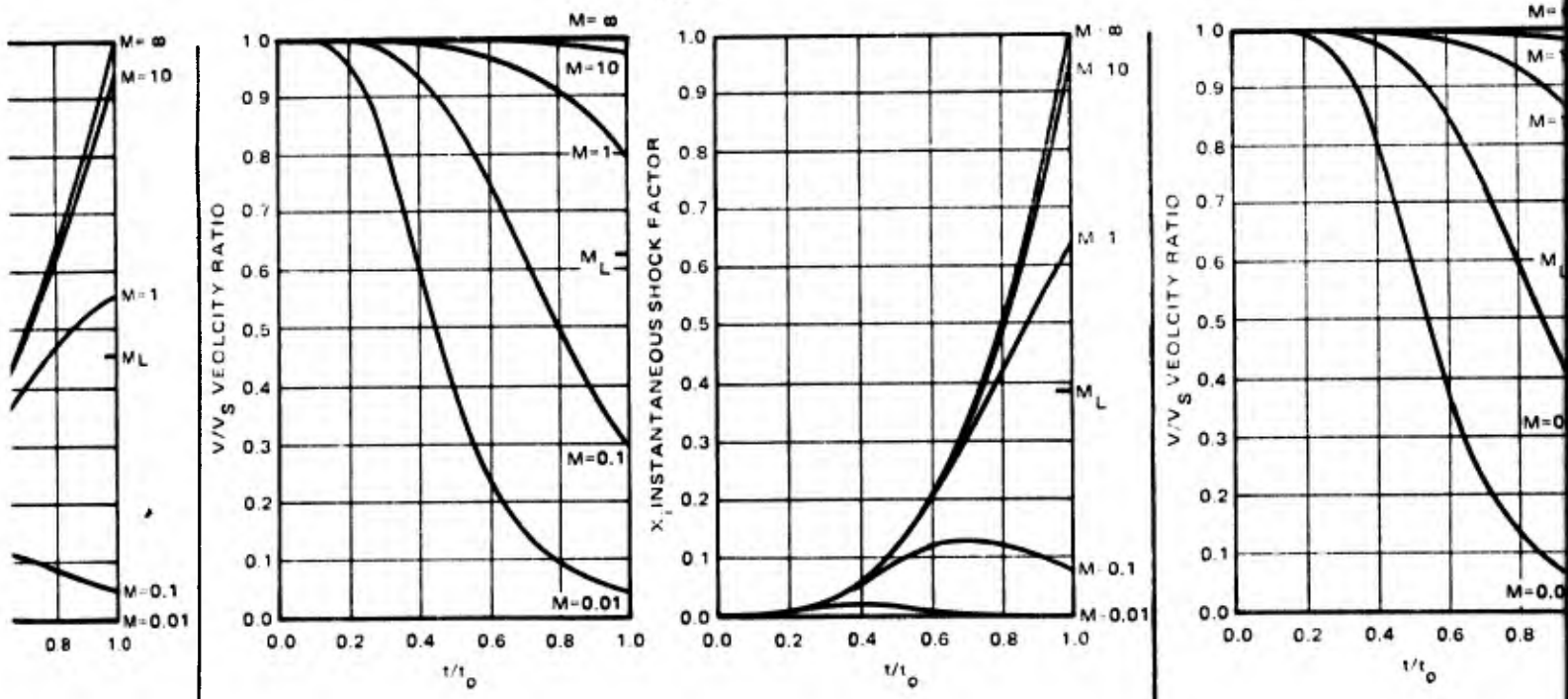


$\tau = 0.2; j = 2$

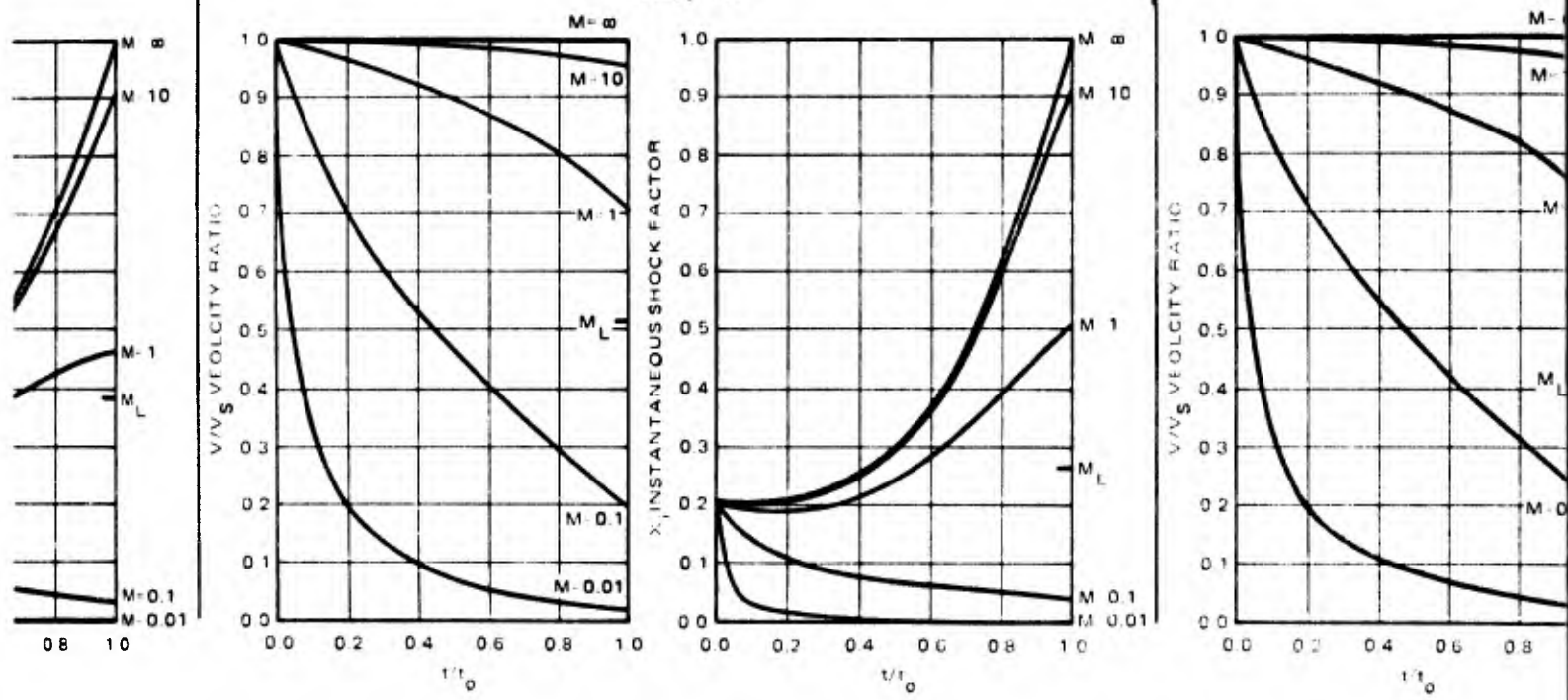


295

$\tau = 0; j = 3$

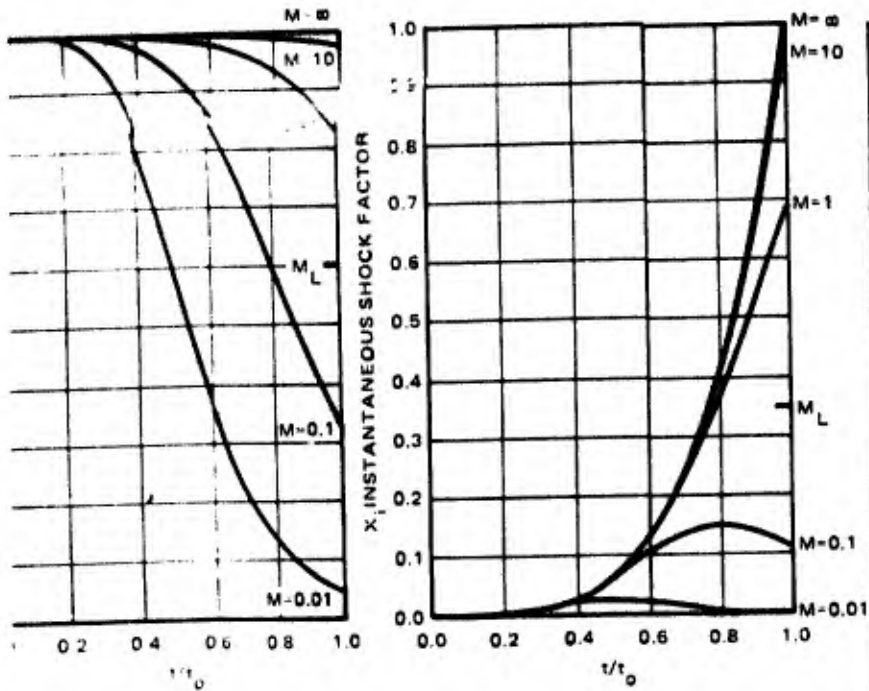


$\tau = 0.2; j = 3$

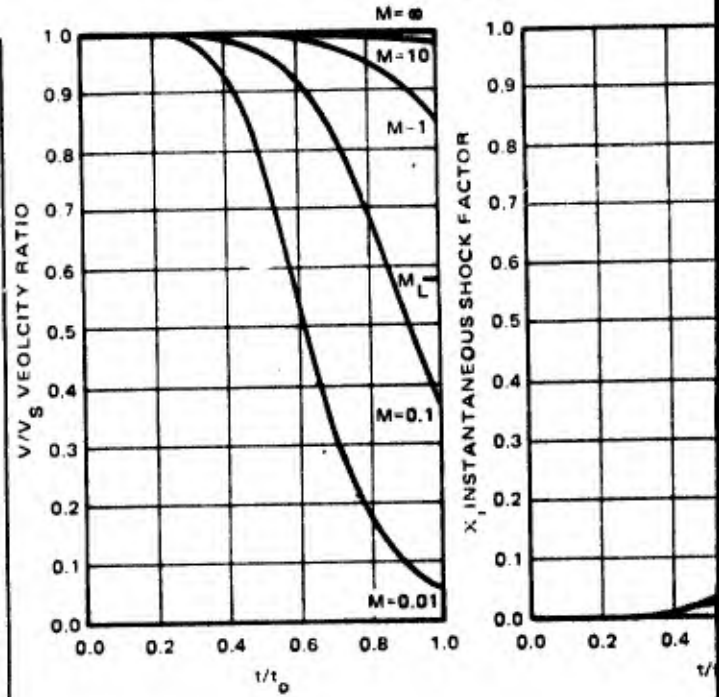


3185

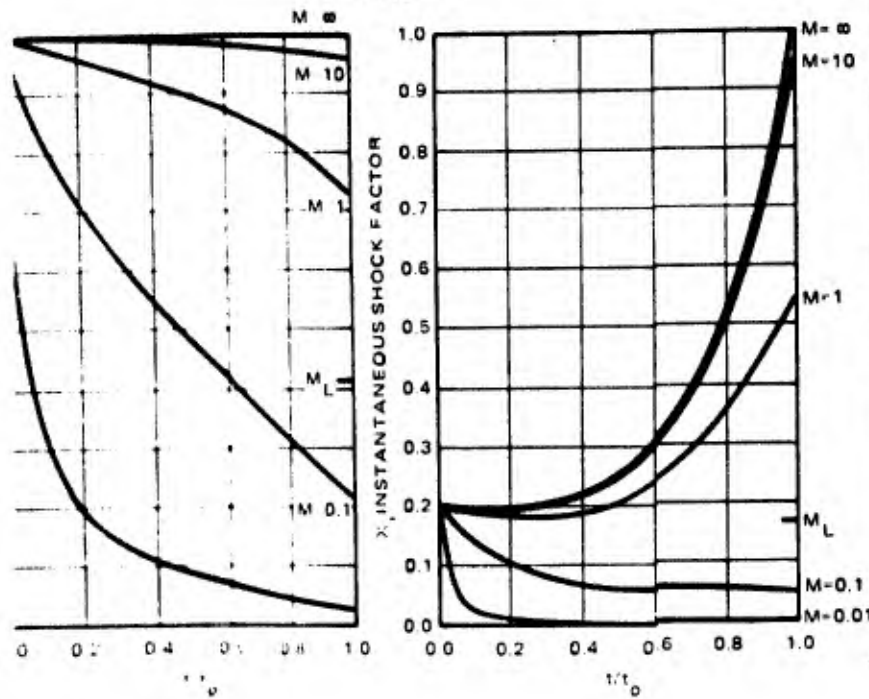
$\tau = 0; j = 4$



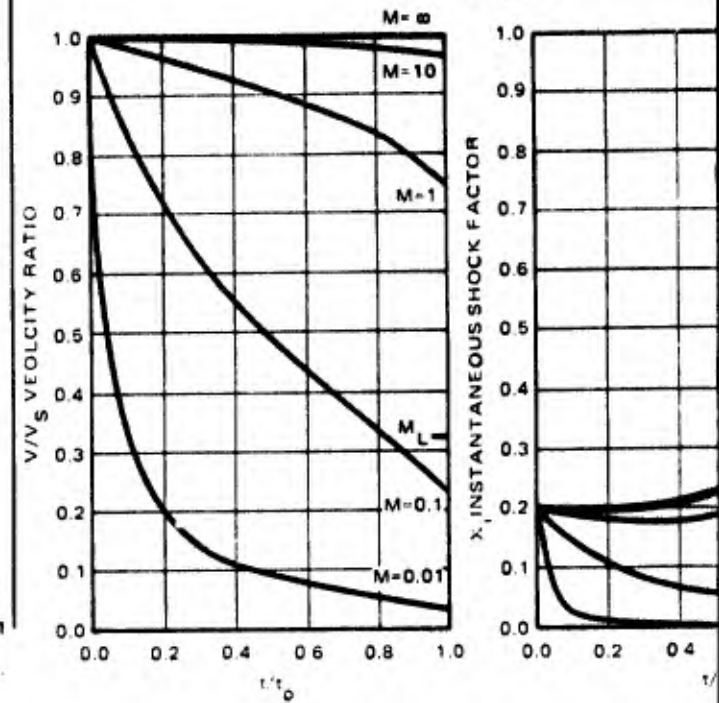
$\tau = 0; j = 5$



$\tau = 0.2; j = 4$



$\tau = 0.2; j = 5$



485

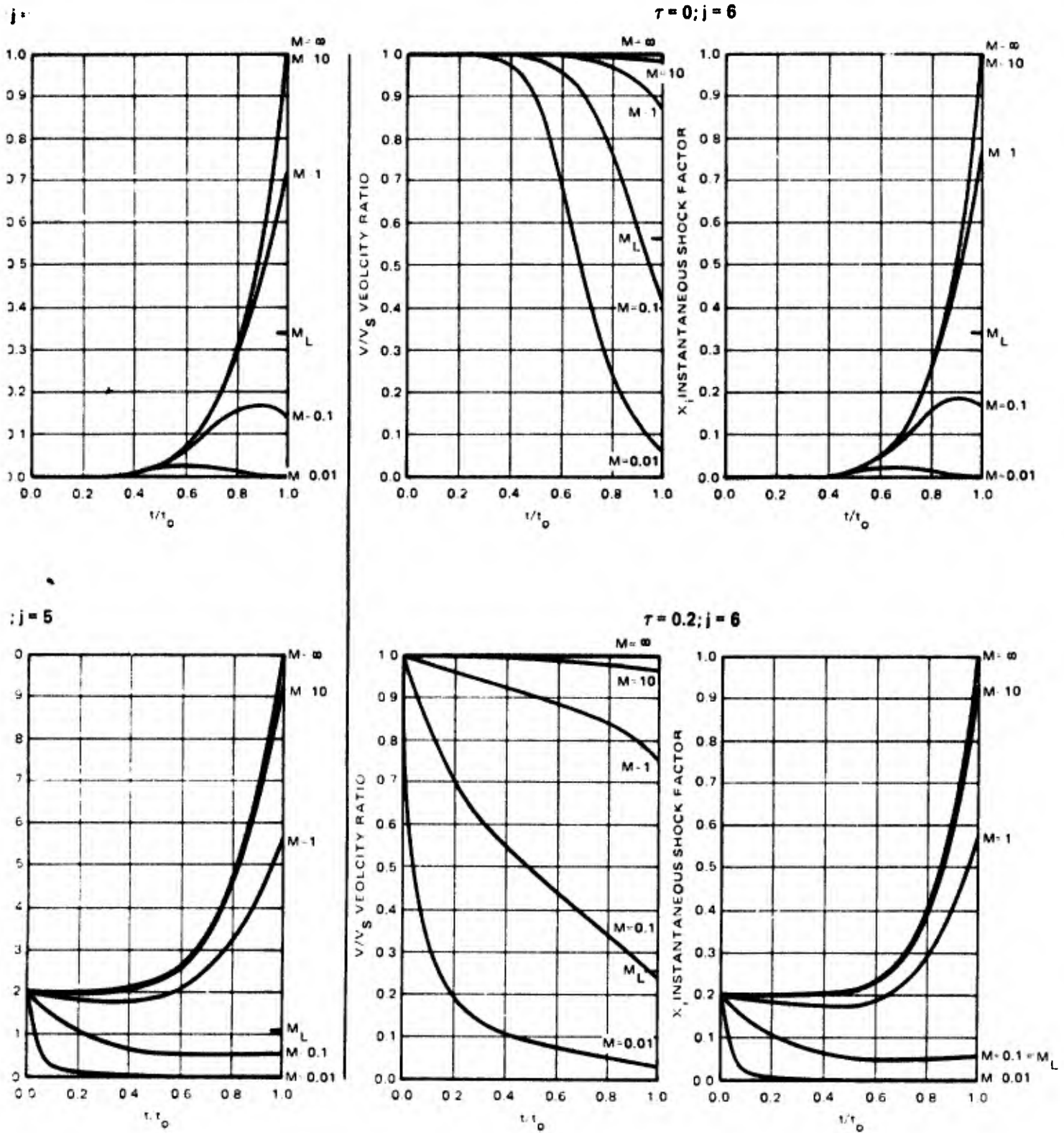


FIGURE 12. EFFECT OF INITIAL AREA AND BALLISTIC MASS RATIO ON THE SHOCK FACTOR AND VELOCITY RATIO DURING THE UNFOLDING PHASE FOR SEVERAL VALUES OF  $j$ .

595

$$\frac{C_{DS}}{C_{DS0}} = \left( \frac{t}{t_0} \right)^j$$

The value of  $j$  in the elastic phase of inflation may be maintained as the same value used in the unfolding phase of deployment. However, if test data indicate that a different  $j$  value improves the data fit in the elastic phase of deployment, the  $j$  values may be changed at  $t/t_0 = 1$ . Inspection of Figure 9 for values of  $t/t_0 > 1$  indicates that a higher value than  $j = 6$  may have given a better data fit.

The subscript zero indicates a condition that exists at the time  $t = t_0$ . The general case velocity ratio at the time  $t = t_0$ .

$$\frac{v_0}{v_s} = \frac{1}{1 + \frac{1}{M} \left[ \frac{(1-\tau)}{(j+1)} + \tau \right]} \quad (15)$$

The general case shock factor at the time  $t = t_0$ .

$$x_0 = \left( \frac{v_0}{v_s} \right)^2 = \frac{1}{\left[ 1 + \frac{1}{M} \left[ \frac{(1-\tau)}{(j+1)} + \tau \right] \right]^2} \quad (16)$$

#### THE ELASTIC PHASE OF INFLATION

The force diagram of Figure 1 and the Ballistic Mass Ratio developed in the unfolding phase of inflation are valid for the elastic phase. Rewriting Equation 4 between new limits,

$$\begin{aligned} \frac{1}{t_0} \int_{t_0}^t \frac{C_{DS}}{C_{DS0}} dt &= M v_s \int_{v_0}^v \frac{dv}{(-v)^2} \\ \frac{1}{t_0} \int_{t_0}^t \left( \frac{t}{t_0} \right)^j dt &= M v_s \left( \frac{1}{v} - \frac{1}{v_0} \right) \end{aligned} \quad (17)$$

$$\frac{v}{v_s} = \frac{1}{\frac{v_s}{v_0} + \frac{1}{(j+1)M} \left[ \left( \frac{t}{t_0} \right)^{j+1} - 1 \right]} \quad (18)$$

$$\begin{aligned} x_i &= \left( \frac{v}{v_s} \right)^2 \frac{C_{DS}}{C_{DS0}} \\ x_i &= \frac{\left( \frac{t}{t_0} \right)^j}{\left[ \frac{v_s}{v_0} + \frac{1}{(j+1)M} \left[ \left( \frac{t}{t_0} \right)^{j+1} - 1 \right] \right]^2} \end{aligned} \quad (19)$$

Calculate the initial elongation,  $\epsilon_0$ , from Equation (20) and determine  $C_{D S_{max}}/C_{D S_0}$  from Figure 15, page A-10.

$$\epsilon_0 = \frac{X_0 F_S}{F_C} \epsilon_{max} \quad (20)$$

In some applications the steady-state drag force,  $F_S$ , exceeds the parachute constructed strength,  $F_C$ . This indicates that the direct opening of parachutes of light construction is limited to finite mass systems that experience sufficient velocity reduction during deployment to assure success. Light construction parachutes should not be used in infinite mass, high-speed systems without reefing.

Then

$$\left(\frac{t_f}{t_0}\right)^j = \frac{C_{D S_{max}}}{C_{D S_0}}$$

$$\frac{t_f}{t_0} = \left(\frac{C_{D S_{max}}}{C_{D S_0}}\right)^{1/j} \quad (21)$$

The inflation time  $t_f$

$$t_f = \left(\frac{C_{D S_{max}}}{C_{D S_0}}\right)^{1/j} t_0 \quad (21a)$$

The maximum shock factor can be determined by Equation 19 and

$$F_{max} = x_{i_{max}} F_S$$

The derived formulae for the several values of  $j$  are summarized in Table 1.

The inflation times  $t_0$  and  $t_f$  are vital analysis inputs. Theoretical inflation time analyses are very difficult due to the many factors involved. Section IV of Appendix A, page A-5, describes a method for calculating the inflation time,  $t_0$ , for solid cloth parachutes ( $j = 6$ ). At low altitudes, Equation 13, page A-7, yields a more realistic inflation time than Equation 14. However, the simplifying assumption of  $n = 1/2$  provided a closed form solution. For altitudes above 40,000 feet, Equations 13 and 14 give essentially the same value. See Figure 12, page A-8. A close study of Section IV and its assumptions should give the reader an appreciation for what is involved. A value of  $j = 1$  is representative of ribbon and ringslot parachute performance.

Numerous simplified filling time equations have been published in many reports and will not be repeated here. Generally there are two forms:

$$(a) \quad t_f = \frac{n D_0}{V_S 0.9} \quad (22)$$

UNFOLDING PHASE OF DEPLOYMENT $0 < t/t_0 \leq 1$							
	DRAG AREA RATIO $C_D S/C_{D0} S_0$		VELOCITY RATIO $V/V_0$		SHOCK FACTOR $X_i$		TIME OF OCC $t/t_0$
	GENERAL CASE	$\tau = 0$	GENERAL CASE	$\tau = 0$	GENERAL CASE	$\tau = 0$	GENERAL CA
	EQ. 10		EQ. 11		EQ. 12		EQ. 13
$j$	$(1-\tau)\left(\frac{t}{t_0}\right)^j + \tau$	$\left(\frac{t}{t_0}\right)^j$	$\frac{1}{1 + \frac{1}{M} \left[ \frac{(1-\tau)}{j+1} \left(\frac{t}{t_0}\right)^{j+1} + \tau \left(\frac{t}{t_0}\right) \right]}$	$\frac{1}{1 + \frac{1}{j+1} M \left(\frac{t}{t_0}\right)^{j+1}}$	$\frac{(1-\tau)\left(\frac{t}{t_0}\right)^j + \tau}{\left[ 1 + \frac{1}{M} \left[ \frac{(1-\tau)}{j+1} \left(\frac{t}{t_0}\right)^{j+1} + \tau \left(\frac{t}{t_0}\right) \right] \right]^2}$	$\frac{\left(\frac{t}{t_0}\right)^j}{\left[ 1 + \frac{1}{j+1} M \left(\frac{t}{t_0}\right)^{j+1} \right]^2}$	NO CLOSED SOLUTION
$1/2$	$(1-\tau)\left(\frac{t}{t_0}\right)^{1/2} + \tau$	$\left(\frac{t}{t_0}\right)^{1/2}$	$\frac{1}{1 + \frac{1}{M} \left[ \frac{2(1-\tau)}{3} \left(\frac{t}{t_0}\right)^{3/2} + \tau \left(\frac{t}{t_0}\right) \right]}$	$\frac{1}{1 + \frac{2}{3M} \left(\frac{t}{t_0}\right)^{3/2}}$	$\frac{(1-\tau)\left(\frac{t}{t_0}\right)^{1/2} + \tau}{\left[ 1 + \frac{1}{M} \left[ \frac{2(1-\tau)}{3} \left(\frac{t}{t_0}\right)^{3/2} + \tau \left(\frac{t}{t_0}\right) \right] \right]^2}$	$\frac{\left(\frac{t}{t_0}\right)^{1/2}}{\left[ 1 + \frac{2}{3M} \left(\frac{t}{t_0}\right)^{3/2} \right]^2}$	
$1$	$(1-\tau)\left(\frac{t}{t_0}\right)^2 + \tau$	$\left(\frac{t}{t_0}\right)^2$	$\frac{1}{1 + \frac{1}{M} \left[ \frac{(1-\tau)}{2} \left(\frac{t}{t_0}\right)^2 + \tau \left(\frac{t}{t_0}\right) \right]}$	$\frac{1}{1 + \frac{1}{2M} \left(\frac{t}{t_0}\right)^2}$	$\frac{(1-\tau)\left(\frac{t}{t_0}\right)^2 + \tau}{\left[ 1 + \frac{1}{M} \left[ \frac{(1-\tau)}{2} \left(\frac{t}{t_0}\right)^2 + \tau \left(\frac{t}{t_0}\right) \right] \right]^2}$	$\frac{\left(\frac{t}{t_0}\right)^2}{\left[ 1 + \frac{1}{2M} \left(\frac{t}{t_0}\right)^2 \right]^2}$	
$2$	$(1-\tau)\left(\frac{t}{t_0}\right)^3 + \tau$	$\left(\frac{t}{t_0}\right)^3$	$\frac{1}{1 + \frac{1}{M} \left[ \frac{(1-\tau)}{3} \left(\frac{t}{t_0}\right)^3 + \tau \left(\frac{t}{t_0}\right) \right]}$	$\frac{1}{1 + \frac{1}{3M} \left(\frac{t}{t_0}\right)^3}$	$\frac{(1-\tau)\left(\frac{t}{t_0}\right)^3 + \tau}{\left[ 1 + \frac{1}{M} \left[ \frac{(1-\tau)}{3} \left(\frac{t}{t_0}\right)^3 + \tau \left(\frac{t}{t_0}\right) \right] \right]^2}$	$\frac{\left(\frac{t}{t_0}\right)^3}{\left[ 1 + \frac{1}{3M} \left(\frac{t}{t_0}\right)^3 \right]^2}$	
$3$	$(1-\tau)\left(\frac{t}{t_0}\right)^4 + \tau$	$\left(\frac{t}{t_0}\right)^4$	$\frac{1}{1 + \frac{1}{M} \left[ \frac{(1-\tau)}{4} \left(\frac{t}{t_0}\right)^4 + \tau \left(\frac{t}{t_0}\right) \right]}$	$\frac{1}{1 + \frac{1}{4M} \left(\frac{t}{t_0}\right)^4}$	$\frac{(1-\tau)\left(\frac{t}{t_0}\right)^4 + \tau}{\left[ 1 + \frac{1}{M} \left[ \frac{(1-\tau)}{4} \left(\frac{t}{t_0}\right)^4 + \tau \left(\frac{t}{t_0}\right) \right] \right]^2}$	$\frac{\left(\frac{t}{t_0}\right)^4}{\left[ 1 + \frac{1}{4M} \left(\frac{t}{t_0}\right)^4 \right]^2}$	
$4$	$(1-\tau)\left(\frac{t}{t_0}\right)^5 + \tau$	$\left(\frac{t}{t_0}\right)^5$	$\frac{1}{1 + \frac{1}{M} \left[ \frac{(1-\tau)}{5} \left(\frac{t}{t_0}\right)^5 + \tau \left(\frac{t}{t_0}\right) \right]}$	$\frac{1}{1 + \frac{1}{5M} \left(\frac{t}{t_0}\right)^5}$	$\frac{(1-\tau)\left(\frac{t}{t_0}\right)^5 + \tau}{\left[ 1 + \frac{1}{M} \left[ \frac{(1-\tau)}{5} \left(\frac{t}{t_0}\right)^5 + \tau \left(\frac{t}{t_0}\right) \right] \right]^2}$	$\frac{\left(\frac{t}{t_0}\right)^5}{\left[ 1 + \frac{1}{5M} \left(\frac{t}{t_0}\right)^5 \right]^2}$	
$5$	$(1-\tau)\left(\frac{t}{t_0}\right)^6 + \tau$	$\left(\frac{t}{t_0}\right)^6$	$\frac{1}{1 + \frac{1}{M} \left[ \frac{(1-\tau)}{6} \left(\frac{t}{t_0}\right)^6 + \tau \left(\frac{t}{t_0}\right) \right]}$	$\frac{1}{1 + \frac{1}{6M} \left(\frac{t}{t_0}\right)^6}$	$\frac{(1-\tau)\left(\frac{t}{t_0}\right)^6 + \tau}{\left[ 1 + \frac{1}{M} \left[ \frac{(1-\tau)}{6} \left(\frac{t}{t_0}\right)^6 + \tau \left(\frac{t}{t_0}\right) \right] \right]^2}$	$\frac{\left(\frac{t}{t_0}\right)^6}{\left[ 1 + \frac{1}{6M} \left(\frac{t}{t_0}\right)^6 \right]^2}$	
$6$	$(1-\tau)\left(\frac{t}{t_0}\right)^7 + \tau$	$\left(\frac{t}{t_0}\right)^7$	$\frac{1}{1 + \frac{1}{M} \left[ \frac{(1-\tau)}{7} \left(\frac{t}{t_0}\right)^7 + \tau \left(\frac{t}{t_0}\right) \right]}$	$\frac{1}{1 + \frac{1}{7M} \left(\frac{t}{t_0}\right)^7}$	$\frac{(1-\tau)\left(\frac{t}{t_0}\right)^7 + \tau}{\left[ 1 + \frac{1}{M} \left[ \frac{(1-\tau)}{7} \left(\frac{t}{t_0}\right)^7 + \tau \left(\frac{t}{t_0}\right) \right] \right]^2}$	$\frac{\left(\frac{t}{t_0}\right)^7}{\left[ 1 + \frac{1}{7M} \left(\frac{t}{t_0}\right)^7 \right]^2}$	

103

TABLE 1. SUMMARY OF THE PERFORMANCE ANALYSIS DURING PARACHUTE DEPLOYMENT FOR SELECTED

$t/t_0 < 1$				AT THE TIME $t = t_0$				
				TIME OF OCCURRENCE OF $\lambda_{i \max}$ $(t/t_0) @ X_{i \max}$		MAXIMUM FINITE MASS SHOCK FACTOR $X_{i \max}$		DRAG AREA RATIO $C_D S/C_{D0} S_0$
GENERAL CASE		$\tau = 0$	GENERAL CASE	$\tau = 0$	GENERAL CASE	GENERAL CASE	$\tau = 0$	GENERAL CASE
EQ. 13						EQ. 15		EQ. 16
$\left[ \frac{1}{j+1} \right]^2$	NO CLOSED SOLUTION	$\left( \frac{j(j+1)M}{(j+2)} \right)^{\frac{1}{j+1}}$	NO CLOSED SOLUTION	$\left[ \frac{(j+2)}{2(j+1)} \right]^2 \left( \frac{j(j+1)M}{(j+2)} \right)^{\frac{1}{j+1}}$	1.0	$\frac{1}{1 + \frac{1}{M} \left[ \frac{(1-\tau)}{(j+1)} + \tau \right]}$	$\frac{1}{1 + \frac{1}{(j+1)M}}$	$\frac{1}{\left[ 1 + \frac{1}{M} \left[ \frac{(1-\tau)}{(j+1)} + \tau \right] \right]^2}$
$\left[ \frac{1}{2} \right]^2$		$\left( \frac{3M}{10} \right)^{2/3}$		$\frac{25}{36} \left( \frac{3M}{10} \right)^{1/3}$	1.0	$\frac{1}{1 + \frac{1}{M} \left[ \frac{2(1-\tau)}{3} + \tau \right]}$	$\frac{1}{1 + \frac{2}{3M}}$	$\frac{1}{\left[ 1 + \frac{1}{M} \left[ \frac{2(1-\tau)}{3} + \tau \right] \right]^2}$
$\left[ \frac{1}{3} \right]^2$		$\left( \frac{2M}{3} \right)^{1/2}$		$\frac{9}{16} \left( \frac{2M}{3} \right)^{1/2}$	1.0	$\frac{1}{1 + \frac{1}{M} \left[ \frac{(1-\tau)}{2} + \tau \right]}$	$\frac{1}{1 + \frac{1}{2M}}$	$\frac{1}{\left[ 1 + \frac{1}{M} \left[ \frac{(1-\tau)}{2} + \tau \right] \right]^2}$
$\left[ \frac{1}{4} \right]^2$		$\left( \frac{3M}{2} \right)^{1/3}$		$\frac{4}{9} \left( \frac{3M}{2} \right)^{2/3}$	1.0	$\frac{1}{1 + \frac{1}{M} \left[ \frac{(1-\tau)}{3} + \tau \right]}$	$\frac{1}{1 + \frac{1}{3M}}$	$\frac{1}{\left[ 1 + \frac{1}{M} \left[ \frac{(1-\tau)}{3} + \tau \right] \right]^2}$
$\left[ \frac{1}{5} \right]^2$		$\left( \frac{12M}{5} \right)^{1/4}$		$\frac{25}{64} \left( \frac{12M}{5} \right)^{3/4}$	1.0	$\frac{1}{1 + \frac{1}{M} \left[ \frac{(1-\tau)}{4} + \tau \right]}$	$\frac{1}{1 + \frac{1}{4M}}$	$\frac{1}{\left[ 1 + \frac{1}{M} \left[ \frac{(1-\tau)}{4} + \tau \right] \right]^2}$
$\left[ \frac{1}{6} \right]^2$		$\left( \frac{10M}{3} \right)^{1/5}$		$\frac{9}{25} \left( \frac{10M}{3} \right)^{4/5}$	1.0	$\frac{1}{1 + \frac{1}{M} \left[ \frac{(1-\tau)}{5} + \tau \right]}$	$\frac{1}{1 + \frac{1}{5M}}$	$\frac{1}{\left[ 1 + \frac{1}{M} \left[ \frac{(1-\tau)}{5} + \tau \right] \right]^2}$
$\left[ \frac{1}{7} \right]^2$		$\left( \frac{30M}{7} \right)^{1/6}$		$\frac{49}{144} \left( \frac{30M}{7} \right)^{5/6}$	1.0	$\frac{1}{1 + \frac{1}{M} \left[ \frac{(1-\tau)}{6} + \tau \right]}$	$\frac{1}{1 + \frac{1}{6M}}$	$\frac{1}{\left[ 1 + \frac{1}{M} \left[ \frac{(1-\tau)}{6} + \tau \right] \right]^2}$
$\left[ \frac{1}{8} \right]^2$		$\left( \frac{21M}{4} \right)^{1/7}$		$\frac{16}{49} \left( \frac{21M}{4} \right)^{6/7}$	1.0	$\frac{1}{1 + \frac{1}{M} \left[ \frac{(1-\tau)}{7} + \tau \right]}$	$\frac{1}{1 + \frac{1}{7M}}$	$\frac{1}{\left[ 1 + \frac{1}{M} \left[ \frac{(1-\tau)}{7} + \tau \right] \right]^2}$

R SELECTED VALUES OF j.

E TIME $t = t_0$				ELASTIC PHASE OF DEPLOYMENT $1 < t/t_0 \leq t_f/t_0$			
SHOCK FACTOR $X_0$		LIMITING MASS RATIO $M_L$		VELOCITY RATIO $V/V_s$	SHOCK FACTOR $X_j$	INITIAL ELONGATION $\epsilon_0$	INFLATE TIME $t_f/t_0$
GENERAL CASE	$r = 0$	GENERAL CASE	$r = 0$	GENERAL CASE	GENERAL CASE	GENERAL CASE	GENERAL CASE
EQ. 16		EQ. 13b		EQ. 18	EQ. 19	EQ. 20	EQ. 21
$\frac{1}{M \left[ \frac{(1-r)}{(j+1)} + r \right]^2}$	$\frac{1}{\left[ 1 + \frac{1}{(j+1)M} \right]^2}$	$\frac{2}{j(1-r)} - \frac{(1-r)}{(j+1)} - r$	$\frac{(j+2)}{j(j+1)}$	$\frac{1}{\frac{V_s}{V_0} + \frac{1}{(j+1)M} \left[ \left( \frac{t}{t_0} \right)^{j+1} - 1 \right]}$	$\frac{\left( \frac{t}{t_0} \right)^j}{\left[ \frac{V_s}{V_0} + \frac{1}{(j+1)M} \left[ \left( \frac{t}{t_0} \right)^{j+1} - 1 \right] \right]^2}$	$\epsilon_0 = \frac{X_0 F_s}{F_c} \epsilon_{max}$	$\left( \frac{C_D S_{max}}{C_D S_0} \right)^{1/j}$
$\frac{1}{\left[ \frac{2(1-r)}{3} + r \right]^2}$	$\frac{1}{\left[ 1 + \frac{2}{3M} \right]^2}$	$\frac{4}{(1-r)} - \frac{2(1-r)}{3} - r$	$\frac{10}{3}$	$\frac{1}{\frac{V_s}{V_0} + \frac{2}{3M} \left[ \left( \frac{t}{t_0} \right)^{3/2} - 1 \right]}$	$\frac{\left( \frac{t}{t_0} \right)^{1/2}}{\left[ \frac{V_s}{V_0} + \frac{2}{3M} \left[ \left( \frac{t}{t_0} \right)^{3/2} - 1 \right] \right]^2}$	$\epsilon_0 = \frac{X_0 F_s}{F_c} \epsilon_{max}$	$\left( \frac{C_D S_{max}}{C_D S_0} \right)^2$
$\frac{1}{M \left[ \frac{(1-r)}{2} + r \right]^2}$	$\frac{1}{\left[ 1 + \frac{1}{2M} \right]^2}$	$\frac{2}{(1-r)} - \frac{(1-r)}{2} - r$	$\frac{3}{2}$	$\frac{1}{\frac{V_s}{V_0} + \frac{1}{2M} \left[ \left( \frac{t}{t_0} \right)^2 - 1 \right]}$	$\frac{\left( \frac{t}{t_0} \right)}{\left[ \frac{V_s}{V_0} + \frac{1}{2M} \left[ \left( \frac{t}{t_0} \right)^2 - 1 \right] \right]^2}$	$\epsilon_0 = \frac{X_0 F_s}{F_c} \epsilon_{max}$	$\frac{C_D S_{max}}{C_D S_0}$
$\frac{1}{\frac{1}{4} \left[ \frac{(1-r)}{3} + r \right]^2}$	$\frac{1}{\left[ 1 + \frac{1}{3M} \right]^2}$	$\frac{1}{(1-r)} - \frac{(1-r)}{3} - r$	$\frac{2}{3}$	$\frac{1}{\frac{V_s}{V_0} + \frac{1}{3M} \left[ \left( \frac{t}{t_0} \right)^3 - 1 \right]}$	$\frac{\left( \frac{t}{t_0} \right)^2}{\left[ \frac{V_s}{V_0} + \frac{1}{3M} \left[ \left( \frac{t}{t_0} \right)^3 - 1 \right] \right]^2}$	$\epsilon_0 = \frac{X_0 F_s}{F_c} \epsilon_{max}$	$\left( \frac{C_D S_{max}}{C_D S_0} \right)^{1/2}$
$\frac{1}{\frac{1}{4} \left[ \frac{(1-r)}{4} + r \right]^2}$	$\frac{1}{\left[ 1 + \frac{1}{4M} \right]^2}$	$\frac{2}{3(1-r)} - \frac{(1-r)}{4} - r$	$\frac{5}{12}$	$\frac{1}{\frac{V_s}{V_0} + \frac{1}{4M} \left[ \left( \frac{t}{t_0} \right)^4 - 1 \right]}$	$\frac{\left( \frac{t}{t_0} \right)^3}{\left[ \frac{V_s}{V_0} + \frac{1}{4M} \left[ \left( \frac{t}{t_0} \right)^4 - 1 \right] \right]^2}$	$\epsilon_0 = \frac{X_0 F_s}{F_c} \epsilon_{max}$	$\left( \frac{C_D S_{max}}{C_D S_0} \right)^{1/3}$
$\frac{1}{\frac{1}{4} \left[ \frac{(1-r)}{5} + r \right]^2}$	$\frac{1}{\left[ 1 + \frac{1}{5M} \right]^2}$	$\frac{1}{2(1-r)} - \frac{(1-r)}{5} - r$	$\frac{3}{10}$	$\frac{1}{\frac{V_s}{V_0} + \frac{1}{5M} \left[ \left( \frac{t}{t_0} \right)^5 - 1 \right]}$	$\frac{\left( \frac{t}{t_0} \right)^4}{\left[ \frac{V_s}{V_0} + \frac{1}{5M} \left[ \left( \frac{t}{t_0} \right)^5 - 1 \right] \right]^2}$	$\epsilon_0 = \frac{X_0 F_s}{F_c} \epsilon_{max}$	$\left( \frac{C_D S_{max}}{C_D S_0} \right)^{1/4}$
$\frac{1}{\left[ \frac{(1-r)}{6} + r \right]^2}$	$\frac{1}{\left[ 1 + \frac{1}{6M} \right]^2}$	$\frac{2}{5(1-r)} - \frac{(1-r)}{6} - r$	$\frac{7}{30}$	$\frac{1}{\frac{V_s}{V_0} + \frac{1}{6M} \left[ \left( \frac{t}{t_0} \right)^6 - 1 \right]}$	$\frac{\left( \frac{t}{t_0} \right)^5}{\left[ \frac{V_s}{V_0} + \frac{1}{6M} \left[ \left( \frac{t}{t_0} \right)^6 - 1 \right] \right]^2}$	$\epsilon_0 = \frac{X_0 F_s}{F_c} \epsilon_{max}$	$\left( \frac{C_D S_{max}}{C_D S_0} \right)^{1/5}$
$\frac{1}{\left[ \frac{(1-r)}{7} + r \right]^2}$	$\frac{1}{\left[ 1 + \frac{1}{7M} \right]^2}$	$\frac{1}{3(1-r)} - \frac{(1-r)}{7} - r$	$\frac{4}{21}$	$\frac{1}{\frac{V_s}{V_0} + \frac{1}{7M} \left[ \left( \frac{t}{t_0} \right)^7 - 1 \right]}$	$\frac{\left( \frac{t}{t_0} \right)^6}{\left[ \frac{V_s}{V_0} + \frac{1}{7M} \left[ \left( \frac{t}{t_0} \right)^7 - 1 \right] \right]^2}$	$\epsilon_0 = \frac{X_0 F_s}{F_c} \epsilon_{max}$	$\left( \frac{C_D S_{max}}{C_D S_0} \right)^{1/6}$

393

and

$$(b) \quad t_f = \frac{nD_0}{V_S} \quad (23)$$

Figure 13 shows that when  $V_S$  is raised to the 0.9 power, the result is nearly the same as dividing  $V_S$  by 2. So equation (a) can be simplified by multiplying  $n$  by 2. Table 2 is from Reference 2 and itemizes the canopy fill factors,  $n$ , for the (b) form of the inflation time equations. Knacke's equations for the filling time of various stages of reefed parachutes are as follows:

First stage reefing inflation time.

$$t_{f1} = \frac{nD_0}{V_S} \left[ \frac{C_{DSr}}{C_{DS0}} \right]^{1/2} \quad (24)$$

Second stage reefing inflation time.

$$t_{f2} = \frac{nD_0}{V_r} \left[ \frac{C_{DS0} - C_{DSr}}{C_{DS0}} \right]^{1/2} \quad (25)$$

where  $V_r$  is the velocity at disreef and  $C_{DSr}$  is the reefed drag area.

#### ANALYSIS APPLICATION TO AN APPARENT SOLID CLOTH PARACHUTE DEPLOYMENT ANOMALY

In 1944 Lt. Col. F.G. Hall, et al., of the Aero Medical Laboratory, Wright Field, measured the opening shock forces of silk and nylon solid cloth parachutes at altitudes of 7,000, 15,000, 26,000 and 40,000 feet at a constant sea level indicated air speed of 111 mph. These tests, reported in the April 1945 Air Corps Technical Digest, were a part of the lecture notes presented at the Naval Surface Weapons Center by Mr. T.W. Knacke in October 1983. They showed that the parachute-opening shock increased as the test altitude increased, and that the 24-foot parachute had a higher opening-shock force than the 28-foot canopy for similar conditions.

The analysis developed in this report shows the diameter effect measured by Col. Hall. Unfortunately, the digest article did not record the inflation-time-altitude data. Inflation-time data should always be reported in parachute test reports, since they are very important in analysis, especially altitude-inflation data. The following example demonstrates that inflation-time data is a key factor in opening-force determination.

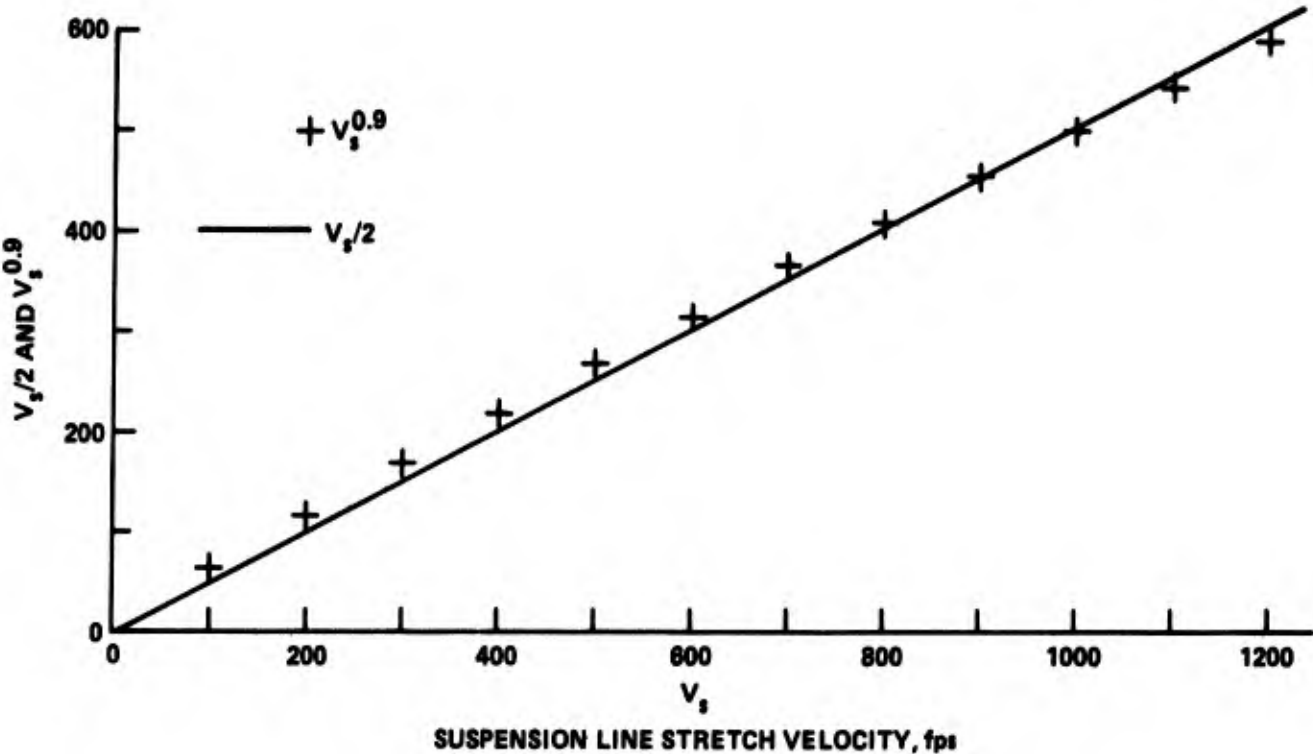


FIGURE 13. EFFECT OF THE FILLING TIME EQUATION EXPONENT 0.9 ON THE TRAJECTORY VELOCITY AT PARACHUTE SUSPENSION LINE STRETCH

TABLE 2. CANOPY FILL FACTOR,  $n$ , FOR VARIOUS PARACHUTE TYPES.

PARACHUTE TYPE	CANOPY FILL FACTOR, $n$		
	REEFED OPENING	DISREEF OPENING	UNREEFED OPENING
SOLID FLAT CIRCULAR	ID <sup>1/</sup>	ID	8
EXTENDED SKIRT, 10%	16-18	4-6	10
EXTENDED SKIRT, FULL	16-18	7	12
CROSS	ID	ID	11.7
RIBBON	10	6	14
RINGSLOT	ID	ID	14
RINGSAIL	7-8	2	7
RIBLESS GUIDE SURFACE	...	...	4-6

<sup>1/</sup>ID = INSUFFICIENT DATA AVAILABLE FOR MEANINGFUL EVALUATION

Reproduced from Reference 2

Example 1. Two 200-pound total weight parachute systems are to be launched simultaneously from the wing racks of an aircraft in level flight near sea level. One system contains a 24-foot flat circular parachute and the other a 28-foot diameter canopy. Determine the magnitudes of the opening-shock forces for a line-stretch velocity of 125 knots indicated air speed. Compare the performance with two ribbon-type parachutes of equivalent drag areas.

Data:  $V_g = 211$  fps,  $\rho = 0.002373$  slugs/ft<sup>3</sup>,  $C_D = 0.75$ ,  $W = 200$  lb.,  $n = 8$ , and  $D_0 = 24$  ft. and 28 ft.

Solution: For values of  $j = 6$  and  $\tau = 0$ , the results are tabulated in Table 3.

TABLE 3 SOLID CLOTH CALCULATIONS FOR EXAMPLE 1

		24 ft DIAMETER FLAT CIRCULAR	28 ft DIAMETER FLAT CIRCULAR
$C_D S_0 = C_D \frac{\pi}{4} D_0^2$ $C_D S_0 = 0.75 \frac{\pi}{4} D_0^2$	ft <sup>2</sup>	339.29	461.82
$t_0 = \frac{n D_0}{V_s}$ $t_0 = \frac{8 D_0}{211}$	sec	0.9094	1.061
$M = \frac{2W}{\rho g C_D S_0 V_s t_0}$	-	0.0797	0.0502
$\left(\frac{t}{t_0}\right)^* \text{ at } x_{imax} = \left(\frac{21M}{4}\right)^{1/7}$	-	0.883	0.827
$x_{imax} = \frac{16}{49} \left(\frac{21M}{4}\right)^{6/7}$	-	0.1548	0.1041
$F_s = \frac{1}{2} \rho V_s^2 C_D S_0$ $F_s = \frac{0.002378}{2} (211)^2 C_D S_0$	lb	17981.9	24475.4
$F_{max} = x_{imax} F_s$	lb	2783.8	2549.0

\*A TIME RATIO VALUE OF LESS THAN 1.0 DENOTES A FINITE MASS DEPLOYMENT

The Ballistic Mass Ratio, the exponent  $j$ , and  $\tau$ , determine what percentage of the steady-state drag force is to be realized as opening shock. Since the finite mass time of occurrence and maximum shock factor are only a function of the mass ratio,  $j$ , and  $\tau$  the lesser percentage correlates with the larger parachute for  $j = 6$ . The larger drag area and longer inflation time of the 28-foot diameter canopy reduce the mass ratio. However, the larger diameter parachute produces a higher steady state drag force. The result depends on which of the factors  $M$ ,  $j$ ,  $\tau$ , or  $F_s$  has the greatest influence.

$$\frac{C_{DS}}{C_{DS0}} = \left(\frac{\tau}{\tau_0}\right)^j$$

$$\frac{v}{v_s} = \frac{1}{1 + \frac{1}{(j+1)M} \left(\frac{\tau}{\tau_0}\right)^{j+1}}$$

$$x_1 = \frac{\left(\frac{\tau}{\tau_0}\right)^j}{\left[1 + \frac{1}{(j+1)M} \left(\frac{\tau}{\tau_0}\right)^{j+1}\right]^2}$$

Figure 14 presents the variations of drag area, velocity ratios, and the opening-shock factor for the 24-foot and 28-foot example parachutes as a function of the time ratio. When viewed in this manner the drag-area ratio, which is not dependent on the mass ratio, is the same for both canopies. The 28-foot canopy slows down more rapidly, and the smaller canopy develops the higher shock force.

The larger parachute requires additional time to inflate. If the inflation process is envisioned as two parachutes side-by-side inflating from a common zero time coordinate, the 28-foot canopy is still developing when the 24-foot canopy is fully inflated. Real time performance is illustrated in Figures 15 and 16. The circle and triangle data markers denote the time ratios of the particular data points. These data indicate that at a given time the drag area of the 24-foot parachute, until a short time after the time of full inflation, is larger than the 28-foot parachute. At the same time the system velocity is less than the 28-foot parachute. On this basis it is difficult to judge which parachute has the maximum shock force. The resulting forces plotted in Figure 16 verify the 24-foot parachute effect.

Col. Hall found that the parachute-opening shock force increased as the altitude increased. Examination of the Ballistic Mass Ratio shows that for constant system weight the mass ratio becomes larger as the air density approaches zero. Also, it is known that solid cloth parachutes open more rapidly at higher altitudes, which further increases the mass ratio. Testing at constant dynamic pressure provides a constant steady-state drag force at all altitudes. Therefore, a higher mass ratio at altitude realizes a larger percentage of the constant steady-state drag as opening force.

The substitution of ribbon parachutes of equal drag areas for the 24-foot and 28-foot solid cloth canopies into the system of example 1 shows that parachute type is a variable in the expected results. In this case the larger parachute does see the larger opening-shock force even though the larger parachute has the minimum mass ratio. Equivalent drag-area ribbon parachutes are larger in diameter than solid cloth canopies because of the reduced drag coefficients, thereby adding to the inflation time. The inflation time constant is  $n = 14$  for ribbon parachutes which also increases the filling time. In this example the mass ratios of the ribbon parachutes are less than the solid cloth parachutes. The significant reason for the turnaround of the small parachute effect is the linear ( $j = 1$ ) drag-area ratio signature of ribbon and ringslot parachutes. Sample calculations for the ribbon parachute are listed in Table 4; for  $j = 1$ ,  $\tau = 0$ , and  $C_D = 0.5$ .

#### IMPULSE AND MOMENTUM DURING PARACHUTE INFLATION

Reference 3, beginning on page 39, discusses impulse and momentum during parachute inflation. The development of an average shock factor during the inflation sequence permits the system impulse, during inflation, to be represented as a rectangular plot of average shock factor versus time. However, the calculations were limited to a  $j$  value of 6. In this report the analysis is extended to the several values of  $j$  for the generalized Pflanz equation. With reference to Figure 17, the impulse in the interval  $0 \leq t \leq t_0$  is:

$j = 6, \tau = 0$

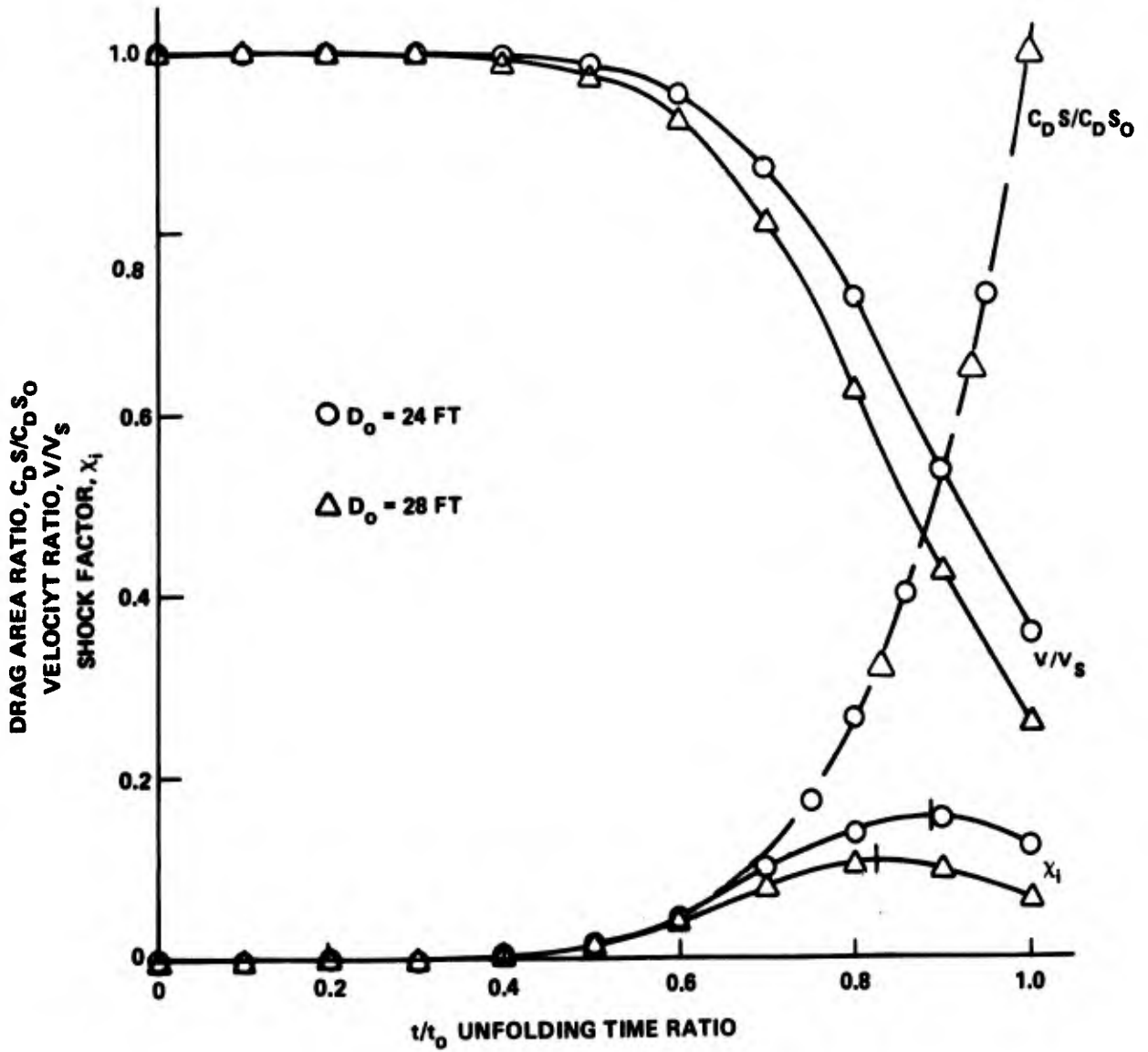


FIGURE 14. FINITE MASS RATIO FORM OF DEPLOYMENT PERFORMANCE PROFILE FOR THE 24-FOOT AND 28-FOOT FLAT CIRCULAR PARACHUTES OF EXAMPLE 1

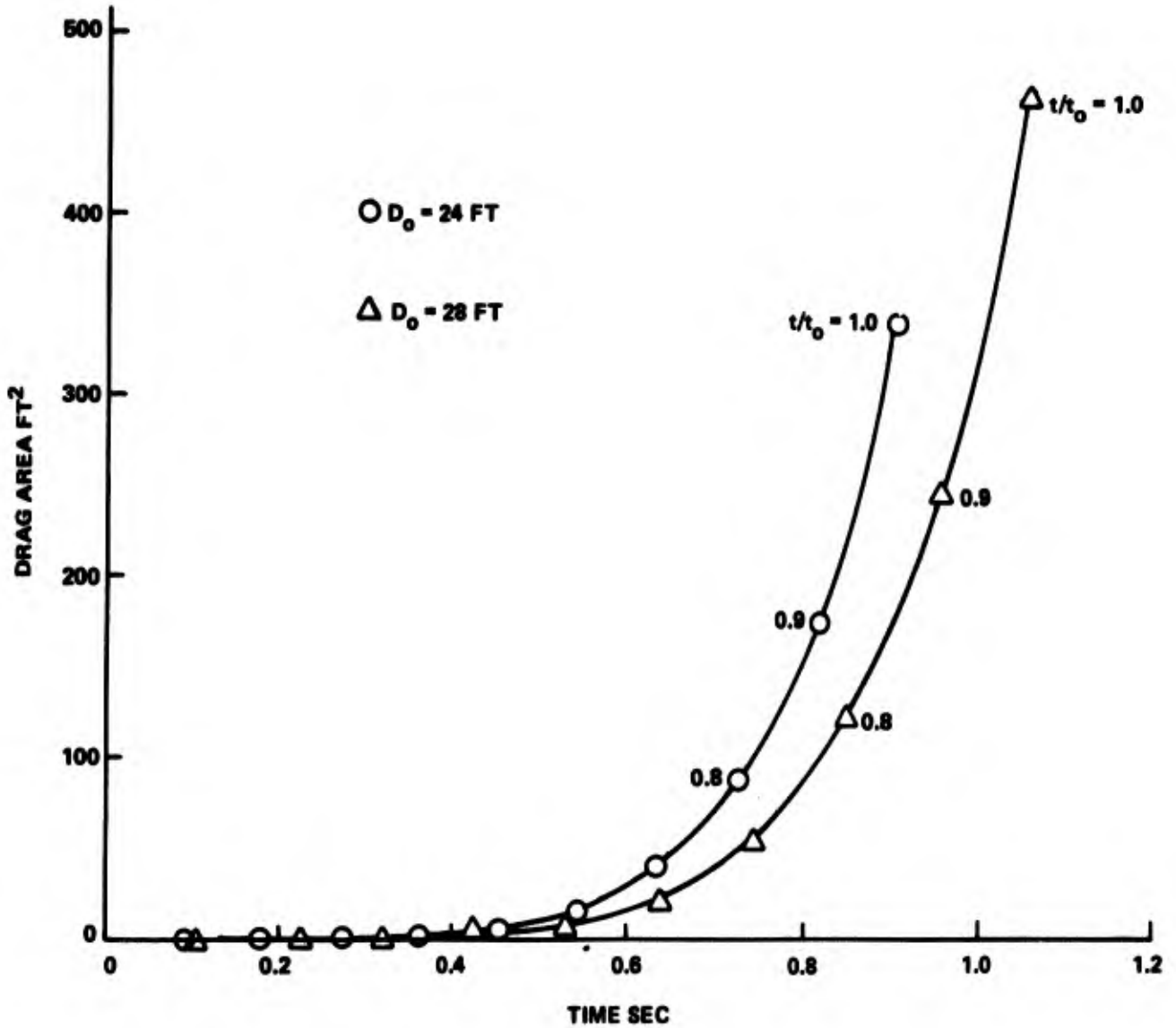


FIGURE 15. FINITE MASS REAL TIME DEPLOYMENT DRAG AREA PROFILES FOR THE 24-FOOT AND 28-FOOT FLAT CIRCULAR PARACHUTES OF EXAMPLE 1

$j = 6, \tau = 0$

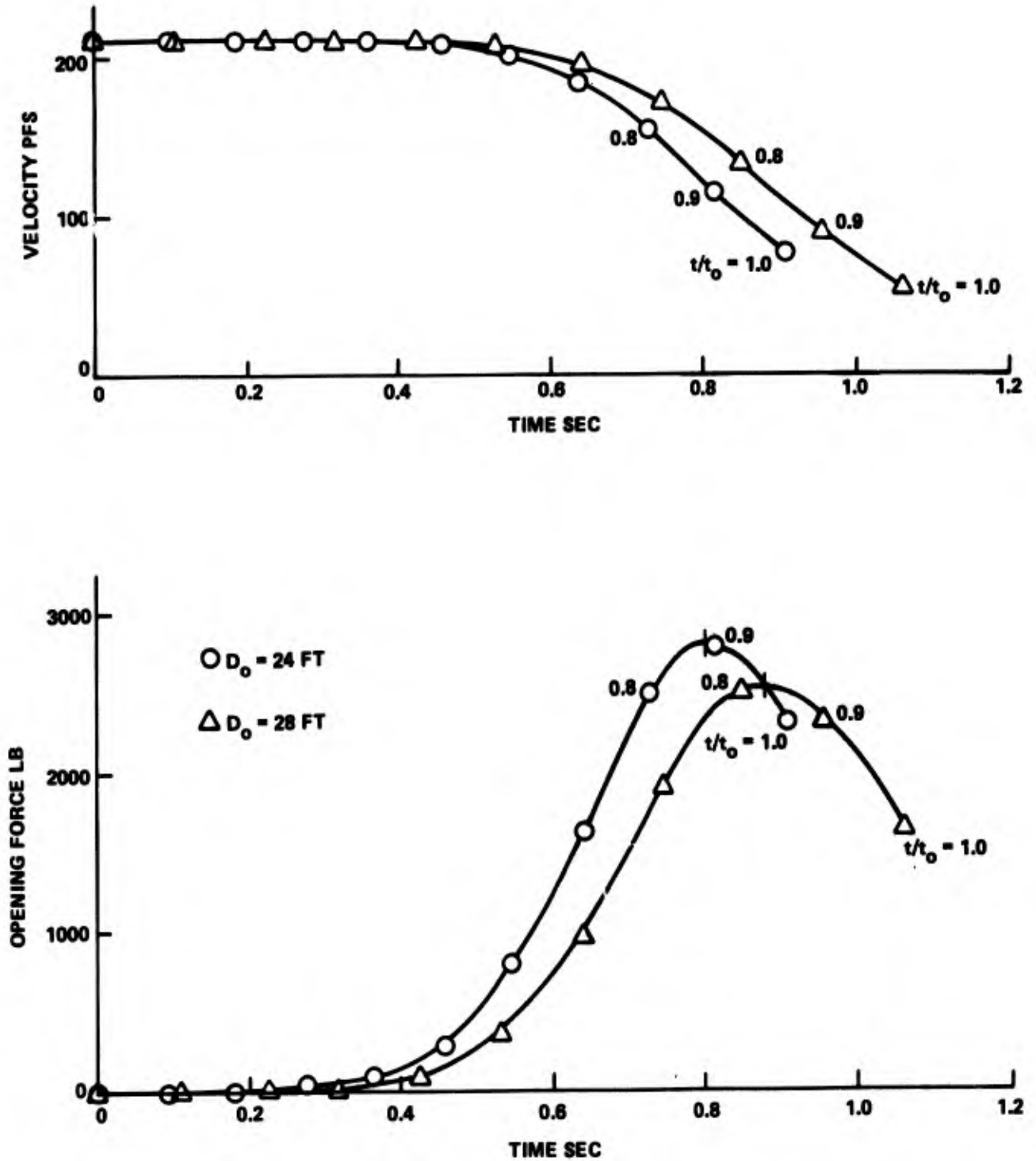


FIGURE 16. FINITE MASS REAL TIME DEPLOYMENT VELOCITY AND OPENING FORCE PROFILES FOR THE 24-FOOT AND 28-FOOT FLAT CIRCULAR PARACHUTES OF EXAMPLE 1

TABLE 4. RIBBON PARACHUTE CALCULATIONS FOR EXAMPLE 1.

		EQUIVALENT 24 ft FLAT CIRCULAR	EQUIVALENT 28 ft FLAT CIRCULAR
$C_D S_o$	ft <sup>2</sup>	339.29	461.82
$S_o = \frac{C_D S_o}{C_D}$	ft <sup>2</sup>		
$S_o = \frac{C_D S_o}{0.5}$		678.58	923.64
$D_o = \sqrt{\frac{4 S_o}{\pi}}$	ft	29.394	34.293
$t_o = \frac{n D_o}{V_s}$	sec		
$t_o = \frac{\sqrt{4} D_o}{211}$		1.950	2.275
$M = \frac{2W}{\rho g C_D S_o V_s t_o}$	-		
$M = \frac{2 \times 200}{0.077 \times C_D S_o \times 211 t_o}$		0.0372	0.0234
$\left(\frac{t}{t_o}\right)_{\text{at } X_{\text{imax}}} = \sqrt{\left(\frac{2M}{3}\right)}$	-	0.1575	0.1250
$X_{\text{imax}} = \frac{9}{16} \sqrt{\left(\frac{2M}{3}\right)}$	-	0.0886	0.0703
$F_s = \frac{1}{2} \rho V_s^2 C_D S_o$	lb		
$F_s = \frac{0.002378}{2} (211)^2 C_D S_o$		17960.5	24446.7
$F_{\text{max}} = X_{\text{imax}} F_s$	lb	1591.3	1718.6

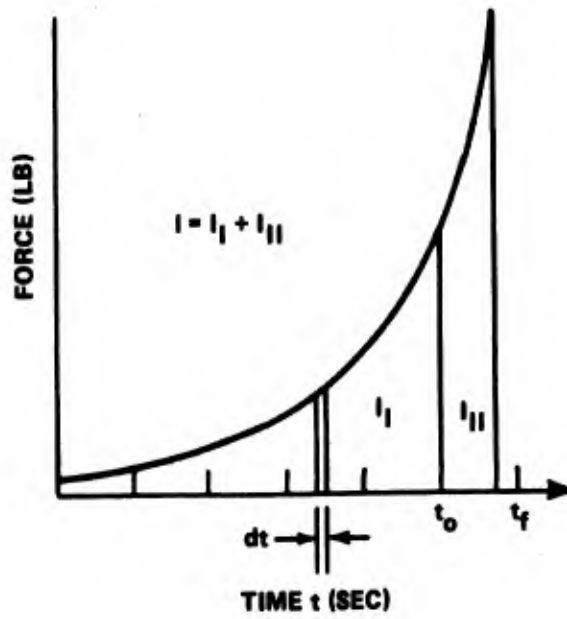


FIGURE 17. IMPULSE OF THE INFLATING CANOPY OF EXAMPLE 2

Reproduced from Reference 3

$$\int_0^t -F dt = \frac{W}{g} \int_{V_S}^V dV$$

$$F = F_S x_1$$

$$x_1 = \frac{C_D S}{C_D S_0} \left( \frac{V}{V_S} \right)^2$$

The generalized Pflanz shock factor, Equation (12).

$$-F_S \int_0^t x_1 dt = \frac{W}{g} \int_{V_S}^V dV$$

$$\int_0^t x_1 dt = \frac{-W}{g F_S} \int_{V_S}^V dV$$

$$\int_0^t x_1 dt = \frac{-2W t_0}{\rho g V_S t_0 C_D S_0} \times \frac{1}{V_S} \int_{V_S}^V dV$$

$$x_{iav} = \frac{1}{t_0} \int_0^t x_1 dt = M \left( 1 - \frac{V}{V_S} \right)$$

At any time ratio, the average shock factor,  $x_{iav}$ , may be considered as the area under the  $x_1 - t$  curve divided by  $t_0$ .

$$x_{iav} = \frac{1}{t_0} \int_0^t \frac{\left[ (1-\tau) \left( \frac{t}{t_0} \right)^j + \tau \right] dt}{\left[ 1 + \frac{1}{M} \left[ \frac{(1-\tau)}{(j+1)} \left( \frac{t}{t_0} \right)^{j+1} + \tau \left( \frac{t}{t_0} \right) \right] \right]^2} = M \left( 1 - \frac{V}{V_S} \right)$$

$$\frac{V}{V_S} = \frac{1}{1 + \frac{1}{M} \left[ \frac{(1-\tau)}{(j+1)} \left( \frac{t}{t_0} \right)^{j+1} + \tau \left( \frac{t}{t_0} \right) \right]} \quad (11)$$

$$x_{iav} = M \left( 1 - \frac{V}{V_S} \right) = \frac{M \left[ \frac{(1-\tau)}{(j+1)} \left( \frac{t}{t_0} \right)^{j+1} + \tau \left( \frac{t}{t_0} \right) \right]}{M + \left[ \frac{(1-\tau)}{(j+1)} \left( \frac{t}{t_0} \right)^{j+1} + \tau \left( \frac{t}{t_0} \right) \right]} \quad (26)$$

The average shock factor in the unfolding phase of inflation for the particular time interval  $t = 0$  to  $t = t_0$  is:

$$x_{iav} = \frac{1}{t_0} \int_0^{t_0} \frac{[(1-\tau) \left(\frac{t}{t_0}\right)^j + \tau] dt}{\left[1 + \frac{1}{M} \left[\frac{(1-\tau)}{(j+1)} \left(\frac{t}{t_0}\right)^{j+1} + \tau \left(\frac{t}{t_0}\right)\right]\right]^2} = M \left(1 - \frac{v_0}{v_s}\right)$$

where

$$\frac{v_0}{v_s} = \frac{1}{1 + \left[\frac{1}{M} \left(\frac{1-\tau}{(j+1)} + \tau\right)\right]} \quad (15)$$

then

$$x_{iav} = M \left(1 - \frac{v_0}{v_s}\right) = \frac{M \left[\frac{(1-\tau)}{(j+1)} + \tau\right]}{M + \frac{(1-\tau)}{(j+1)} + \tau} \quad (27)$$

For the special case of  $\tau = 0$

$$x_{iav} = \frac{1}{t_0} \int_0^{t_0} \frac{\left(\frac{t}{t_0}\right)^j dt}{\left[1 + \frac{1}{(j+1)M} \left(\frac{t}{t_0}\right)^{j+1}\right]^2} = M \left(1 - \frac{v_0}{v_s}\right)$$

$$\frac{v_0}{v_s} = \frac{1}{1 + \frac{1}{(j+1)M}} = \frac{(j+1)M}{(j+1)M + 1}$$

$$x_{iav} = \frac{M}{(j+1)M + 1} \quad (28)$$

For deployments where the Ballistic Mass Ratio is less than  $M_L$ , the inflation time,  $t_f$ , is equal to the reference time,  $t_0$ . When the Ballistic Mass Ratio exceeds the  $M_L$ , an additional impulse is imparted during the time from  $t_0$  to  $t_f$ .

$$-F_s \int_{t_0}^t x_1 dt = \frac{W}{g} \int_{v_0}^v dv$$

$$x_{1av} = \frac{1}{t_0} \int_{t_0}^t x_1 dt = M \left(\frac{v_0}{v_s} - \frac{v}{v_s}\right)$$

where

$$\frac{v}{v_s} = \frac{1}{\frac{v_s}{v_0} + \frac{1}{(j+1)M} \left[ \left( \frac{t}{t_0} \right)^{j+1} - 1 \right]}$$

and  $v_0/v_s$  is defined by Equation (15).

at  $t = t_f$

$$x_{i_{av}} = \frac{1}{t_0} \int_{t_0}^{t_f} \frac{\left( \frac{t}{t_0} \right)^j dt}{\left[ \frac{v_s}{v_0} + \frac{1}{(j+1)M} \left[ \left( \frac{t}{t_0} \right)^{j+1} - 1 \right] \right]^2} = M \left[ \frac{v_0}{v_s} - \frac{v_f}{v_s} \right]$$

where

$$\frac{v_f}{v_s} = \frac{1}{\frac{v_s}{v_0} + \frac{1}{(j+1)M} \left[ \left( \frac{t_f}{t_0} \right)^{j+1} - 1 \right]}$$

The average shock factor for finite mass deployment is expressed by Equation (27) or (28). The average shock factor for deployments in the intermediate and infinite mass ranges are the summation of the unfolding phase and elastic phase shock factors.

$$\begin{aligned} x_{i_{av} \text{ Total}} &= x_{i_{av}} \Big|_{t=0}^{t=t_0} + x_{i_{av}} \Big|_{t=t_0}^{t=t_f} \\ x_{i_{av} \text{ Total}} &= M \left( 1 - \frac{v_0}{v_s} \right) + M \left( \frac{v_0}{v_s} - \frac{v_f}{v_s} \right) \\ x_{i_{av} \text{ Total}} &= M \left( 1 - \frac{v_f}{v_s} \right) \end{aligned} \tag{29}$$

Figure 18 is reproduced from example 2 of Reference 3 to illustrate the rectangular impulse approach. Note the effects of altitude on the inflation time and total system impulse. Example 2, of Reference 3, examined the results of testing a recovery system at altitudes from sea level to 80,000 feet at constant Ballistic Mass Ratio and dynamic pressure.

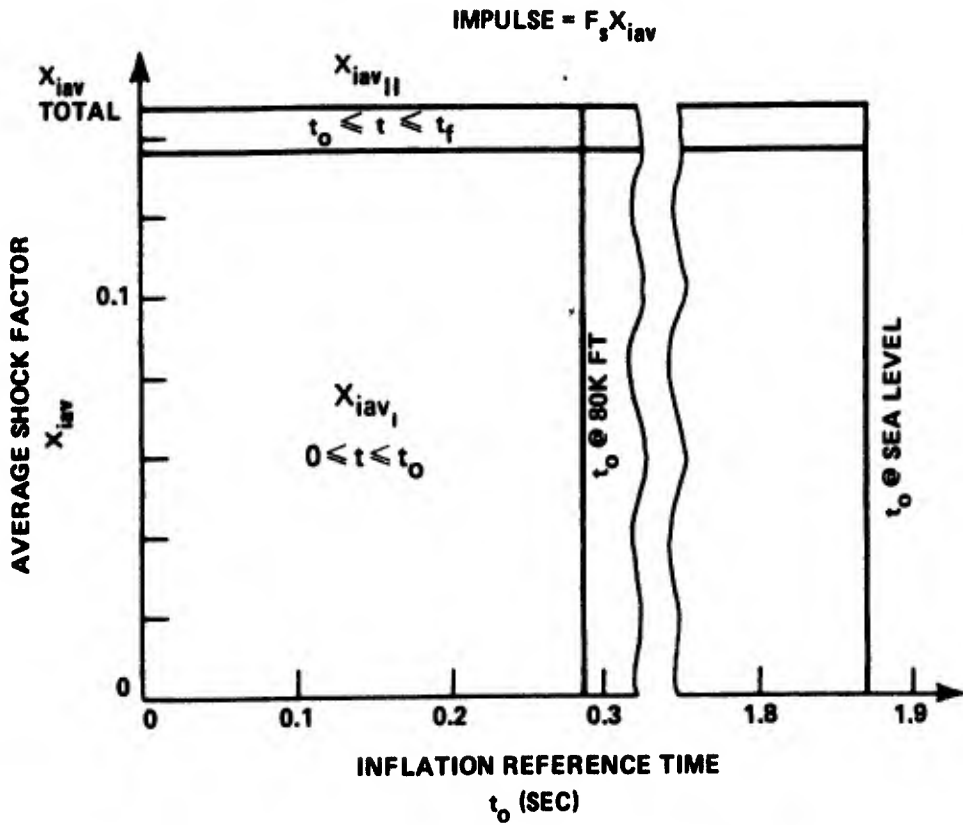


FIGURE 18. EFFECT OF ALTITUDE AND INFLATION REFERENCE TIME ON THE IMPULSE OF THE INFLATING CANOPY OF EXAMPLE 2

Reproduced from Reference 3

## CONCLUSIONS

A closed form generic parachute opening shock force analysis was developed which can be applied to the various drag-area signatures developed by Pfanz and Ludtke. The exceptions were the time of occurrence of the maximum force for the general case with initial drag area and the resultant shock factor. The drag-area signatures obtained by using the variable exponent  $j$  denote different types of parachutes. The Pfanz method was generalized to account for initial drag-area effects. The interaction of the study variables is presented graphically in Figure 12 as an aid to visualizing their combined effects. The developed equations for the several values of  $j$  and the initial drag-area effects are summarized in Table 1 for the convenience of the reader.

In application the analysis demonstrates the same effects on finite mass solid cloth parachutes as noted by Col. Hall in his 1944 test series. The analysis also demonstrates that, if ribbon parachutes were tested in the same manner, the results would be just the opposite from the solid cloth parachutes. This would be an interesting experiment since ribbon parachutes were not available in 1944.

The Ballistic Mass Ratio meets the requirements for a genuine performance scale factor because it directly or indirectly affects all of the elements which define the parachute-inflation process.

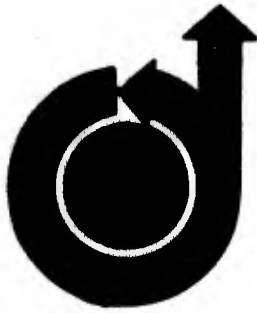
When a given parachute system is tested at constant Ballistic Mass Ratio and dynamic pressure, at any test altitude, the maximum opening shock force and stress distributions are the same. Therefore, it is theoretically possible to adjust the system weight and test at an alternate altitude that can be more convenient, less costly, or allow use of available test assets and obtain identical test results. The requirements and methods for accomplishing alternate altitude testing are described in Reference 3.

For a given type of parachute,  $j$ , and deployment system,  $\tau$ , the effects of altitude on the parachute opening shock force depend upon the Ballistic Mass Ratio. For solid cloth canopies, an increase in altitude reduces the inflation distance,  $V_{st_0}$ . This, together with the reduction of the air density, results in an increase in the Ballistic Mass Ratio scale factor, which determines the percentage of the steady state drag force,  $F_g$ , that is to be realized as opening shock force. The steady state drag force is constant for all altitudes when tests are performed at constant dynamic pressure. Therefore, the increase in the Ballistic Mass Ratio causes the increase of opening shock force with altitude. Analysis of other types of canopies requires definitions of the inflation distance as a function of altitude.

The method of addressing the impulse and momentum of an inflating parachute canopy, derived in Reference 3, for a fixed  $j$  value of 6 has been updated for a variable exponent and initial drag area. When viewed in this manner the average shock factor during canopy inflation was shown to be a function of the Ballistic Mass Ratio, exponent  $j$ , and initial drag area.

REFERENCES

1. Ludtke, W. P., Observations on Parachute Scale Factors for Modeling Parachute Deployment and Steady State Performance, NSWC/WOL TR 78-189.
2. Knacke, T., Lecture Notes from the Helmut G. Heinrich Short Course on Decelerator Systems Technology. Presented at the Sandia National Laboratories, July 1985.
3. Ludtke, W. P., Alternate Altitude Testing of Solid Cloth Parachute Systems, NSWC TR 85-24.
4. Air Force Flight Dynamics Laboratory, Recovery Systems Design Guide, AFFDL-TR-78-151.



NSWC TR 86-142

Appendix A

**AIAA Paper  
No. 73-477**

**A TECHNIQUE FOR THE CALCULATION OF THE  
OPENING-SHOCK FORCES FOR SEVERAL TYPES OF  
SOLID CLOTH PARACHUTES**

by  
**W. P. LUDTKE**  
Naval Ordnance Laboratory  
Silver Spring, Maryland

# **AIAA 4th Aerodynamic Deceleration Systems Conference**

**PALM SPRINGS, CALIFORNIA / MAY 21-23, 1973**

First publication rights reserved by American Institute of Aeronautics and Astronautics,  
1290 Avenue of the Americas, New York, N. Y. 10019. Abstracts may be published without  
permission if credit is given to author and to AIAA. (Price: AIAA Member \$1.50. Nonmember \$2.00).

Note: This paper available at AIAA New York office for six months;  
thereafter, photoprint copies are available at photocopy prices from  
AIAA Library, 750 3rd Avenue, New York, New York 10017

## A TECHNIQUE FOR THE CALCULATION OF THE OPENING-SHOCK FORCES FOR SEVERAL TYPES OF SOLID CLOTH PARACHUTES

W. P. Ludtke  
Naval Ordnance Laboratory  
Silver Spring, Maryland

Abstract

An analytical method of calculating parachute opening-shock forces based upon wind-tunnel derived drag area time signatures of several solid cloth parachute types in conjunction with a scale factor and retardation system steady-state parameters has been developed. Methods of analyzing the inflation time, geometry, cloth airflow properties and materials elasticity are included. The effects of mass ratio and altitude on the magnitude and time of occurrence of the maximum opening shock are consistent with observed field test phenomena.

I. Introduction

In 1965, the Naval Ordnance Laboratory (NOL) was engaged in a project which utilized a 35-foot-diameter, 10-percent extended-skirt parachute (type T-10) as the second stage of a retardation system for a 250-pound payload. Deployment of the T-10 parachute was to be accomplished at an altitude of 100,000 feet. In this rarefied atmosphere, the problem was to determine the second stage deployment conditions for successful operation. A search of available field test information indicated a lack of data on the use of solid cloth parachutes at altitudes above 30,000 feet.

The approach to this problem was as follows: Utilizing existing wind-tunnel data, low-altitude field test data, and reasonable assumptions, a unique engineering approach to the inflation time and opening-shock problem was evolved that provided satisfactory results. Basically, the method combines a wind-tunnel derived drag area ratio signature as a function of deployment time with a scale factor and Newton's second law of motion to analyze the velocity and force profiles during deployment. The parachute deployment sequence is divided into two phases. The first phase, called "unfolding phase," where the canopy is undergoing changes in shape, is considered to be inelastic as the parachute inflates initially to its steady-state aerodynamic size for the first time. At this point, the "elastic phase" is entered where it is considered that the elasticity of the parachute materials enters the problem and resists the applied forces until the canopy has reached full inflation.

The developed equations are in agreement with the observed performance of solid cloth parachutes in the field, such as the decrease of inflation time as

altitude increases, effects of altitude on opening-shock force, finite and infinite mass operation, and inflation distance.

II. Development of Velocity Ratio and Force Ratio Equations During the Unfolding Phase of Parachute Deployment

---

The parachute deployment would take place in a horizontal attitude in accordance with Newton's second law of motion.

$$\Sigma F = ma$$

$$-\frac{1}{2} \rho v^2 C_D S = \frac{W}{g} \frac{dv}{dt}$$

It was recognized that other factors, such as included air mass, apparent mass, and their derivatives, also contribute forces acting on the system. Since definition of these parameters was difficult, the analysis was conducted in the simplified form shown above. Comparison of calculated results and test results indicated that the omitted terms have a small effect.

$$\int_0^t C_D S dt = \frac{-2W}{\rho g} \int_{V_s}^V \frac{dV}{V^2} \quad (1)$$

Multiplying the right-hand side of equation (1) by

$$1 = \frac{V_s t_0 C_D S_0}{V_s t_0 C_D S_0}$$

and rearranging

$$\begin{aligned} & \frac{1}{t_0} \int_0^t \frac{C_D S}{C_D S_0} dt \\ &= \frac{-2W}{\rho g V_s t_0 C_D S_0} V_s \int_{V_s}^V \frac{dV}{V^2} \quad (2) \end{aligned}$$

In order to integrate the left-hand term of equation (2), the drag area ratio must be defined for the type of parachute under

analysis as a function of deployment reference time,  $t_0$ .

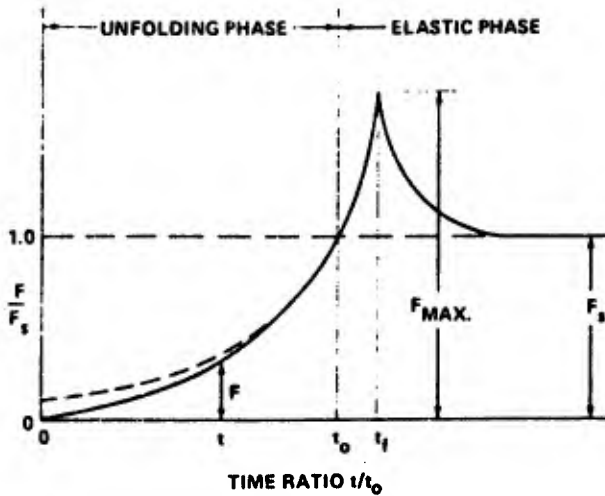


FIG. 1 TYPICAL INFINITE MASS FORCE-TIME HISTORY OF A SOLID CLOTH PARACHUTE IN A WIND TUNNEL

Figure 1 illustrates a typical solid cloth parachute wind-tunnel infinite mass force-time history after snatch. In infinite mass deployment, the maximum size and maximum shock force occur at the time of full inflation,  $t_f$ . However,  $t_f$  is inappropriate for analysis since it is dependent upon the applied load, structural strength, and materials elasticity. The reference time,  $t_0$ , where the parachute has attained its steady-state aerodynamic size for the first time, is used as the basis for performance calculations.

At any instant during the unfolding phase, the force ratio  $F/F_s$  can be determined as a function of the time ratio,  $t/t_0$ .

$$F = \frac{1}{2} \rho v^2 C_D S$$

$$F_s = \frac{1}{2} \rho v_s^2 C_D S_0$$

Since the wind-tunnel velocity and density are constant during infinite mass deployment

$$\frac{F}{F_s} = \frac{C_D S}{C_D S_0}$$

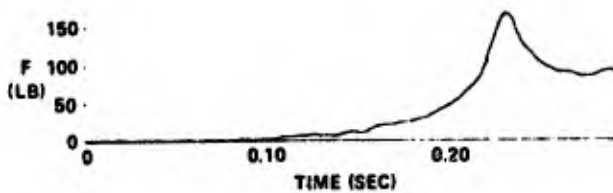
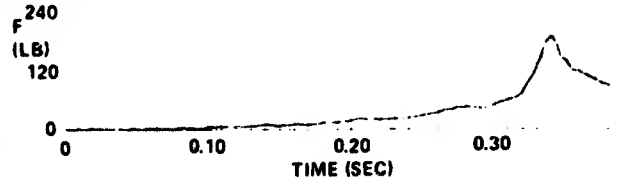
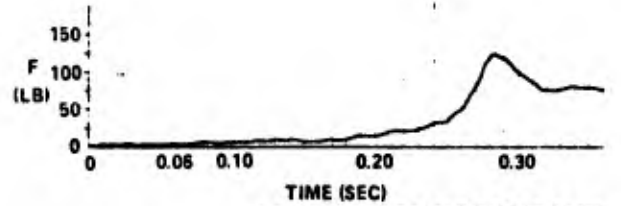


FIG. 2 TYPICAL FORCE-TIME CURVE FOR A SOLID FLAT PARACHUTE UNDER INFINITE MASS CONDITIONS.



REPRODUCED FROM REFERENCE (1)

FIG. 3 TYPICAL FORCE-TIME CURVE FOR A 10% EXTENDED SKIRT PARACHUTE UNDER INFINITE MASS CONDITIONS.



REPRODUCED FROM REFERENCE (1)

FIG. 4 TYPICAL FORCE-TIME CURVE FOR A PERSONNEL GUIDE SURFACE PARACHUTE UNDER INFINITE MASS CONDITIONS

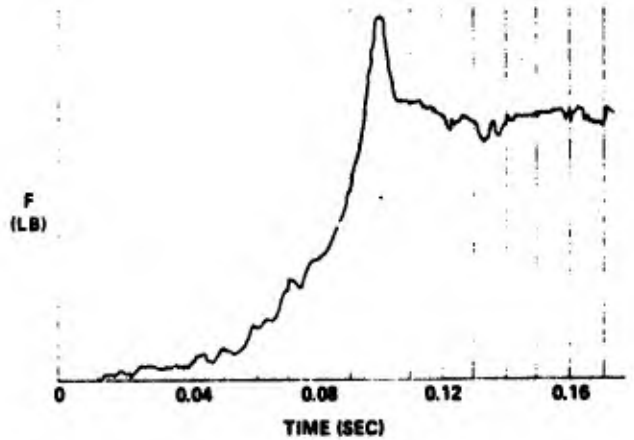


FIG. 5 TYPICAL FORCE-TIME SIGNATURE FOR THE ELLIPTICAL PARACHUTE UNDER INFINITE MASS CONDITIONS

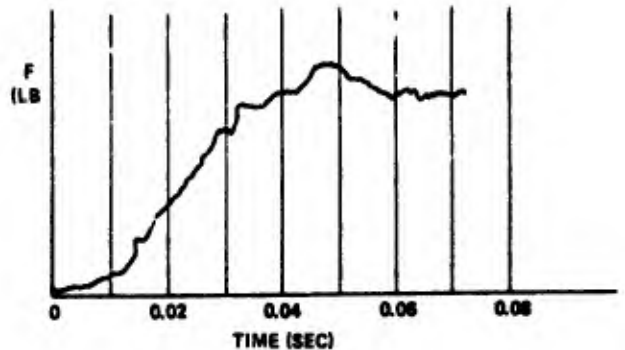


FIG. 6 TYPICAL FORCE-TIME SIGNATURE FOR THE RING SLOT PARACHUTE 20% GEOMETRIC POROSITY UNDER INFINITE MASS CONDITIONS

Infinite mass opening-shock signatures of several types of parachutes are presented in Figures 2 through 6. Analysis of these signatures using the force ratio,  $F/F_s$ , - time ratio,  $t/t_0$ , technique indicated a similarity in the performance of the various solid cloth types of

parachutes which were examined. The geometrically porous ring slot parachute displayed a completely different signature, as was expected. These data are illustrated in Figure 7. If an initial boundary

$$\frac{C_D S}{C_{D0} S_0} = (1-\eta)^2 \left(\frac{t}{t_0}\right)^6 + 2\eta(1-\eta) \left(\frac{t}{t_0}\right)^3 + \eta^2 \quad (5)$$

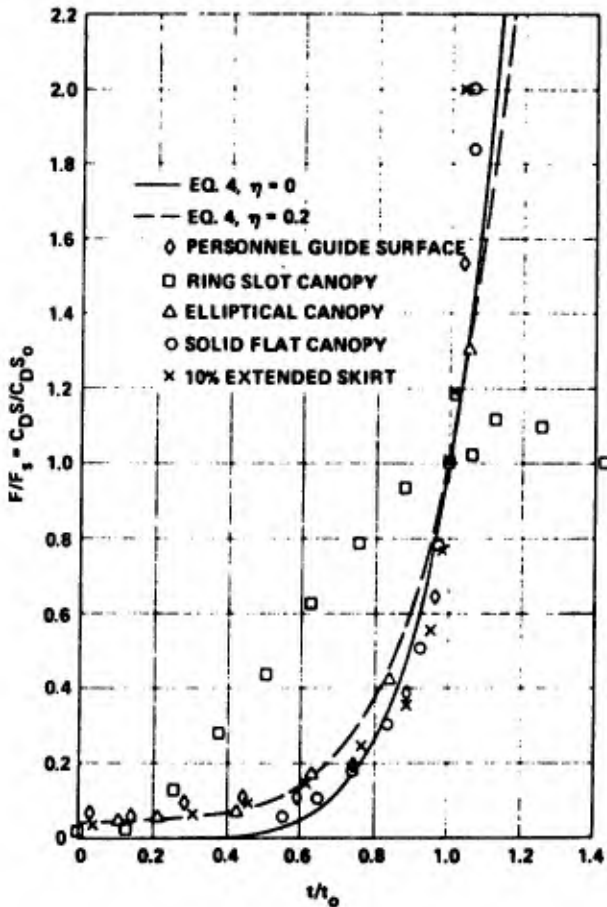


FIG. 7 DRAG AREA RATIO VS. TIME RATIO

condition of  $C_D S / C_{D0} S_0 = 0$  at time  $t/t_0 = 0$  is assumed, then, the data can be approximated by fitting a curve of the form

$$\frac{C_D S}{C_{D0} S_0} = \left(\frac{t}{t_0}\right)^6 \quad (3)$$

A more realistic drag area ratio expression was determined which includes the effect of initial area at line stretch.

$$\frac{C_D S}{C_{D0} S_0} = \left[ (1-\eta) \left(\frac{t}{t_0}\right)^3 + \eta \right]^2 \quad (4)$$

where  $\eta$  is the ratio of the projected mouth area at line stretch to the steady-state projected frontal area. Expanding equation (4)

At the time that equation (5) was ascertained, it suggested that the geometry of the deploying parachute was independent of density and velocity. It was also postulated that although this expression had been determined for the infinite mass condition, it would also be true for the finite mass case. This phenomenon has since been independently observed and confirmed by Berndt and De Weese in reference (2).

Since the drag area ratio was determined from actual parachute deployments, it was assumed that the effects of apparent mass and included mass on the deployment force history were accommodated.

The right-hand term of equation (2) contains the expression

$$\frac{2W}{\rho g V_s t_0 C_{D0} S_0} = M \quad (6)$$

This term can be visualized as shown in Figure 8 to be a ratio of the retarded mass (including the parachute) to an associated mass of atmosphere contained in a right circular cylinder which is generated by moving an inflated parachute of area  $C_{D0} S_0$  for a distance equal to the product of  $V_s t_0$  through an atmosphere of density,  $\rho$ .

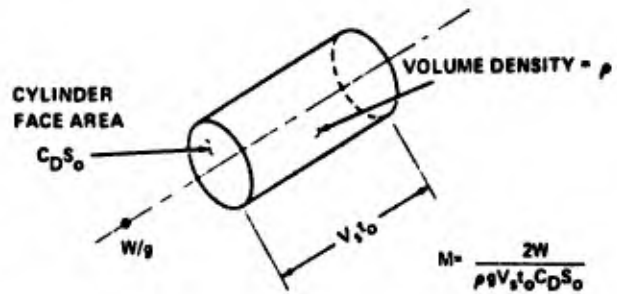


FIG. 8 VISUALIZATION OF THE MASS RATIO CONCEPT

The mass ratio,  $M$ , is the scale factor which controls the velocity and force profiles during parachute deployment. Substituting  $M$  and  $C_D S / C_{D0} S_0$  into equation (2), integrating, and solving for  $V/V_s$

$$\frac{V}{V_s} = \frac{1}{1 + \frac{1}{M} \left[ \frac{(1-\eta)^2}{7} \left(\frac{t}{t_0}\right)^7 + \frac{\eta(1-\eta)}{2} \left(\frac{t}{t_0}\right)^4 + \eta^2 \frac{t}{t_0} \right]} \quad (7)$$

The instantaneous shock factor is defined as

$$x_1 = \frac{F}{F_s} = \frac{\frac{1}{2} \rho v^2 C_D S}{\frac{1}{2} \rho v_s^2 C_D S_0}$$

If the altitude variation during deployment is small, then, the density may be considered as constant

$$x_1 = \frac{C_D S}{C_D S_0} \left( \frac{v}{v_s} \right)^2$$

from equations (5) and (7)

$$x_1 = \frac{(1-\eta)^2 \left(\frac{t}{t_0}\right)^6 + 2\eta(1-\eta) \left(\frac{t}{t_0}\right)^3 + \eta^2}{\left[1 + \frac{1}{M} \left[ \frac{(1-\eta)^2}{7} \left(\frac{t}{t_0}\right)^7 + \frac{\eta(1-\eta)}{2} \left(\frac{t}{t_0}\right)^4 + \eta^2 \frac{t}{t_0} \right] \right]^2} \quad (8)$$

**III. Maximum Shock Force and Time of Occurrence During the Unfolding Phase**

The time of occurrence of the maximum instantaneous shock factor,  $x_1$ , is difficult to determine for the general case. However, for  $\eta = 0$ , the maximum shock factor and time of occurrence are readily calculated. For  $\eta = 0$

$$x_1 = \frac{\left(\frac{t}{t_0}\right)^6}{\left[1 + \frac{1}{7M} \left(\frac{t}{t_0}\right)^7\right]^2}$$

Setting the derivative of  $x_1$  with respect to time equal to zero and solving for  $t/t_0$  at  $x_1$  max

$$\left(\frac{t}{t_0}\right) @ x_1 \text{ max} = \left(\frac{21M}{4}\right)^{\frac{1}{7}} \quad (9)$$

and the maximum shock factor is

$$x_1 \text{ max} = \frac{16}{49} \left(\frac{21M}{4}\right)^{\frac{6}{7}} \quad (10)$$

Equations (9) and (10) are valid for values of  $M \leq \frac{4}{21}$  (0.19), since for larger values of  $M$ , the maximum shock force occurs in the elastic phase of inflation.

Figures 9 and 10 illustrate the velocity and force profiles generated from equations (7) and (8) for initial projected area ratios of  $\eta = 0$ , and 0.2 with various mass ratios.

**IV. Methods for Calculation of the Reference Time,  $t_0$**

The ratio concept is an ideal method to analyze the effects of the various parameters on the velocity and force profiles of the opening parachutes; however, a means of calculating  $t_0$  is required before specific values can be computed. Methods for computing the varying mass flow into the inflating canopy mouth, the varying mass flow out through the varying inflated canopy surface area, and the volume of air,  $V_0$ , which must be collected during the inflation process are required.

Figure 11 represents a solid cloth-type parachute canopy at some instant during inflation. At any given instant, the parachute drag area is proportional to the maximum inflated diameter. Also, the maximum diameter in conjunction with the suspension lines determines the inflow mouth area (A-A) and the pressurized canopy area (B-B-B). This observation provided the basis for the following assumptions. The actual canopy shape is of minor importance.

a. The ratio of the instantaneous mouth inlet area to the steady-state mouth area is in the same ratio as the instantaneous drag area.

$$\frac{A_M}{A_{M0}} = \frac{C_D S}{C_D S_0}$$

b. The ratio of the instantaneous pressurized cloth surface area to the canopy surface area is in the same ratio as the instantaneous drag area.

$$\frac{S}{S_0} = \frac{C_D S}{C_D S_0}$$

c. Since the suspension lines in the unpressurized area of the canopy are straight, a pressure differential has not developed, and, therefore, the net air-flow in this zone is zero.

Based on the foregoing assumptions, the mass flow equation can be written

$$dm = m \text{ inflow} - m \text{ outflow}$$

$$\rho \frac{dV}{dt} = \rho V A_M - \rho A_S P$$

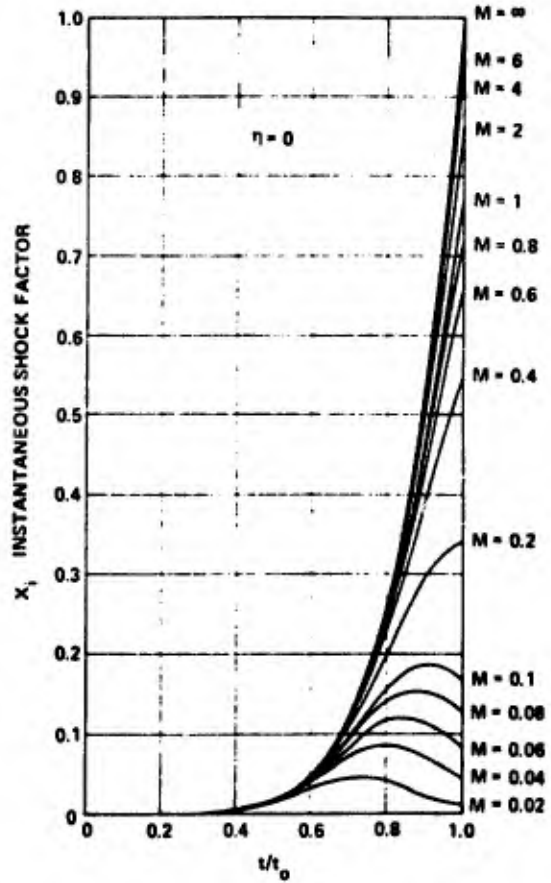
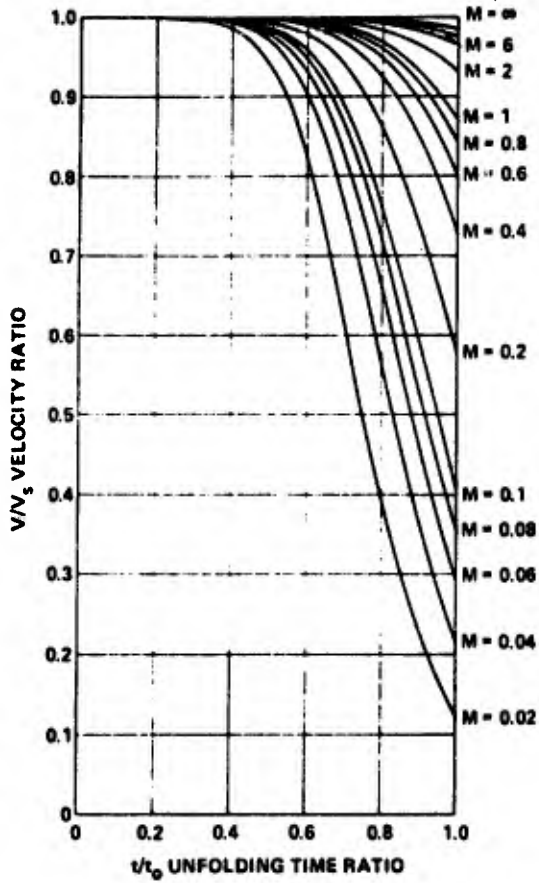


FIG. 9 EFFECT OF INITIAL AREA AND MASS RATIO ON THE SHOCK FACTOR AND VELOCITY RATIO DURING THE UNFOLDING PHASE FOR  $\eta = 0$ .

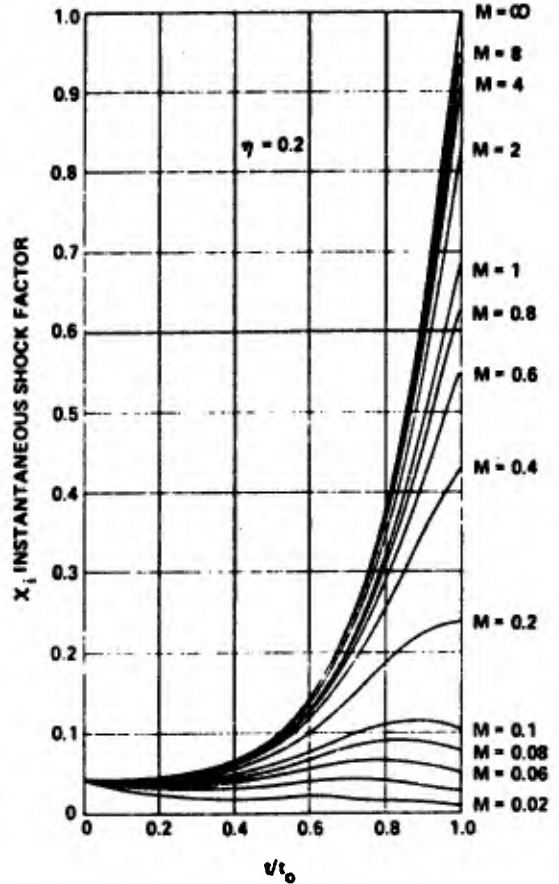
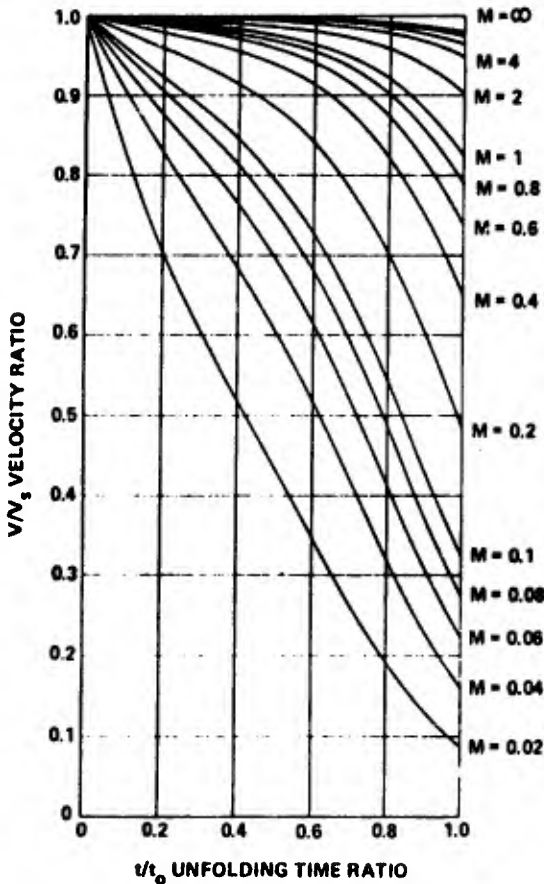


FIG. 10 EFFECT OF INITIAL AREA AND MASS RATIO ON THE SHOCK FACTOR AND VELOCITY RATIO DURING THE UNFOLDING PHASE FOR  $\eta = 0.2$ .

$$\rho \frac{dv}{dt} = \rho v A_{\eta=0} \frac{C_D S}{C_D S_0} - \rho A_{S_0} \frac{C_D S}{C_D S_0} P \quad (11)$$

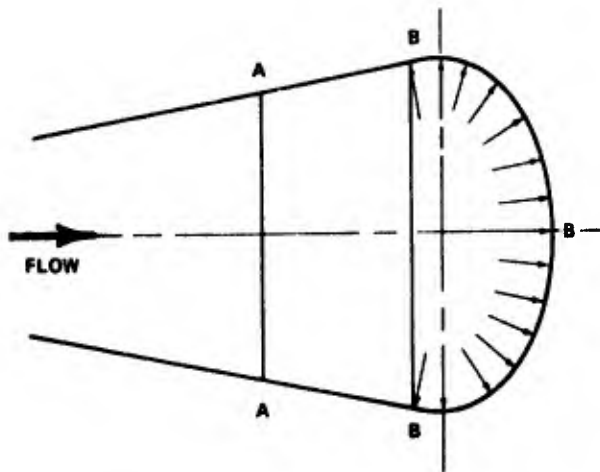


FIG. 11 PARTIALLY INFLATED PARACHUTE CANOPY

From equation (3)

$$\frac{C_D S}{C_D S_0} = \left(\frac{t}{t_0}\right)^6 ; \text{ for } \eta = 0$$

From equation (7)

$$v = \frac{V_s}{1 + \frac{1}{7M} \left(\frac{t}{t_0}\right)^7} ; \eta = 0$$

From equation (26)

$$P = k \left(\frac{C_F \rho}{2}\right)^n v^{2n}$$

$$\int_0^{V_0} dV = A_{M_0} V_s \int_0^{t_0} \frac{\left(\frac{t}{t_0}\right)^6}{1 + \frac{1}{7M} \left(\frac{t}{t_0}\right)^7} dt$$

$$-A_{S_0} k \left(\frac{C_F \rho}{2}\right)^n \int_0^{t_0} \left(\frac{t}{t_0}\right)^6 \left[ \frac{V_s}{1 + \frac{1}{7M} \left(\frac{t}{t_0}\right)^7} \right]^{2n} dt \quad (12)$$

Integrating:

$$V_0 = A_{M_0} V_s t_0^M \ln \left[ 1 + \frac{1}{7M} \right]$$

$$-A_{S_0} k \left(\frac{C_F \rho}{2}\right)^n \int_0^{t_0} \left(\frac{t}{t_0}\right)^6 \left[ \frac{V_s}{1 + \frac{1}{7M} \left(\frac{t}{t_0}\right)^7} \right]^{2n} dt \quad (13)$$

Measured values of n indicate a data range from 0.574 through 0.771. A convenient solution to the reference time equation evolves when n is assigned a value of 1/2. Integrating equation (13) and using

$$V_s t_0 M = \frac{2W}{\rho C_D S_0}$$

$$\text{LET } K_1 = \frac{\rho V_0}{2W} \left[ \frac{C_D S_0}{A_{M_0} - A_{S_0} k \left(\frac{C_F \rho}{2}\right)^{1/2}} \right]$$

$$t_0 = \frac{14W}{\rho V_s C_D S_0} \left[ e^{K_1} - 1 \right] \quad (14)$$

Equation (14) expresses the unfolding reference time,  $t_0$ , in terms of mass, altitude, snatch velocity, airflow characteristics of the cloth, and the steady-state parachute geometry. Note that the term  $\rho V_0/W$  is the ratio of the included air mass to the mass of the retarded hardware. Multiplying both sides of equation (14) by  $V_s$  demonstrates that

$$V_s t_0 = \text{a constant which is a function of altitude}$$

Figures 12 and 13 indicate the parachute unfolding time and unfolding distance for values of  $n = 1/2$  and  $n = 0.63246$ . Note the variation and convergence with rising altitude. The opening-shock force is strongly influenced by the inflation time. Because of this, the

value of  $t_0$  calculated by using a realistic value of  $n$  should be used in the lower atmosphere.

As an example of this method of opening-shock analysis, let us examine the effect of altitude on the opening-shock force of a T-10-type parachute retarding a 200-pound weight from a snatch velocity of  $V_s = 400$  feet per second at sea level. Conditions of constant velocity and constant dynamic pressure are investigated. The results are presented in Figure 14. At low altitudes, the opening-shock force is less than the steady-state drag force; however, as altitude rises, the opening shock eventually exceeds the steady-state drag force at some altitude. This trend is in agreement with field test observations.

V. Correction of  $t_0$  for Initial Area Effects

The unfolding reference time,  $t_0$ , calculated by the previous methods assumes that the parachute inflates from zero drag area. In reality, a parachute has a drag

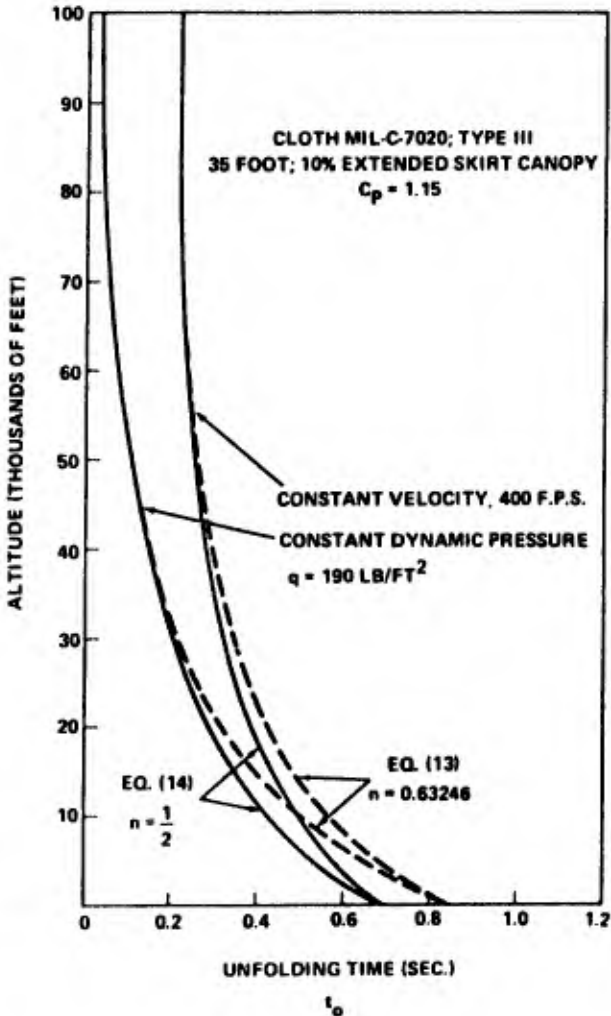


FIG. 12 EFFECT OF ALTITUDE ON THE UNFOLDING TIME " $t_0$ " AT CONSTANT VELOCITY AND CONSTANT DYNAMIC PRESSURE FOR  $n = 1/2$  AND  $n = 0.63296$

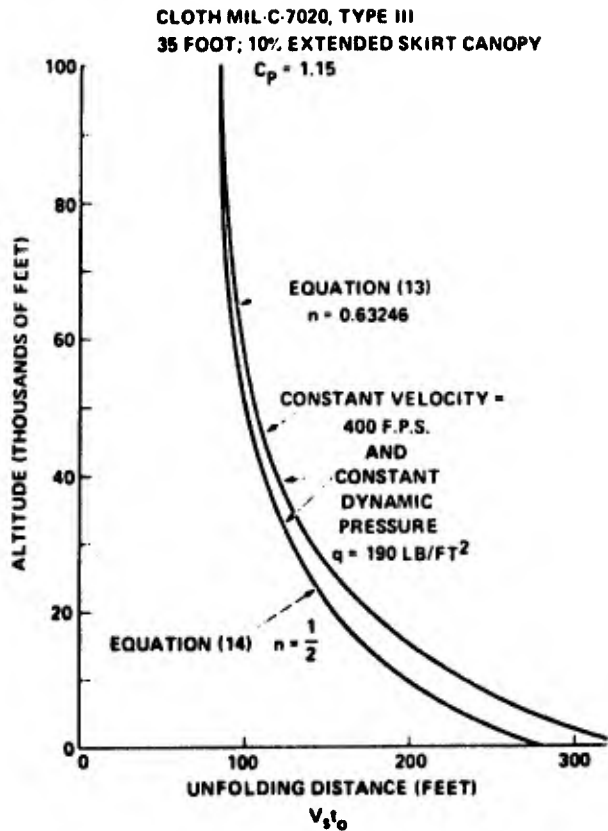


FIG. 13 EFFECT OF ALTITUDE ON THE UNFOLDING DISTANCE AT CONSTANT VELOCITY AND CONSTANT DYNAMIC PRESSURE FOR  $n = 1/2$  AND  $n = 0.63246$ .

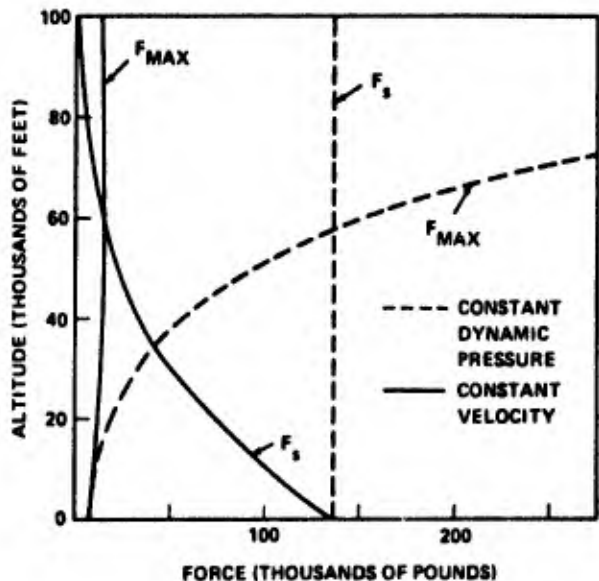


FIG. 14 VARIATION OF STEADY-STATE DRAG,  $F_s$ , AND MAXIMUM OPENING SHOCK WITH ALTITUDE FOR CONSTANT VELOCITY AND CONSTANT DYNAMIC PRESSURE

area at the beginning of inflation. Once  $t_0$  has been calculated, a correction can be applied, based upon what is known about the initial conditions.

Case A - When the initial projected area is known

$$\frac{A_i}{A_c} = \left(\frac{t_i}{t_o}\right)^3$$

$$t_i = \left(\frac{A_i}{A_c}\right)^{1/3} t_{o\text{calculated}}$$

$$t_{o\text{corrected}} = \left[1 - \left(\frac{A_i}{A_c}\right)^{1/3}\right] t_{o\text{calculated}} \quad (15)$$

Case B - When the initial drag area is known

$$\frac{C_D S_i}{C_D S_o} = \left(\frac{t_i}{t_o}\right)^6$$

$$t_i = \left(\frac{C_D S_i}{C_D S_o}\right)^{1/6} t_{o\text{calculated}}$$

$$t_{o\text{corrected}} = \left[1 - \left(\frac{C_D S_i}{C_D S_o}\right)^{1/6}\right] t_{o\text{calculated}} \quad (16)$$

The mass ratio should now be adjusted for the corrected  $t_o$  before velocity and force profiles are determined.

#### VI. Opening-Shock Force, Velocity Ratio, and Inflation Time During the Elastic Phase of Parachute Inflation

The mass ratio,  $M$ , is an important parameter in parachute analysis. For values of  $M \ll 4/21$ , the maximum opening-shock force occurs early in the inflation process, and the elastic properties of the canopy are not significant. As the mass ratio approaches  $M = 4/21$ , the magnitude of the opening-shock force increases, and the time of occurrence happens later in the deployment sequence. For mass ratios  $M > 4/21$ , the maximum shock force will occur after the reference time,  $t_o$ . Parachutes designed for high mass ratio operation must provide a structure of sufficient constructed strength,  $F_c$ , so that the actual elongation of the canopy under load is less

than the maximum extensibility,  $\epsilon_{\text{max}}$ , of the materials.

Development of the analysis in the elastic phase of inflation is similar to the technique used in the unfolding phase. Newton's second law of motion is used, together with the drag area ratio signature and mass ratio

$$\frac{C_D S}{C_D S_o} = \left(\frac{t}{t_o}\right)^6$$

which is still valid, as shown in Figure 7

$$\frac{1}{Mt_o} \int_{t_o}^t \left(\frac{t}{t_o}\right)^6 dt = v_s \int_{v_o}^v \frac{-dv}{v^2}$$

Integrating and solving for  $\frac{v}{v_s}$

$$\frac{v}{v_s} = \frac{1}{\frac{v_s}{v_o} + \frac{1}{7M} \left[ \left(\frac{t}{t_o}\right)^7 - 1 \right]} \quad (17)$$

where  $\frac{v_o}{v_s}$  is the velocity ratio of the unfolding process at time  $t = t_o$ .

$$\frac{v_o}{v_s} = \frac{1}{1 + \frac{1}{M} \left[ \frac{(1-\eta)^2}{7} + \frac{\eta(1-\eta)}{2} + \eta^2 \right]} \quad (18)$$

The instantaneous shock factor in the elastic phase becomes

$$x_i = \frac{C_D S}{C_D S_o} \left(\frac{v}{v_s}\right)^2$$

$$x_i = \frac{\left(\frac{t}{t_o}\right)^6}{\left[ \frac{v_s}{v_o} + \frac{1}{7M} \left[ \left(\frac{t}{t_o}\right)^7 - 1 \right] \right]^2} \quad (19)$$

The end point of the inflation process depends upon the applied loads, elasticity of the canopy, and the constructed strength of the parachute. A linear load elongation

relationship is utilized to determine the maximum drag area.

$$\frac{\epsilon}{F} = \frac{\epsilon_{\max}}{F_c}$$

$$\epsilon = \frac{F \epsilon_{\max}}{F_c} \quad (20)$$

The force, F, is initially the instantaneous force at the end of the unfolding process

$$F = X_0 F_S \quad (21)$$

where  $X_0$  is the shock factor of the unfolding phase at  $t = t_0$

$$X_0 = \frac{1}{\left[ 1 + \frac{1}{M} \left[ \frac{(1-\eta)^2}{7} + \frac{\eta(1-\eta)}{2} + \eta^2 \right] \right]^2} \quad (22)$$

Since the inflated shape is defined, the drag coefficient is considered to be constant, and the instantaneous force is proportional to the dynamic pressure and projected area. The maximum projected area would be developed if the dynamic pressure remained constant during the elastic phase. Under very high mass ratios, this is nearly the case over this very brief time period; but as the mass ratio decreases, the velocity decay has a more significant effect. The simplest approach for all mass ratios is to determine the maximum drag area of the canopy as if elastic inflation had occurred at constant dynamic pressure. Then utilizing the time ratio determined as an end point, intermediate shock factors can be calculated from equation (19) and maximum force assessed.

The initial force,  $X_0 F_S$ , causes the canopy to increase in projected area. The new projected area in turn increases the total force on the canopy which produces a secondary projected area increase. The resulting series of events are resisted by the parachute materials. The parachute must, therefore, be constructed of sufficient strength to prevent the elongation of the materials from exceeding the maximum elongation.

$$\epsilon_0 = \frac{X_0 F_S}{F_c} \epsilon_{\max} \quad (23)$$

The next force in the series at constant q

$$F_1 = X_0 F_S \frac{A_1}{A_c}$$

where

$$\frac{A_1}{A_c} = (1 + \epsilon_0)^2$$

Subsequent elongations in the system can be shown to be

$$\epsilon_1 = \epsilon_0 (1 + \epsilon_0)^2$$

$$\epsilon_2 = \epsilon_0 (1 + \epsilon_0 (1 + \epsilon_0)^2)^2$$

The required canopy constructed strength can be determined for a given set of deployment conditions. The limiting value of the series ( $\epsilon_L$ ) determines the end point time ratio.

$$\left( \frac{t_f}{t_0} \right)^6 = \frac{C_{D S_{\max}}}{C_{D S_0}} = (1 + \epsilon_L)^2$$

$$\left( \frac{t_f}{t_0} \right) = \left( \frac{C_{D S_{\max}}}{C_{D S_0}} \right)^{1/6} = (1 + \epsilon_L)^{1/3} \quad (24)$$

Figure 15 illustrates the maximum drag area ratio as a function of  $\epsilon_0$ .

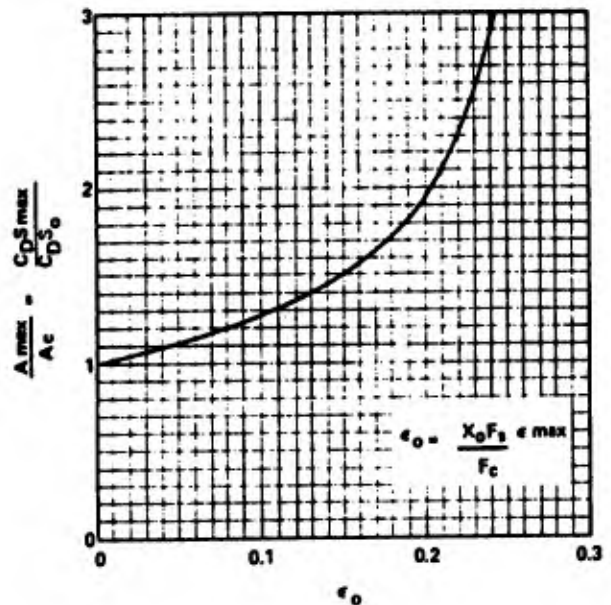


FIG. 15 MAXIMUM DRAG AREA RATIO VS. INITIAL ELONGATION

### VII. Application of Cloth Permeability to the Calculation of the Inflation Time of Solid Cloth Parachutes

The mass outflow through the pressurized region of an inflating solid cloth parachute at any instant is dependent upon the canopy area which is subjected to airflow and the rate of airflow through that area. The variation of pressurized area as a function of reference time,  $t_0$ , was earlier assumed to be proportional to the instantaneous drag area ratio, leaving the rate-of-airflow problem to solve. The permeability parameter of cloth was a natural choice for determining the rate of airflow through the cloth as a function of pressure differential across the cloth. Heretofore, these data have been more of a qualitative, rather than quantitative, value. A new method of analysis was developed wherein a generalized curve of the form  $P = k(\Delta P)^n$  was fitted to cloth permeability data for a number of different cloths and gives surprisingly good agreement over the pressure differential range of available data. The pressure differential was then related to the trajectory conditions to give a generalized expression which can be used in the finite mass ratio range, as well as the infinite mass case. The permeability properties were transformed into a mass flow ratio,  $M'$ , which shows agreement with the effective porosity concept.

Measured and calculated permeability pressure data for several standard cloths are illustrated in Figure 16. This method has been applied to various types of cloth between the extremes of a highly permeable 3-momme silk to a relatively impervious parachute pack container cloth with reasonably good results, see Figure 17.

The canopy pressure coefficient,  $C_p$ , is defined as the ratio of the pressure differential across the cloth to the dynamic pressure of the free stream.

$$C_p = \frac{\Delta P}{q} = \frac{P(\text{internal}) - P(\text{external})}{1/2 \rho V^2} \quad (25)$$

where  $V$  is based on equation (7).

The permeability expression,  $P = k(\Delta P)^n$  becomes

$$P = k \left( C_p \frac{\rho V^2}{2} \right)^n \quad (26)$$

Although some progress has been made by Melzig and others on the measurement of the variation of the pressure coefficient on an actual inflating canopy, this dimension and its variation with time are still dark areas at the time of this writing. At the present time, a constant average value of pressure coefficient is

used in these calculations. Figure 18 presents the effect of pressure coefficient and altitude on the unfolding time for constant deployment conditions.

It is well known that the inflation time of solid cloth parachutes decreases as the operational altitude increases. This effect can be explained by considering the ratio of the mass outflow through a unit cloth area to the mass inflow through a unit mouth area.

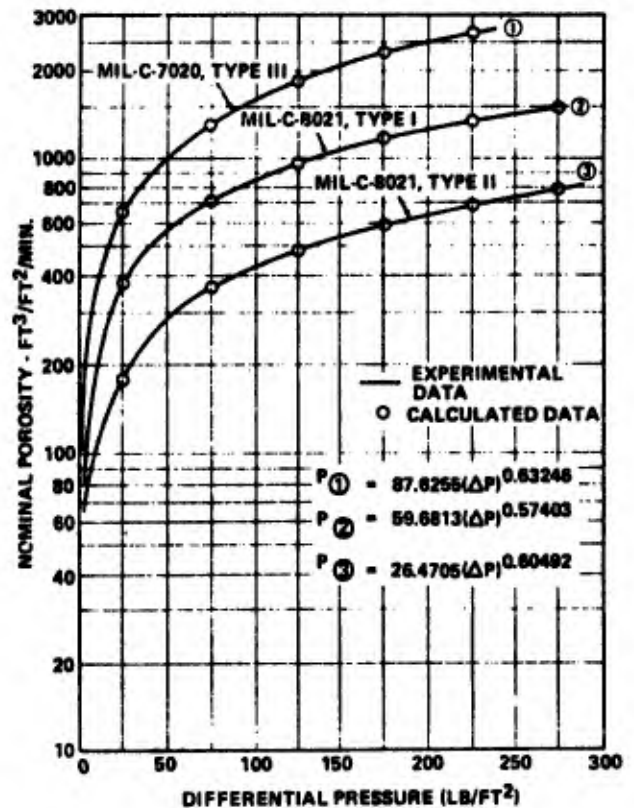
$$M' = \text{mass flow ratio} = \frac{\text{mass outflow}}{\text{mass inflow}}$$

where

$$\text{mass outflow} = P \frac{\text{slugs}}{\text{ft}^2\text{-sec}} \text{ (per ft}^2 \text{ cloth area)}$$

and

$$\text{mass inflow} = V \frac{\text{slugs}}{\text{ft}^2\text{-sec}} \text{ (per ft}^2 \text{ inflow area)}$$



REPRODUCED FROM REFERENCE (4)

FIG. 18 NOMINAL POROSITY OF PARACHUTE MATERIAL VS DIFFERENTIAL PRESSURE.

Therefore, the mass flow ratio becomes

$$M' = \frac{P}{V} = \frac{P}{V}$$

$$M' = k \left( \frac{C_p \rho}{2} \right)^n v^{(2n-1)} \quad (27)$$

Effective porosity,  $C$ , is defined as the ratio of the velocity through the cloth,  $u$ , to a fictitious theoretical velocity,  $v$ , which will produce the particular  $\Delta P = 1/2\rho v^2$ .

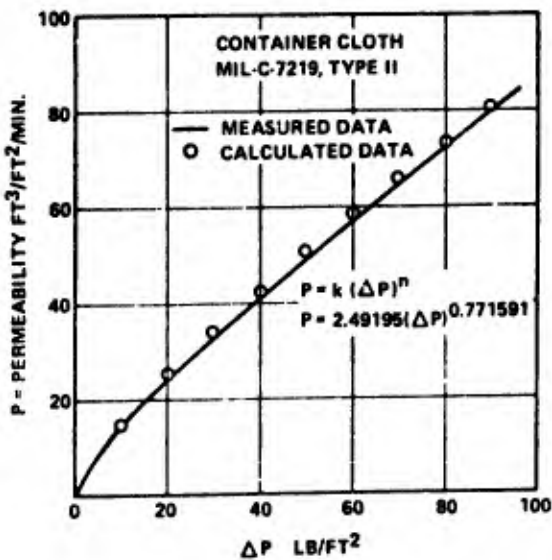
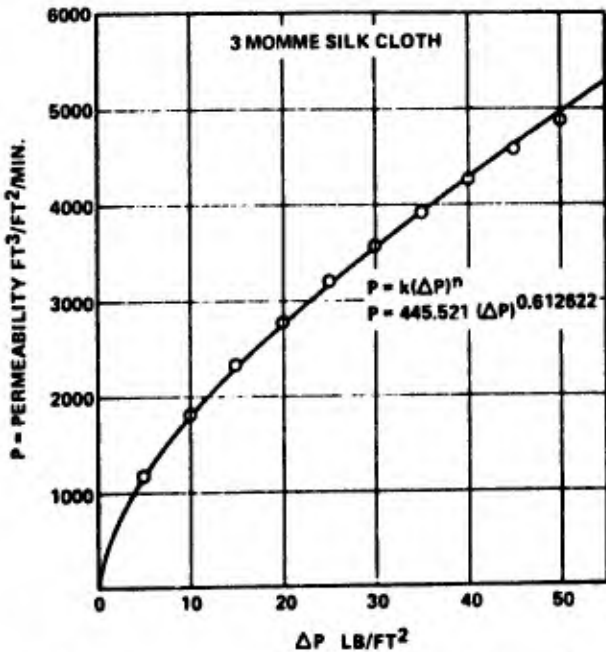


FIG. 17 COMPARISON OF MEASURED AND CALCULATED PERMEABILITY FOR RELATIVELY PERMEABLE AND IMPERMEABLE CLOTHS

AVERAGE CANOPY PRESSURE COEFFICIENT DURING INFLATION INCLUDING THE VENT

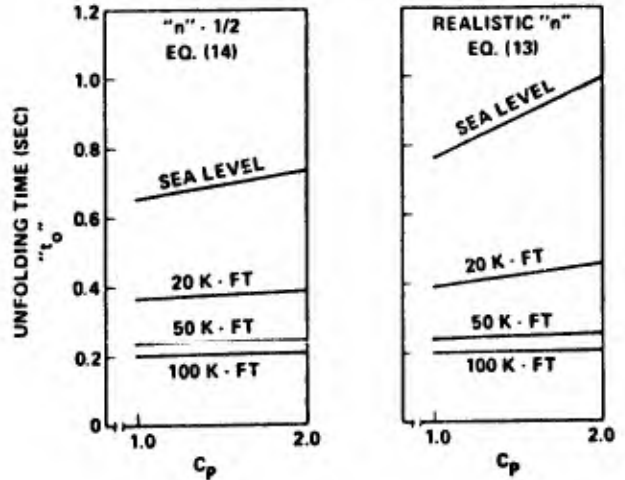
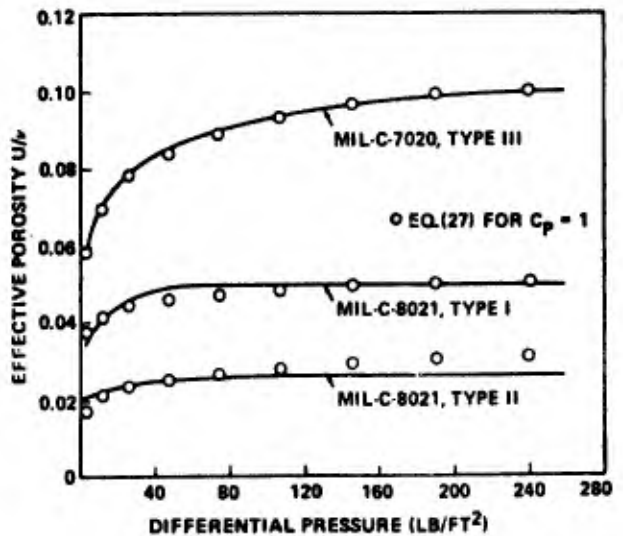


FIG. 18 EFFECT OF PRESSURE COEFFICIENT AND ALTITUDE ON THE UNFOLDING TIME.

effective porosity,  $C = \frac{u}{v}$  (28)

Comparison of the mass flow ratio and previously published effective porosity data is shown in Figure 19. The effects of altitude and velocity on the mass flow ratio are presented in Figures 20, and 21 for constant velocity and constant altitude. The decrease of cloth permeability with altitude is evident.

The permeability constants "k" and "n" can be determined from the permeability pressure differential data as obtained from an instrument such as a Frazier Permeameter. Two data points, "A" and



REPRODUCED FROM REFERENCE (4)

FIG. 19 THE EFFECTIVE POROSITY OF PARACHUTE MATERIALS VS. DIFFERENTIAL PRESSURE

"B," are selected in such a manner that point "A" is in a low-pressure zone below the knee of the curve, and point "B" is located in the upper end of the high-pressure zone, as shown in Figure 22.

The two standard measurements of 1/2 inch of water and 20 inches of water appear to be good data points if both are

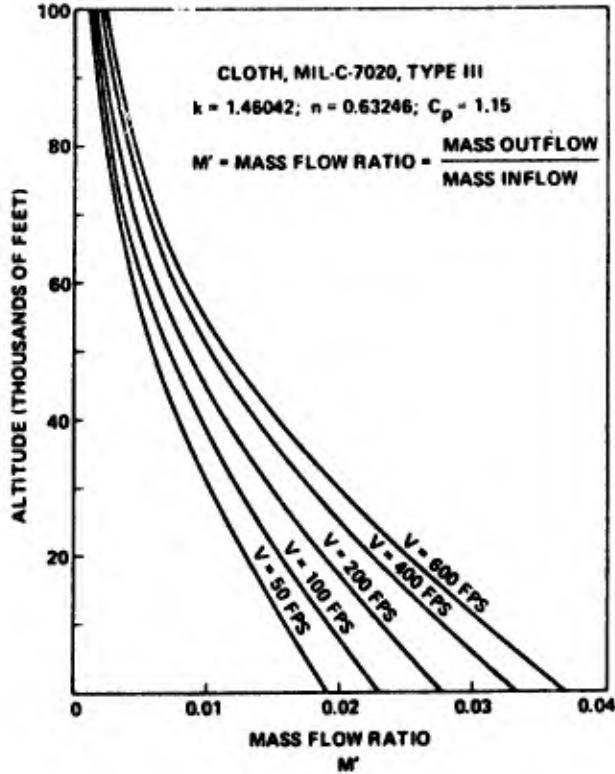


FIG. 20 EFFECT OF ALTITUDE ON MASS FLOW RATIO AT CONSTANT VELOCITY

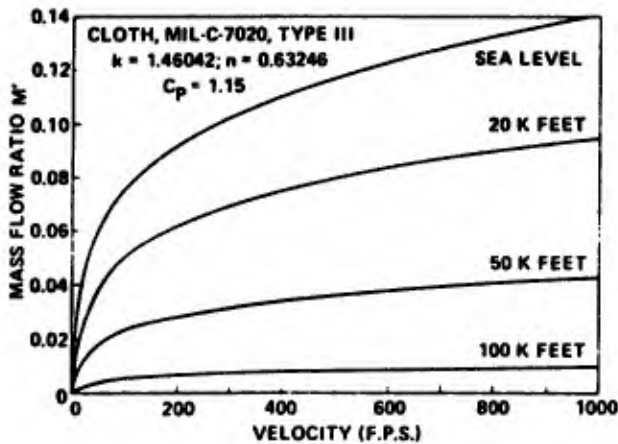


FIG. 21 EFFECT OF VELOCITY ON MASS FLOW RATIO AT CONSTANT DENSITY

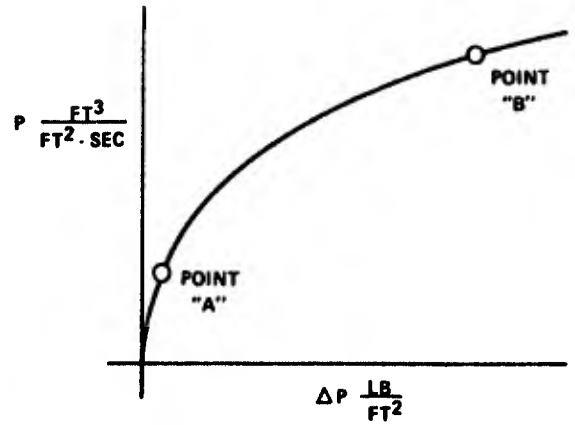


FIG. 22 LOCATION OF DATA POINTS FOR DETERMINATION OF "k" AND "n"

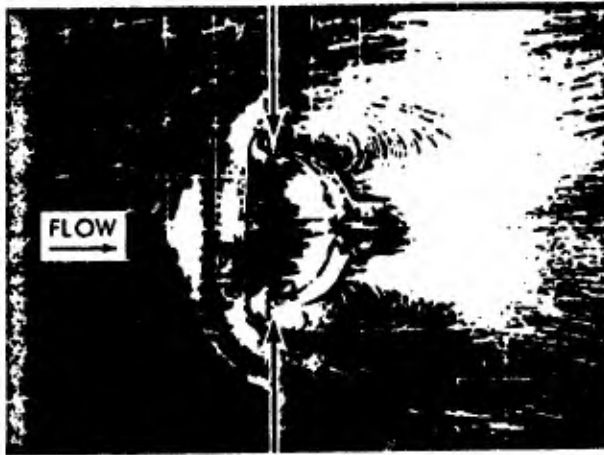
available on the same sample. Substituting the data from points "A" and "B" into  $P = k(\Delta P)^n$  :

$$n = \frac{\ln\left(\frac{P_B}{P_A}\right)}{\ln\left(\frac{\Delta P_B}{\Delta P_A}\right)} \quad (29)$$

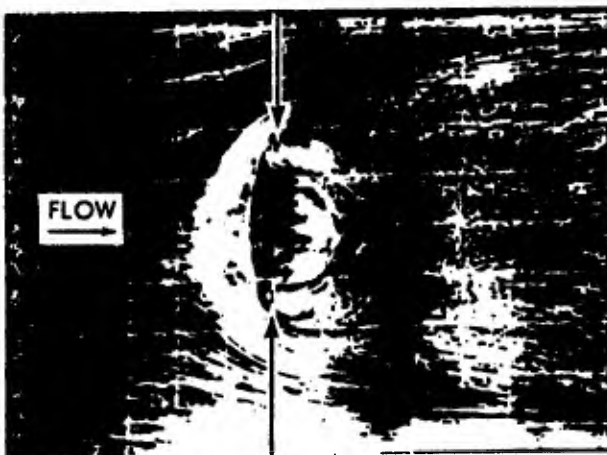
$$k = \frac{P_A}{(\Delta P_A)^n} = \frac{P_B}{(\Delta P_B)^n} \quad (30)$$

VIII. Determination of the Parachute Included Volume and Associated Air Mass

Before the reference time,  $t_0$ , and inflation time,  $t_f$ , can be calculated, the volume of atmosphere,  $V_0$ , which is to be collected during the inflation process must be accurately known. This requirement dictates that a realistic inflated canopy shape and associated volume of atmosphere be determined. Figure 23 was reproduced from reference (5). The technique of using lampblack coated plates to determine the airflow patterns around metal models of inflated canopy shapes was used by the investigator of reference (5) to study the stability characteristics of contemporary parachutes, i.e., 1943. A by-product of this study is that it is clearly shown that the volume of air within the canopy bulges out of the canopy mouth (indicated by arrows) and extends ahead of the canopy hem. This volume must be collected during the inflation process. Another neglected, but significant, source of canopy volume exists in the billowed portion of the gore panels.



HEMISPHERE



VENT PARACHUTE

REPRODUCED FROM REFERENCE (5)

FIG. 23 AIRFLOW PATTERNS SHOWING AIR VOLUME  
AHEAD OF CANOPY HEM

The steady-state canopy shape has been observed in wind-tunnel and field tests to be elliptical in profile. Studies of the inflated shape and included volume of several parachute types (flat circular, 10 percent extended skirt, elliptical, hemispherical, ring slot, ribbon, and cross) are documented in references (6) and (7). These studies demonstrated that the steady-state profile shape of inflated canopies of the various types can be approximated to be two ellipses of common major diameter,  $2\bar{a}$ , and dissimilar minor diameters,  $b$  and  $b'$ , as shown in Figure 24. It was also shown that the volume of the ellipsoid of revolution formed by revolving the profile shape about the canopy axis was a good approximation of the volume of atmosphere to be collected during canopy inflation and included the air volume extended ahead of the parachute skirt hem together with the billowed gore volume.

$$\bar{V}_0 = \frac{2}{3} \pi \bar{a}^3 \left[ \frac{b}{\bar{a}} + \frac{b'}{\bar{a}} \right] \quad (31)$$

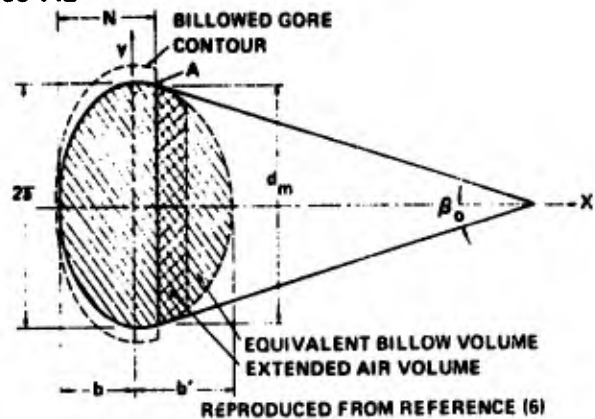


FIG. 24 PARACHUTE CROSS SECTION NOMENCLATURE

Tables I and II are summaries of test results reproduced from references (6) and (7), respectively, for the convenience of the reader.

#### IX. References

1. "A Method to Reduce Parachute Inflation Time with a Minor Increase in Opening Force," WADD Report TR 60-761
2. Berndt, R. J., and DeWesse, J. H., "Filling Time Prediction Approach for Solid Cloth Type Parachute Canopies," AIAA Aerodynamic Deceleration Systems Conference, Houston, Texas, 7-9 Sep 1966
3. "Theoretical Parachute Investigations," Progress Report No. 4, Project No. 5, WADC Contract AF33 (616)-3955, University of Minnesota
4. "Performance of and Design Criteria for Deployable Aerodynamic Decelerators," TR ASK-TR-61-579, AFFDL, AIRFORCESYSCOM, Dec 1963
5. "Investigation of Stability of Parachutes and Development of Stable Parachutes from Fabric of Normal Porosity," Count Zeppelin Research Institute Report No. 300, 23 Mar 1943
6. Ludtke, W. P., "A New Approach to the Determination of the Steady-State Inflated Shape and Included Volume of Several Parachute Types," NOLTR 69-159, 11 Sep 1969
7. Ludtke, W. P., "A New Approach to the Determination of the Steady-State Inflated Shape and Included Volume of Several Parachute Types in 24-Gore and 30-Gore Configurations," NOLTR 70-178, 3 Sep 1970

**TABLE I SUMMARY OF PARACHUTE SHAPE TEST RESULTS FOR 12-GORE AMD 16-GORE CONFIGURATIONS**

Parachute Type	No. of Gores	Suspension Line Length inches	Velocity		Scale Factor, K				$\frac{N}{a}$	Axes Ratio				Volume in <sup>3</sup>			$\frac{V_o}{V_H}$
			mph	fps	$\frac{2\bar{a}}{D_o}$	$\frac{2\bar{a}}{D_F}$	$\frac{2\bar{a}}{D_R}$	$\frac{2\bar{a}}{L}$		$\frac{b}{a}$	$\frac{b'}{a}$	$\frac{b}{a}, \frac{b'}{a}$	$V_H$	$V_C$	$V_o$		
Flat Circular	12	34	50	73	.645	.650			.856	.6115	.8817	1.4932	4476	4481	6980	1.56	
	16	34	50	73	.663	.669			.820	.5558	.9039	1.4597	4450	4100	7325	1.65	
10% Extended Skirt	12	34	100	147	.663	.652			.881	.6424	.8860	1.5284	3928	4400	6783	1.73	
	16	34	17	25	.654	.640			.785	.5580	.8502	1.4082	4051	3920	6197	1.53	
Elliptical	12	34	75	110			.916		.812	.5626	.9657	1.5283		3322	5405		
	16	34	17	25			.875		.800	.6169	.8163	1.4332		2726	4405		
Hemispherical	12	34	125	183			.996		1.254	1.0005	.9080	1.9085		6224	8666		
	16	34	75	110			.994		1.185	.9129	.9380	1.8509		5921	8370		
Ringslot 16% Geometric Porosity	12	34	25	37	.607	.654			.853	.6566	.8735	1.530	3800	3650	5903	1.55	
	12	34	100	147	.616	.663			.922	.6566	.8735	1.530	3800	4198	6166	1.62	
	12	34	200	293	.637	.686			.918	.6566	.8735	1.530	3800	4624	6826	1.90	
	16	34	25	37	.611	.658			.827	.6004	.8890	1.4894	3800	3763	5685	1.50	
	16	34	100	147	.617	.664			.864	.6004	.8890	1.4894	3800	3985	6030	1.59	
	16	34	200	293	.645	.695			.844	.6004	.8890	1.4894	3800	4430	6897	1.82	
Ribbon 24% Geometric Porosity	12	34	25	37	.586	.632			.859	.6558	.8768	1.5326	3800	3323	5335	1.40	
	12	34	100	147	.615	.663			.837	.6558	.8768	1.5326	3800	3714	6163	1.62	
	12	34	200	293	.632	.681			.877	.6558	.8768	1.5326	3800	4280	6683	1.76	
	16	34	25	37	.603	.650			.797	.5570	.8578	1.4148	3800	3438	5358	1.41	
	16	34	100	147	.626	.674			.791	.5570	.8578	1.4148	3800	3804	5983	1.57	
	16	34	200	293	.648	.698			.781	.5570	.8578	1.4148	3800	4164	6656	1.75	
Cross Chute W/L = .264	34	25	37	.710		543	1.242	.8867	1.2776	2.1643	1928	3768	5798	3.01			
	34	100	147	.707		540	1.270	.8867	1.2776	2.1643	1928	3810	5712	2.96			
	34	200	293	.716		547	1.285	.8867	1.2776	2.1643	1928	4212	5925	3.07			
	47	25	37	.759		580	1.113	.8494	1.2512	2.1006	1928	4052	6868	3.56			
	47	100	147	.729		557	1.205	.8494	1.2512	2.1006	1928	3973	5958	3.09			
	47	200	293	.775		592	1.110	.8494	1.2512	2.1006	1928	4292	7303	3.79			

REPRODUCED FROM REFERENCE (6)

**TABLE II SUMMARY OF PARACHUTE SHAPE TEST RESULTS FOR 24-GORE AND 30-GORE CONFIGURATIONS**

Parachute Type	No. of Gores	Suspension Line Length inches	Velocity		Scale Factor, K		$\frac{N}{a}$	Axes Ratio			Volume in <sup>3</sup>			$\frac{V_o}{V_H}$
			mph	fps	$\frac{2\bar{a}}{D_o}$	$\frac{2\bar{a}}{D_F}$		$\frac{b}{a}$	$\frac{b'}{a}$	$\frac{b}{a} + \frac{b'}{a}$	$V_H$	$V_C$	$V_o$	
Flat Circulars	24	34	50	73	.677	.679	.795	.5758	.8126	1.3884	4362	4695	7273	1.67
	30	34	17	25	.668	.669	.827	.6214	.7806	1.4020	4342	4626	7027	1.62
10% Extended* Skirt	24	34	100	147	.665	.648	.834	.5949	.8771	1.4720	4138	4446	6930	1.67
	30	34	17	25	.650	.633	.825	.6255	.7962	1.4127	4172	4076	6265	1.50
Ring Slot 16% Geometrically Porous	24	34	25	37	.663	.665	.824	.5800	.9053	1.4853	3591	3878	6031	1.68
	24	34	100	147	.680	.682	.819	.5800	.9053	1.4853	3591	4079	6510	1.81
	24	34	200	293	.694	.696	.809	.5800	.9053	1.4853	3591	4270	6924	1.93
	30	34	25	37	.677	.678	.788	.5800	.9053	1.4853	3582	3826	6404	1.79
	30	34	100	147	.684	.685	.802	.5800	.9053	1.4853	3582	4023	6588	1.84
	30	34	200	293	.698	.699	.800	.5800	.9053	1.4853	3582	4260	7012	1.96
Ribbon 24% Geometrically Porous	24	34	25	37	.671	.673	.770	.5980	.8187	1.4167	3591	3591	5968	1.66
	24	34	100	147	.676	.678	.813	.5980	.8187	1.4167	3591	3927	6097	1.70
	24	34	200	293	.687	.689	.804	.5980	.8187	1.4167	3591	4061	6389	1.78
	30	34	25	37	.655	.657	.782	.6021	.8463	1.4484	3582	3396	5666	1.58
	30	34	100	147	.669	.670	.784	.6021	.8463	1.4484	3582	3622	6022	1.68
	30	34	200	293	.677	.679	.823	.6021	.8463	1.4484	3582	4002	6256	1.75

\*Since this parachute was "breathing" during the test, several photographs were taken at each speed. The data were reduced from the photograph which most reasonably appeared to represent the equilibrium state.

REPRODUCED FROM REFERENCE (7)

## X. List of Symbols

$A_C$	- Steady-state projected area of the inflated parachute, $ft^2$	$P$	- Cloth permeability - rate of air-flow through a cloth at an arbitrary differential pressure, $ft^3/ft^2/sec$
$A_M$	- Instantaneous canopy mouth area, $ft^2$	$q$	- Dynamic pressure, $lb/ft^2$
$A_{Mo}$	- Steady-state inflated mouth area, $ft^2$	$S$	- Instantaneous inflated canopy surface area, $ft^2$
$a$	- Acceleration, $ft/sec^2$	$S_O = A_{SO}$	- Canopy surface area, $ft^2$
$2\bar{a}$	- Maximum inflated parachute diameter of gore mainseam, $ft$	$t$	- Instantaneous time, $sec$
$b$	- Minor axis of the ellipse bounded by the major axis ( $2\bar{a}$ ) and the vent of the canopy, $ft$	$t_O$	- Reference time when the parachute has reached the design drag area for the first time, $sec$
$b'$	- Minor axis of the ellipse which includes the skirt hem of the canopy, $ft$	$t_f$	- Canopy inflation time when the inflated canopy has reached its maximum physical size, $sec$
$C$	- Effective porosity	$u$	- Air velocity through cloth in effective porosity, $ft/sec$
$C_D$	- Parachute coefficient of drag	$v$	- Fictitious theoretical velocity used in effective porosity, $ft/sec$
$C_P$	- Parachute pressure coefficient, relates internal and external pressure ( $\Delta P$ ) on canopy surface to the dynamic pressure of the free stream	$V$	- Instantaneous system velocity, $ft/sec$
$D_O$	- Nominal diameter of the aerodynamic decelerator = $\sqrt{4S_O/\pi}$ , $ft$	$V_O$	- System velocity at the time $t = t_O$ , $ft/sec$
$F$	- Instantaneous force, $lbs$	$V_S$	- System velocity at the end of suspension line stretch, $ft/sec$
$F_S$	- Steady-state drag force that would be produced by a fully open parachute at velocity $V_S$ , $lbs$	$\underline{V}_O$	- Volume of air which must be collected during the inflation process, $ft^3$
$F_C$	- Constructed strength of the parachute, $lbs$	$W$	- Hardware weight, $lb$
$F_{max}$	- Maximum opening-shock force, $lbs$	$x_1$	- Instantaneous shock factor
$g$	- Gravitational acceleration, $ft/sec^2$	$X_O$	- Shock factor at the time $t = t_O$
$k$	- Permeability constant of canopy cloth	$\rho$	- Air density, $slugs/ft^3$
$m$	- Mass, $slugs$	$\eta$	- Ratio of parachute projected mouth area at line stretch to the steady-state projected area
$M$	- Mass ratio - ratio of the mass of the retarded hardware (including parachute) to a mass of atmosphere contained in a right circular cylinder of length ( $V_S t_O$ ), face area ( $C_D S_O$ ), and density ( $\rho$ )	$\epsilon$	- Instantaneous elongation
$M'$	- Mass flow ratio - ratio of atmosphere flowing through a unit cloth area to the atmosphere flowing through a unit inlet area at arbitrary pressure	$\epsilon_{max}$	- Maximum elongation
$n$	- Permeability constant of canopy cloth	$\epsilon_O$	- Initial elongation at the beginning of the elastic phase of inflation
		S.F.	- Parachute safety factor = $F_C/F_{max}$

## Appendix B

## A GUIDE FOR THE USE OF APPENDIX A

At first reading, Appendix A may appear to be a complicated system of analysis because of the many formulae presented. Actually, once understood, the technique is straightforward and uncomplicated. The author has attempted to simplify the algebra wherever possible. This appendix presents, in semi-outline form, a guide to the sequence of calculations because the analysis does require use of formulae from the text, not necessarily in the order in which they were presented. Also, the user can be referred to graphs of performance to illustrate effects.

In order to compute  $t_0$ , other parameters must be obtained from various sources.

## I. Determine System Parameters

1.  $C_{DSO}$ , drag area,  $ft^2$  obtained from design requirement.
2.  $V_S$ , fps, velocity of system at suspension line stretch.
3.  $\rho$ , slugs/ $ft^3$ , air density at deployment altitude.
4.  $W$ , lb, system weight (including weight of the parachute) from design requirements.
5.  $V_O$ ,  $ft^3$ , this volume of air, which is to be collected during inflation, is calculated from the steady-state inflated shape geometry of the particular parachute type. The nomenclature is described in Figure 24, p. A-14. When  $D_O$  or  $D_F$  is known,  $\bar{a}$  can be calculated from data in Table I and Table II, p. A-15, for various parachute types and number of gores. Then the geometric volume  $V_O$  can be calculated by Equation (31), p. A-14, with appropriate values of  $b/\bar{a}$  and  $b'/\bar{a}$  from the tables.
6.  $A_{MO}$ ,  $ft^2$ , steady-state canopy mouth area

$$A_{MO} = \pi \bar{a}^2 \left[ 1 - \left( \frac{N/\bar{a} - b/\bar{a}}{b'/\bar{a}} \right)^2 \right] \quad (B-1)$$

where  $N/\bar{a}$ ,  $b/\bar{a}$ , and  $b'/\bar{x}$  are available from Tables I and II for the particular type of parachute and number of gores.

$$7. A_{SO}, \text{ ft}^2, \text{ canopy surface area} = \frac{\pi D_O^2}{4}$$

8.  $C_p$ , pressure coefficient, see Figure 18, p. A-12. A constant  $C_p = 1.7$  for all altitudes seems to yield acceptable results.

9. Constants  $k$  and  $n$  are derived from measurements of the air flow through the cloth. Only  $k$  is needed for Equation (14), but  $n$  is also required for Equation (13). These parameters can be determined for any cloth using the technique described beginning on p. A-12. The two-point method is adequate if the  $\Delta P$  across the cloth is in the range of  $\Delta P$  for actual operation. Check-points of cloth permeability can be measured and compared to calculated values to verify agreement. If the data are to be extrapolated to operational  $\Delta P$ 's greater than measured, a better method of determining  $k$  and  $n$  from the test data would be a least squares fit through many data points. This way errors due to reading either of the two points are minimized.

## II. Step 1

Calculate the reference time  $t_0$  by use of Equations (13) or (14), p. A-7. If the deployment altitude is 50,000 feet or higher, Equation (14) is preferred due to its simplicity. For altitudes from sea level to 50,000 feet, Equation (13) is preferred. Figure 12, p. A-8, shows the effect of altitude on  $t_0$  and can be taken as a guide for the user to decide whether to use Equation (13) or (14). One should keep in mind that the opening shock force can be a strong function of inflation time, so be as realistic as possible. If Equation (13) is elected, the method in use at the NSWC/WO is to program Equation (13) to compute the parachute volume,  $V_0$ , for an assumed value of  $t_0$ . Equation (14), because of its simplicity, can be used for a first estimate of  $t_0$  at all altitudes. The computed canopy volume is then compared to the canopy volume calculated from the geometry of the parachute as per Equation (31), p. A-14. If the volume computed from the mass flow is within the volume computed from the geometry within plus or minus a specified delta volume, the time  $t_0$  is printed out. If not within the specified limits,  $t_0$  is adjusted, and a new volume calculated. For a 35-foot  $D_0$ , T-10 type canopy, I use plus or minus 10 cubic feet in the volume comparison. The limit would be reduced for a parachute of smaller  $D_0$ .

If  $V_0$  calculated =  $V_0$  geometry  $\pm 10$ , then print answer.

If  $V_0$  calculated  $\neq V_0$  geometry  $\pm 10$ , then correct  $t_0$  as follows:

$$t_0 = t_0 \frac{V_0 \text{ geometry}}{V_0 \text{ calculated}} \quad (\text{B-2})$$

The new value of  $t_0$  is substituted in the "do loop" and the volume recomputed. This calculation continues until the required volume is within the specified limits.

III. Calculate  $t_0$  corrected for initial area. The  $t_0$  of Section II assumes that the parachute inflated from a zero initial area. If this is a reasonable assumption for the particular system under study, then the mass ratio can be determined from Equation (6), p. A-4. For  $\eta = 0$  if the value of  $M \leq 0.19$ , then a finite state of deployment exists, and the time ratio of occurrence and the maximum shock factor can be determined from Equations (9) and (10), respectively, on p. A-5. If  $\eta \neq 0$ , then the limiting mass ratio for finite operations will rise slightly as described in Appendix C. Figures C-1 and C-2 illustrate the effects of initial area on limiting mass ratios and shock factors respectively. If the mass ratio is greater than the limiting mass ratio ( $M_L$ ), then the maximum shock force occurs at a time greater than  $t_0$  and the elasticity of the materials must be considered (see Section VI).

If  $\eta \neq 0$ , then the reference time,  $t_0$ , will be reduced, and the mass ratio will rise due to partial inflation at the line stretch. Figures 9 and 10, p. A-6, illustrate the effects of initial area on the velocities and shock factor during the "unfolding" inflation. Equation (15), p. A-9, can be used to correct  $t_0$  calculated for the cases where  $\eta = A_i/A_c$ . If the initial value of drag area is known, Equation (16), p. A-9, can be used to correct  $t_0$  and rechecked for limiting mass ratios versus  $\eta$  in Appendix C.

IV. Opening shock calculations in the elastic phase of inflation. It has been considered that from time  $t = 0$  to  $t = t_0$  the parachute has been inelastic. At the time  $t = t_0$  the applied aerodynamic load causes the materials to stretch and the parachute canopy increases in size. The increased size results in an increase in load, which causes further growth, etc. This sequence of events continues until the applied forces have been balanced by the strength of materials. The designer must insure that the constructed strength of the materials is sufficient to resist the applied loads for the material elongation expected. Use of materials of low elongation should result in lower opening shock forces as  $C_D S_{max}$  is reduced.

When the mass ratio of the system is greater than the limiting mass ratio, the elasticity of the materials and material strength determine the maximum opening shock force. The maximum elongation  $\epsilon_{max}$  and the ultimate strength of the materials are known from tests or specifications. The technique begins on p. A-9.

At the time  $t = t_0$ , calculate the following quantities for the particular values of  $M$  and  $\eta$ .

- a.  $V_0/V_S$  from Equation (18), p. A-9.

- b.  $X_0$  from Equation (22), p. A-10.
- c.  $\epsilon_0$  from Equation (23), p. A-10.
- d. Determine  $C_{DS_{max}}/C_{DS_0}$  from Figure 15, p. A-10.
- e. Calculate the inflation time ratio  $t_f/t_0$  from Equation (24), p. A-10.
- f. Calculate the maximum shock factor from Equation (19), p. A-9.
- g. Calculate the opening shock force  $F_{max.} = \chi_1 F_s$  where

$$F_s = \frac{1}{2} \rho V_s^2 C_{DS_0}$$

- h. Calculate filling time,  $t_f$ (sec)

$$\chi_1 = \epsilon_0 \left( \frac{\chi_1}{\epsilon_0} \right)$$

V. In order to simplify the required effort, the work sheets of Table B-1 are included on pages B-5 through B-9 to aid the engineer in systematizing the analysis. The work sheets should be reproduced to provide additional copies.

Table B-1. Opening Shock Force

CALCULATION WORK SHEETS

	SYMBOL	VALUE	DIMENSION
1. Parachute type -			
2. System parameters			
a. System weight, W (lb)		W	lb.
b. Gravity, g (ft/sec <sup>2</sup> )		g	ft/sec <sup>2</sup>
c. Deployment altitude (ft)			ft.
d. Deployment air density, ρ (slugs/ft <sup>3</sup> )		ρ	slugs/ft <sup>3</sup>
e. Velocity at line stretch, V <sub>s</sub> (fps)		V <sub>s</sub>	fps.
f. Steady state canopy data			
(1) Diameter, D <sub>o</sub> (ft)		D <sub>o</sub>	ft.
(2) Inflated diameter, 2ā (ft); $\frac{2\bar{a}}{D_o} = *$		2ā	ft.
(3) Surface area, S <sub>o</sub> (ft <sup>2</sup> ); $\frac{\pi}{4} D_o^2$		A <sub>so</sub> = S <sub>o</sub>	ft. <sup>2</sup>
(4) Drag area, C <sub>D</sub> S <sub>o</sub> (ft <sup>2</sup> ); C <sub>D</sub> x S <sub>o</sub>		C <sub>D</sub> S <sub>o</sub>	ft. <sup>2</sup>
(5) Mouth area, A <sub>MO</sub> <sup>*</sup> (ft <sup>2</sup> )			
$A_{MO} = \pi \bar{a}^2 \left[ 1 - \left( \frac{N/\bar{a} - b/\bar{a}}{b'/\bar{a}} \right)^2 \right]$		A <sub>MO</sub>	ft. <sup>2</sup>
(6) Volume, V <sub>o</sub> <sup>*</sup> (ft <sup>3</sup> )			
$V_o = \frac{\pi}{3} \pi \bar{a}^3 \left[ \frac{b}{\bar{a}} + \frac{b'}{\bar{a}} \right]$		V <sub>o</sub>	ft. <sup>3</sup>
g. Cloth data			
(1) k } Calculate using technique beginning on		k	—
(2) n } p. A-12.		n	—
<p>Note: Permeability is usually measured as ft<sup>3</sup>/ft<sup>2</sup>/min. For these calculations permeability must be expressed as ft<sup>3</sup>/ft<sup>2</sup>/sec</p>			

\* Data for these calculations are listed in Tables 1 and 2, p. A-15.

Table B-1. Opening Shock Force  
(cont'd)

(3)  $\epsilon_{max}$ ; determine maximum elongations from pull test data of joints, seams, lines, etc. Use minimum  $\epsilon_{max}$  determined from tests.

(4)  $C_p$ ; pressure coefficient

h. Steady state drag,  $F_s$  (lb),  $F_s = \frac{1}{2} \rho V_s^2 C_D S_o$

i. Parachute constructed strength,  $F_c$  (lb); determined from data on efficiency of seams, joints, lines. Constructed strength is the minimum load required to fail a member times the number of members.

3. Force calculations

a. Calculate  $t_o$  for  $\eta = 0$ ; eq. 14, p. A-7.

$$t_o = \frac{14W}{\rho g V_s C_D S_o} \left[ \epsilon \frac{\rho g V_o}{2W} \left[ \frac{C_D S_o}{A_{MO} - A_{SO} k \left( \frac{C_p \rho}{2} \right)^{\frac{1}{2}}} \right] - 1 \right]$$

Check Figure 13, p. A-8, for advisability of using eq. 13, p. A-7.

b. If  $\eta = 0$ , proceed with steps c through e. If  $\eta \neq 0$ , go to step f.

c. Mass ratio,  $M$ ; eq. 6, p. A-4

$$M = \frac{2W}{\rho g V_s t_o C_D S_o}$$

d. If  $M \leq 4/21$  for  $\eta = 0$ , then finite mass deployment is indicated.

(1) Time ratio at  $x_i max$ ; eq. 9, p. A-5

$$\frac{t}{t_o @ x_i max} = \left( \frac{21M}{4} \right)^{\frac{1}{7}}$$

(2) Max shock factor,  $x_i$ ; eq., 10, p. A-5

$$x_i max = \frac{16}{49} \left( \frac{21M}{4} \right)^{\frac{6}{7}}$$

SYMBOL	VALUE	DIMENSION
	$C_p$	—
	$F_s$	lb.
	$F_c$	lb.
	$t_o$	sec.
	$M$	—
	$\frac{t}{t_o @ x_i max}$	—
	$x_i max$	—

Table B-1. Opening Shock Force (Cont'd)

(3) Max shock force,  $F_{max}$  (lb)

$$F_{max} = X_{i\ max} F_S$$

e. If  $M > 4/21$ ; then intermediate mass or infinite mass deployment is indicated and the elasticity of materials is involved. Calculate the trajectory conditions at time  $t = t_o$ .

(1) Velocity ratio @  $t = t_o$  for  $\eta = 0$

$$\frac{V_o}{V_s} = \frac{1}{1 + \frac{1}{7M}}$$

(2) Shock factor  $X_o$  @  $t = t_o$  for  $\eta = 0$

$$X_o = \frac{1}{\left[1 + \frac{1}{7M}\right]^2} = \left(\frac{V_o}{V_s}\right)^2$$

(3) Initial elongation,  $\epsilon_o$ ; eq. 23, p. A-10

$$\epsilon_o = \frac{X_o F_S}{F_c} \epsilon_{max}$$

(4) Determine  $\frac{C_{D\ S\ max}}{C_{D\ S_o}}$  from Figure 15, p. A-10

$$\frac{C_{D\ S\ max}}{C_{D\ S_o}}$$

p. A-10 (5) Calculate inflation time ratio,  $\frac{t_f}{t_o}$ ; eq. 24,

$$\frac{t_f}{t_o} = \left(\frac{C_{D\ S\ max}}{C_{D\ S_o}}\right)^{\frac{1}{6}}$$

$$\frac{t_f}{t_o}$$

(6) Calculate maximum shock factor,  $X_{i\ max}$ ; eq. 19, p. A-9

$$X_{i\ max} = \frac{\left(\frac{t_f}{t_o}\right)^6}{\left[\frac{V_s}{V_o} + \frac{1}{7M} \left[\left(\frac{t_f}{t_o}\right)^7 - 1\right]\right]^2}$$

$$X_{i\ max}$$

(7) Calculate maximum shock force,  $F_{max}$  (lb),

$$F_{max} = X_{i\ max} F_S$$

$$F_{max}$$

SYMBOL	VALUE	DIMENSION
	$F_{max}$	lb.
	$\frac{V}{V_o}$	-
	$X_o$	-
	$\epsilon_o$	-
	$\frac{C_{D\ S\ max}}{C_{D\ S_o}}$	-
	$\frac{t_f}{t_o}$	-
	$X_{i\ max}$	-
	$F_{max}$	lb.

Table B-1. Opening Shock Force (cont'd)

(8) Inflation time, sec =  $t_f = t_o \left( \frac{t_f}{t_o} \right)$

f. If  $\eta \neq 0$ , correct  $t_o$  for initial area effects; eq. 16, p. A-9

$$t_o = \left[ 1 - \left( \frac{C_D S_i}{C_D S_o} \right)^{1/6} \right] t_o \text{ calculated}$$

g. Mass Ratio, M, eq. 6, p. A-4

$$M = \frac{2W}{\rho g V_s t_o C_D S_o}$$

h. Calculate limiting mass ratio,  $M_L$

$$M_L = \frac{1}{3(1-\eta)} - \left[ \frac{9}{14} \eta^2 + \frac{3}{14} \eta + \frac{1}{7} \right]$$

If  $M \leq M_L$ , finite mass deployment is indicated and  $x_i \text{ max}$  can be determined by eq. 8, p. A-5 by assuming values of  $t/t_o$  and plotting the data using the methods of Appendix C.

i. If  $M > M_L$ , then intermediate mass or infinite mass deployment is indicated and the elasticity of materials is involved. Calculate the trajectory conditions at time  $t = t_o$ .

(1) Velocity ratio @  $t = t_o$  for  $\eta \neq 0$ ; eq. 18, p. A-9

$$\frac{V_o}{V_s} = \frac{1}{\left[ 1 + \frac{1}{M} \left[ \frac{(1-\eta)^2}{7} + \frac{\eta(1-\eta)}{2} + \eta^2 \right] \right]}$$

(2) Shock factor  $X_o$  @  $t = t_o$  for  $\eta \neq 0$ ; eq. 22, p. A-10

$$X_o = \frac{1}{\left[ 1 + \frac{1}{M} \left[ \frac{(1-\eta)^2}{7} + \frac{\eta(1-\eta)}{2} + \eta^2 \right] \right]^2} = \left( \frac{V_o}{V_s} \right)^2$$

(3) Initial elongation,  $\epsilon_o$ ; eq. 23, p. A-10

$$\epsilon_o = \frac{X_o F_s}{F_c} \epsilon_{\text{max}}$$

(4) Determine  $\frac{C_D S_{\text{max}}}{C_D S_o}$  from Figure 15, p. A-10

SYMBOL

VALUE

DIMENSION

$t_f$

Sec.

$t_o$

Sec.

M

-

$M_L$

-

$\frac{V_o}{V_s}$

-

$X_o$

-

$\epsilon_o$

-

$\frac{C_D S_{\text{max}}}{C_D S_o}$

-

Table B-1. Opening Shock Force (Contd.)

	SYMBOL	VALUE	DIMENSION	
p. A-10	(5) Calculate inflation time ratio, $\frac{t_f}{t_0}$ ; eq. 24,	$\frac{t_f}{t_0} = \left( \frac{C_D S_{max}}{C_D S_0} \right)^{\frac{1}{6}}$	$\frac{t_f}{t_0}$	-
eq. 19, p. A-9	(6) Calculate maximum shock factor, $x_{i \max}$ ;	$x_{i \max} = \frac{\left( \frac{t_f}{t_0} \right)^6}{\left[ \frac{V_s}{V_0} + \frac{1}{7M} \left[ \left( \frac{t_f}{t_0} \right)^7 - 1 \right] \right]^2}$	$x_{i \max}$	-
	(7) Calculate maximum shock force, $F_{\max}$ (lb)	$F_{\max} = x_{i \max} F_s$	$F_{\max}$	lb.
	(8) Calculate inflation time, $t_f$ (sec)	$t_f = t_0 \left( \frac{t_f}{t_0} \right)$	$t_f$	Sec.

## Appendix C

EFFECT OF INITIAL AREA RATIO ON THE LIMITING MASS RATIO  
AND SHOCK FACTOR FOR THE FINITE STATE OF  
SOLID CLOTH PARACHUTE DEPLOYMENT

Very low mass ratios are indicative of finite mass parachute deployment, wherein the maximum shock force occurs before the parachute is fully inflated during the unfolding phase of deployment. As the mass ratio is increased, the maximum shock force occurs later in the inflation process. At some value of mass ratio, the maximum shock force will occur at the time  $t_0$ . This particular mass ratio is defined as the limiting mass ratio ( $M_L$ ) for finite mass deployment. A further increase in mass ratio will result in the maximum shock force occurring after the parachute has achieved the design drag area ( $C_D S_0$ ) for the first time.

Equation (8), from p. A-5, Appendix A, defines the instantaneous shock factor during the unfolding phase of parachute deployment.

$$\chi_1 = \frac{(1-\eta)^2 \left(\frac{t}{t_0}\right)^6 + 2\eta(1-\eta) \left(\frac{t}{t_0}\right)^3 + \eta^2}{\left[1 + \frac{1}{M} \left[ \frac{(1-\eta)^2}{7} \left(\frac{t}{t_0}\right)^7 + \frac{\eta(1-\eta)}{2} \left(\frac{t}{t_0}\right)^4 + \eta \frac{t}{t_0} \right]\right]^2}$$

This expression is to be analyzed for the following purposes:

- a. Determine the effect of the initial area ratio ( $\eta$ ) on the limiting mass ratio ( $M_L$ ).
- b. Determine the variations of the instantaneous shock factor during the unfolding phase of deployment as a function of limiting mass ratio and  $\eta$ .
- c. Determine the expression for the time of occurrence of the maximum shock force for finite mass ratios less than the limiting mass ratio.

The maximum shock force occurs at the point in finite mass deployment where  $dx_1/dt = 0$ . Setting the derivative  $dx_1/dt = 0$  and solving for mass ratio as a function of  $\eta$  and  $t/t_0$  results in the following equality:

$$M = \frac{\left[ (1-\eta)^2 \left(\frac{t}{t_0}\right)^6 + 2\eta(1-\eta) \left(\frac{t}{t_0}\right)^3 + \eta^2 \right]^2}{3 \left[ (1-\eta)^2 \left(\frac{t}{t_0}\right)^5 + \eta(1-\eta) \left(\frac{t}{t_0}\right)^2 \right]} - \left[ \frac{(1-\eta)^2}{7} \left(\frac{t}{t_0}\right)^7 + \frac{\eta(1-\eta)}{2} \left(\frac{t}{t_0}\right)^4 + \eta^2 \frac{t}{t_0} \right] \quad (C-1)$$

Since the limiting mass ratio occurs at  $t/t_0 = 1$ , Equation (C-1) can be reduced to:

$$M_L = \frac{1}{3(1-\eta)} - \left[ \frac{9}{14} \eta^2 + \frac{3}{14} \eta + \frac{1}{7} \right] \quad (C-2)$$

The effects of initial area ratio on the limiting mass ratio are described in Equation (C-2) and Figure C-1. Note that the time of occurrence of the maximum shock force for  $\eta = 0$  in Equation (C-1) is:

$$\frac{t}{t_0} \otimes x_{i \max} = \left( \frac{21M}{4} \right)^{\frac{1}{7}} \quad (C-3)$$

which is the same as Equation (9), p. A-5, Appendix A.

The variation of the instantaneous shock factor during the unfolding phase of deployment for limiting mass ratios is presented in Figure C-2. Initial area at the beginning of inflation causes the initial force to increase, but this is compensated for by reduced maximum shock forces. As  $\eta$  increases, the initial loads can be greater than the maximum shock force. However, values of  $\eta$  are usually small and depend on the deployment systems for magnitude and repeatability. Values of  $\eta = 0.4$  are more representative of a parachute being disreefed rather than initially deployed. This does demonstrate, however, that the analysis presented in Appendix A can be adapted to the disreefing of solid cloth parachutes by considering the next stage to be a deployment with a large value of  $\eta$ . Variation in initial area is one of the causes of variation in opening shock forces. The variation of opening shock forces for finite mass, intermediate mass, and infinite mass states of deployment can be evaluated by successive calculations with various expected values of  $\eta$ .

For known mass ratios less than the limiting mass ratio, the time of occurrence of the maximum shock force can be ascertained from Equation C-1. If  $\eta$  approaches zero, then the time ratio of

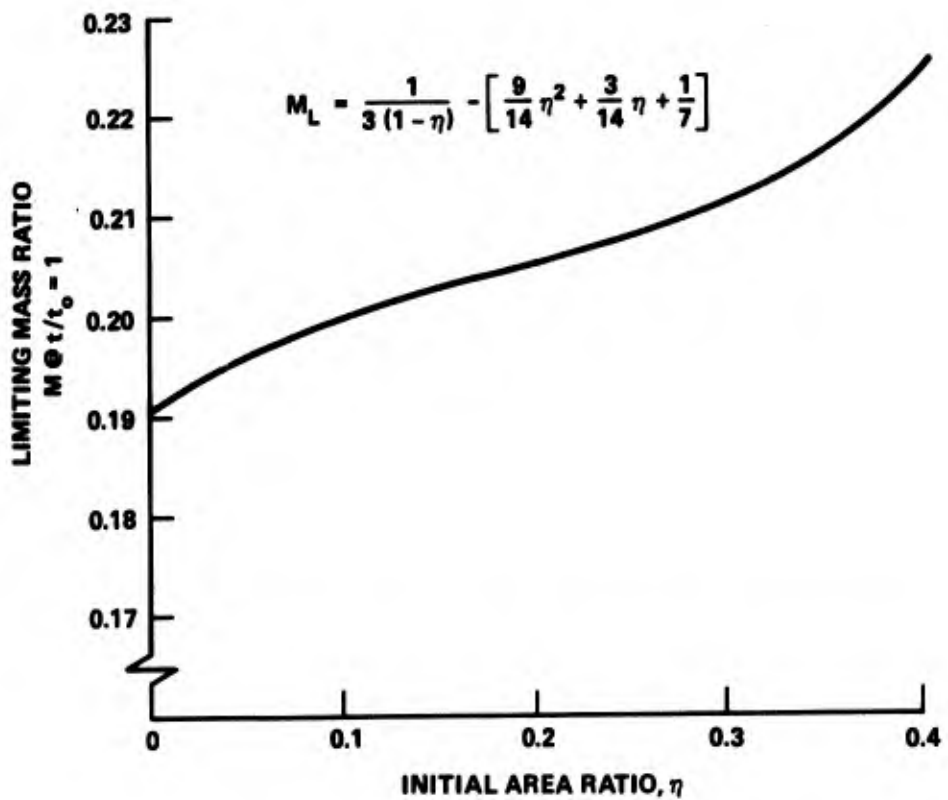


**FIGURE C-1. EFFECT OF INITIAL AREA RATIO ON THE LIMITING MASS RATIO FOR THE FINITE STATE OF PARACHUTE DEPLOYMENT FOR SOLID CLOTH PARACHUTES**

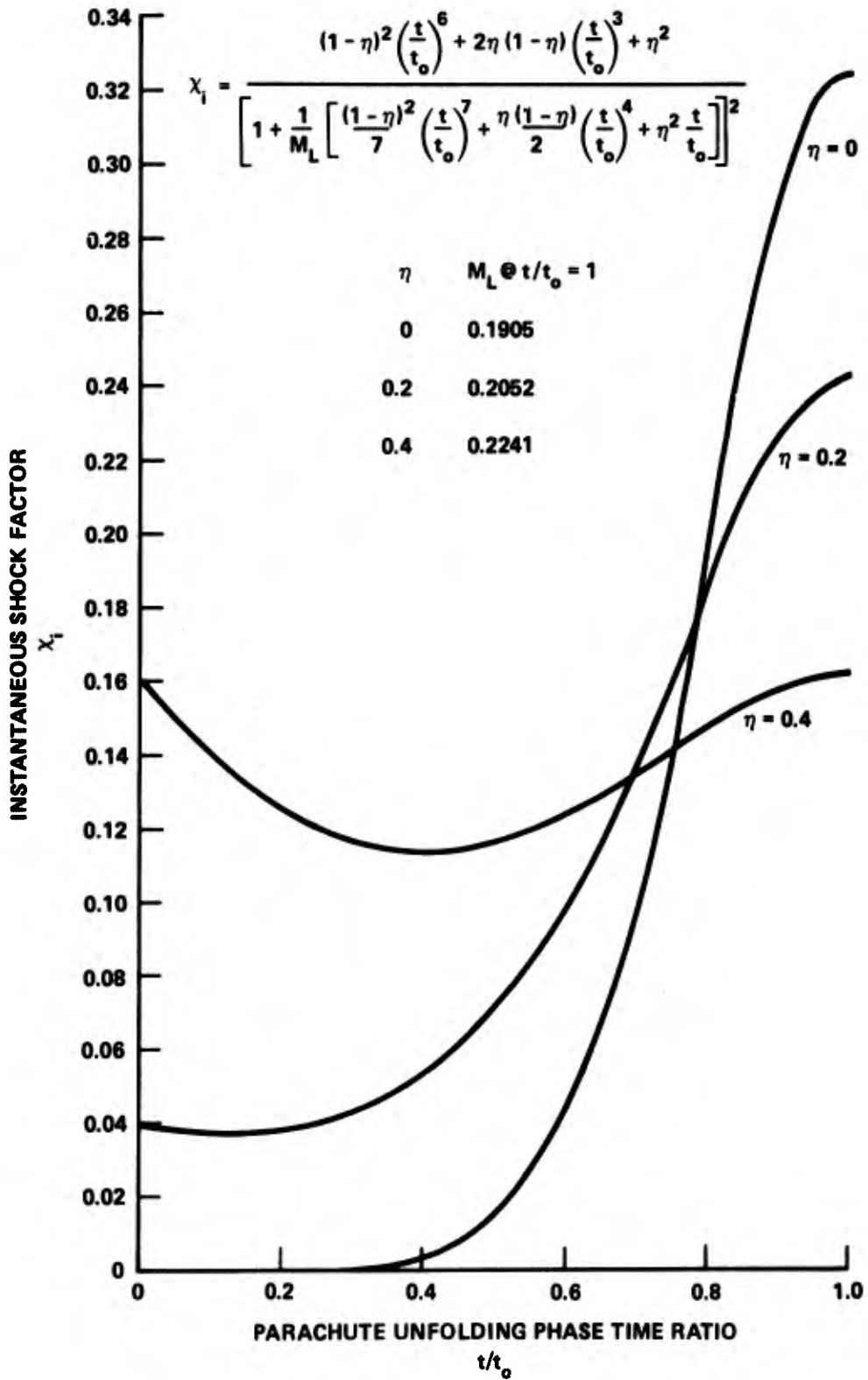


FIGURE C-2. VARIATION OF THE FINITE MASS SHOCK FACTOR DURING THE UNFOLDING PHASE OF SOLID CLOTH PARACHUTES FOR LIMITING MASS RATIOS AND INITIAL AREA EFFECTS

occurrence of the maximum shock force can be initially estimated from Equation (C-3), or determined by plotting

$$x_i = f\left(M, \eta, \frac{t}{t_0}\right)$$

as in Figure C-2.

## DISTRIBUTION

	<u>Copies</u>		<u>Copies</u>
Commander Naval Air Systems Command Attn: Library Department of the Navy Washington, DC 20361	4	Commanding Officer U.S. Army Mobility Equipment Research and Development Center Attn: Technical Document Center Fort Belvoir, VA 22660	2
Commander Naval Sea Systems Attn: Library Washington, DC 20362	4	Commander U.S. Army Aviation Systems Command Attn: Library St. Louis, MO 63166	2
Commanding Officer Naval Personnel Research and Development Center Attn: Library Washington, DC 20007	2	Commander U.S. Army Munitions Command Attn: Technical Library Stanley D. Kahn Dover, NJ 07801	2 1
Office of Naval Research Attn: Library Washington, DC 20360	4	Commander U.S. Army Weapons Command Attn: Technical Library Research and Development Directorate Rock Island, IL 61201	2
U.S. Naval Academy Attn: Library Annapolis, MD 21402	2	Commander U.S. Army ARRADCOM Attn: Library Thomas D. Hoffman DRDAR-LCA-F Ray W. Kline DRDAR-LCA-F Dover, NJ 07801	1 1 1
Commanding Officer U.S. Naval Air Development Center Attn: Library William B. Shope David N. DeSimone Louis A. Daulerio Thomas J. Popp Maria C. Hura Johnsonville, PA 18974	2 1 1 1 1 1		
Commanding Officer U.S. Naval Weapons Support Center Attn: Library Mark T. Little Crane, IN	2 1		

## DISTRIBUTION (Cont.)

	<u>Copies</u>		<u>Copies</u>
Commander		Command Officer	
U.S. Army Natick R&D Labs		Kelly AFB	
Attn: Library	1	Attn: SA-ALC/MMIR	2
James E. Sadek	1	Library	2
Peter Masek	1	TX 78241	
Calvin K. Lee	1	Commanding Officer	
M. P. Gionfrido	1	McCallan AFB	
Joseph Gardella	1	Attn: Library	2
Timothy E. Dowling	1	Library	2
DRDNA-UAS	1	CA 95652	
Kansis Street		Defense Technical Information	
Natick, MA		Center	
Commanding Officer		Cameron Station, Building 4	
Wright-Patterson AFB		Alexandria, VA 22314	12
Attn: William Casey ASD/ENECA	1	Library of Congress	
William Pinnell	1	Attn: Gift and Exchange	10
APWAL/FIER	1	Division	
Robert L. Hesters Jr.	1	Washington, DC 20540	
ASD/YYEE	1	NASA Langley Research Center	
E. Schultz AFWAL/FIER	1	Langley Station	
Daniel J. Kolega	1	Attn: Research Program Recording	
Bldg. 25 Area B	1	Unit, Mail Stop 122	1
Patrick J. O'Brian	1	Raymond L. Zavasky,	
Bldg. 25 Area B	1	Mail Stop 177	1
H. Engel ASD/ENEC	1	Andrew S. Wright, Jr.,	
OH 45433		Mail Stop 401	8
Commanding Officer		Hampton, VA 23365	
Air Force Flight Test Center		NASA Ames Research Center	
Attn: Airframe Systems		Attn: Library, Stop 202-3	1
Division Aerodynamic		Moffett Field, CA 94035	
Decelerator Branch	2	NASA Flight Research Center	
John A. Hed	1	Attn: Library	1
Edwards AFB, CA 93523		P.O. Box 273	
Commanding Officer		Edwards, CA 93523	
Air Force Space Division		NASA Goddard Space Flight	
Attn: Library	2	Center	
P.O. Box 92960		Attn: Library	1
Worldway Postal Center		Greenbelt, MD 20771	
Los Angeles, CA 90009		Jet Propulsion Laboratory	
Commanding Officer		4800 Oak Grove Drive	
Air Force Aerophysics		Attn: Library, Mail 111-113	1
Laboratory		Pasadena, CA 91103	
Attn: Library	2		
Hanscom Field, MA			

## DISTRIBUTION (cont.)

	<u>Copies</u>		<u>Copies</u>
NASA Manned Spacecraft Center Attn: Library, Code BM6 2101 Webster Seabrook Road Houston, TX 77058	1	University of Minnesota Dept. of Aerospace Engineering Attn: Dr. W. L. Garrard Minneapolis, MN 55455	2
NASA Marshall Space Flight Center Attn: Library Huntsville, AL 25812	1	Internal Distribution: U13 (W. P. Ludtke) U13 (J. F. McNelia) U13 (D. W. Fiske) U13 (J. Murphy) U13 (J. G. Velez) U13 (M. L. Fender) U13 (A. G. Fritz) U13 (R. L. Pense) U13 (C. J. Diehlman) U131 (E. Noel) U43 (J. Rosenberg) U43 (B. Delre) E231 E232	175 1 1 1 1 1 1 1 1 1 1 1 9 3
NASA Goddard Space Flight Center/ Wallops Flight Facility Attn: Library Mr. Mendle Silbert Mr. Earl B. Jackson, Code 841.2 Mr. Dave Moltedo, Code 841.2 Mr. Anel Flores Wallops Island, VA 23337	1 1 1 1 1 1 1 1		
NASA Lewis Research Center Attn: Library, Mail Stop 60-3 21000 Brookpark Road Cleveland, OH 44135	1		
NASA John F. Kennedy Space Center Attn: Library, Code IS-CAS-42B Kennedy Space Center, FL 32899	1		
NASA Headquarters Attn: Library Washington, DC 20546	2		
Sandia National Laboratories Attn: Code 1632 Library Dr. Dean Wolf Dr. Carl Peterson R. Kurt Baca Ira T. Holt Donald W. Johnson James W. Purvis Harold E. Widdows Albuquerque, NM 87185	1 1 1 10 1 1 1 1 1 1		